DISSERTATION

PRIMARY VIRAL-SECONDARY BACTERIAL PNEUMONIA: A NOVEL SYRIAN HAMSTER INFECTION MODEL FOR INVESTIGATING MODULATION OF HOST RESPONSE PATHWAYS AS THERAPEUTIC TARGETS.

Submitted by

Ashley Romano

Department of Microbiology, Immunology, and Pathology

In partial fulfillment of the requirements

For the Degree of Doctor of Philosophy

Colorado State University

Fort Collins, Colorado

Summer 2025

Doctoral Committee:

Advisor: Richard Slayden

Zaid Abdo
Angela Bosco-Lauth
Brendan Podell
Ron Tjalkens

ABSTRACT

PRIMARY VIRAL-SECONDARY BACTERIAL PNEUMONIA: A NOVEL SYRIAN HAMSTER INFECTION MODEL FOR INVESTIGATING MODULATION OF HOST RESPONSE PATHWAYS AS THERAPEUTIC TARGETS.

Acute respiratory tract infections remain a significant public health concern. Despite numerous clinical retrospective studies on primary viral-secondary bacterial pneumonia (VBP), there are no experimental reports addressing the influence of SARS-CoV-2 on susceptibility to secondary bacterial infection, VBP studies exploring the effects of biological variables, or assessment of host-directed therapeutics (HDTs) as a treatment strategy for VBP using immunocompetent lab animal model species. As such, I designed a three-pronged research project to address these critical knowledge gaps to create a novel small animal infection model with high translational impact for studying human VBP pathogenesis and treatment options. I first established an infection model characterizing VBP in Syrian hamsters, which is an immunocompetent lab animal species that is naturally susceptible to SARS-CoV-2 and extracellular bacterial species. I found that the ideal infection scenario comprised of: male hamsters older than 39 weeks of age; intranasal SARS-CoV-2 administered on Day 0; non-surgical intratracheal *Haemophilus influenzae* serotype B administered on Day 2.5 post-viral infection (PVI); study endpoints of Day 7 and Day 14 PVI. I then repeated this experiment and included virus-only, bacteria-only, and bacteria followed by virus infection groups to confirm that the pathogen infection sequence impacts disease phenotype. This study demonstrated that the virus followed by bacteria infection group resulted in the greatest amount of weight loss, most severe histopathology, and positive microbial titers on Day 7 post-primary infection (PPI). Moreover, to assess which pathways were most affected on Day 7 PPI, I performed qRT-PCR

relative gene expression on lung tissue homogenates that revealed significant pro- and anti-inflammatory gene dysregulation in a subset of virus followed by bacteria infected hamsters that was not detected in any other infection group. These findings informed the choice of HDTs selected to modulate host pathways implicated in host-pathogen interactions that can lead to severe disease states. I discovered that either modulating expression of host receptors utilized by SARS-CoV-2 for cell entry or modulating host cyclooxygenase-2 function may be viable treatment targets for subsets of VBP patients. Together, this work establishes a new model for assessing VBP in an underutilized laboratory animal species and highlights the utility of HDTs as a treatment option for VBP.

TABLE OF CONTENTS

CHAPTER 1 – INTRODUCTION

DEFINING THE PROBLEM OF PRIMARY VIRAL-SECONDARY BACTERIAL PNEUMONIA

The mammalian respiratory tract constantly interacts with the external environment and must filter harmful or noxious particulates from inspired air for unabated respiration. Despite the intricate defense mechanisms of the upper and lower respiratory tract, various viral, bacterial, and fungal pathogens can overcome these barriers to infect the respiratory tract individually or in combination. One well-known primary respiratory pathogen is severe acute respiratory syndrome coronavirus 2 (SARS-CoV-2), the causative agent of coronavirus disease 2019 (COVID-19). This virus has disproportionately caused severe disease in select individuals, and chronological age is the single greatest risk factor for COVID-19 mortality [2]. Multiple studies have found that secondary bacterial pneumonia significantly contributes to worse clinical outcomes among moderately to critically ill COVID-19 patients [30, 64, 88]. Virus-mediated changes enable endogenous or exogenous bacteria to colonize and infect the host respiratory tract. The pulmonary microenvironment is further disrupted by tissue damage secondary to the host innate immune cell release of nonspecific defense molecules into the extracellular space [39]. Although response mechanisms are often appropriately regulated in patients, aged patients are likelier to exhibit an imbalanced response resulting in a dysregulated pro-inflammatory state [2, 61]. These host and pathogen microenvironment alterations result in complex diseases that are difficult to study in humans.

Published primary viral-secondary bacterial pneumonia (VBP) animal infection models predominantly utilize mice, which unfortunately lack translational rigor due to their various immune deficits [75]. Moreover, SARS-CoV murine models utilize transgenic mice that have not been shown to successfully transmit virus to co-housed naïve, uninfected mice – further underscoring mechanistic differences between humans and mouse models [52]. These issues highlight the need for novel models that better recapitulate human immunological responses to advance our

understanding and treatment of VBP. Syrian hamster biology more closely recapitulates human immune responses and SARS-CoV-2 pathobiology, and thus may more aptly reveal relevant mechanisms engaged during VBP infections.

VBP HISTORICAL SIGNIFICANCE

Most of the recent pandemics have been of viral origin [42]. This is especially true for RNA viruses that successfully generate infectious mutated virions, such as influenza viruses and coronaviruses, which can then evade host immune responses to cause re-infection or extend pandemic situations. The injury incurred from viral pneumonia is oftentimes compounded by secondary bacterial pneumonia and is known to lead to increased morbidity in select patient demographics [57]. One important caveat is that patients hospitalized for viral pneumonia often receive empirical antibiotics, which likely skews data reporting on the true prevalence of secondary bacterial infections [41, 50].

The first well-documented occurrence, and most extreme example, of VBP was the 1918–1919 “Spanish flu” pandemic caused by the founder H1N1 influenza A virus [55, 46]. It has been estimated that most Spanish flu patients with severe influenza-associated pneumonia died from a secondary bacterial pneumonia [55]. Unlike many infectious types of pneumonia, there was a disproportional increase in the frequency of secondary bacterial pneumonia in healthy young adults, as compared to infants and aged adults, which highlighted the possibility of host-related factors such as older adults having been pre-exposed to then-prevalent influenza A viruses containing either H1 or N1 [66, 80]. In a retrospective autopsy series of 68 high-quality tissue specimens from Spanish flu patients, 92% of autopsy lung cultures were positive for at least one bacterial species [55]. The most commonly isolated bacteria was pneumococci [55].

Influenza pandemics with high morbidity and mortality usually occur due to the emergence of a novel influenza A virus where little or no immunity exists among the global population [57]. Such a breach in the respiratory tract barrier across a large populace can provide invading bacteria with

different substrates for adhesion and access to usually inaccessible nutrients to metabolize [56]. Although limited studies from the 2009 H1N1 influenza A virus pandemic reported on bacterial complications, many of those studies found that up to 30% of patients had a secondary bacterial infection, which was associated with admission to intensive care units or death [17, 23, 47, 77]. In these analyses, *Streptococcus pneumoniae* was the most common bacteria isolated. Interestingly, approximately 25% of all seasonal outbreak influenza-related deaths are associated with secondary bacterial infections [56].

Another virus implicated in human VBP cases is respiratory syncytial virus (RSV). Human RSV is the main cause of acute lower respiratory tract infections in children less than five years of age and adults over 65 years of age [56]. Studies have found that, in children, up to 40% of severe RSV cases admitted to intensive care units had lower airway secretions positive for bacteria [45, 51, 81]. Meta-analysis specifically assessing childhood RSV and *S. pneumoniae* infections found an increased disease severity risk when both pathogens were detected simultaneously [5]. Moreover, in aged adults hospitalized with RSV, bacterial-associated pneumonia has been reported in 8-12% of those cases [16, 25, 43]. The most commonly isolated bacteria in the children and adult studies were *S. pneumoniae* or *Haemophilus influenzae*. Beyond influenza viruses and human RSV, there are clusters of published reports that implicate rhinoviruses, adenoviruses, coronaviruses, parainfluenza virus, and human metapneumovirus as contributing viruses in VBP [8, 60].

VBP is not limited to only humans but is a major contributor to respiratory disease in production animal species, such as cattle and swine. Unlike VBP in humans, VBP in production animals occurs most commonly in young, weanling animals exposed to environmental stressors such as overcrowding, transportation, and poor ventilation [22]. VBP is such a well-established phenomenon in production animal medicine that it is often referred to as a “respiratory disease complex” or even “shipping fever” [90]. Common viruses and bacteria implicated in cattle are bovine viral diarrhea virus, bovine respiratory syncytial virus, bovine herpes virus-1, *Mycoplasma bovis*,

Histophilus somni, *Mannheimia haemolytica,* and *Pasteurella multocida* [12]. Pathogens involved in porcine VBP are swine influenza virus, porcine reproductive and respiratory syndrome virus, porcine circovirus type 2, *Mycoplasma hyopneumoniae, Pasteurella multocida*, *Haemophilus parasuis,* and *Streptococcus suis* [67]. The financial burden of cattle and swine respiratory disease is estimated to cost the industries $800 million and $660 million USD, respectively, due to mortality, medical treatments, and labor costs [29, 34].

OVERVIEW OF RESPIRATORY TRACT INNATE HOST DEFENSES

Host defenses are composed of physical barriers, innate immune cells, and the associated signaling pathways that work in concert to minimize the successful deposition of microbes, toxic chemicals, and inert substances into the lower respiratory tract. Understanding the relevance of these defenses and how they are interrelated are critical in selecting model species for translational infectious disease research.

Physical barriers of the respiratory tract system

Nasal cavity

The first major defense that inspired environmental air contacts is the nasal cavity, which is composed of nasal turbinates lined by pseudostratified, ciliated epithelial cells interspersed by goblet and serous cells [90]. Much like other epithelial surfaces throughout the body, respiratory tract epithelia are adhered to one another by tight junctions that aid in providing structural integrity to prevent pathogen invasion and maintain fluid dynamics [24]. Goblet and serous cells secrete a hydrated mucus that can capture inspired contaminants. The scroll-like design of the turbinates increases nasal surface area to aid in trapping particulate matter as small as 2×10^{-6} m in diameter, limiting such particles from depositing in the lower respiratory tract. Although the average diameter of viruses and bacteria is 1×10^{-9} m and 1×10^{-6} m, respectively, respiratory pathogens are

commonly encased in a fomite such as dust or bodily fluids, increasing their relative size [90]. Infectious fomites approximately 1×10^{-6} m or less in diameter can successfully be inhaled into the lower respiratory tract. Regarding animal modeling research, it is important to note that there is species variation in the complexity of the nasal turbinates such that rodent turbinates have a relative surface area approximately 5× greater than humans [83]. As such, rodent nasal turbinates are better at filtering inhaled particulate from inspired air than humans.

In addition to epithelial and turbinate structural barriers, the microbiome is an overlooked defense liaison of the nasal cavity. Commensal bacteria can both interfere with opportunistic pathogen colonization as well as prime the host immune response [14, 37]. Microbiota antagonism can occur if commensal bacteria are superior at nutrient acquisition or engage in rapid nutrient sequestration compared to invading opportunistic bacteria [27]. As for host immunity, nasal commensal bacteria can aid in the modulation of IgA production and stimulate myeloid cell cytokine elaboration [37, 72]. Interestingly, multiple sources have also demonstrated specific inverse relationships of symbiotic commensals versus opportunistic bacteria that exist within the nasal microbial community between health and disease states – underscoring the importance of upper respiratory tract microbial compositions in respiratory health [9, 40, 68].

Conducting zone

Infectious fomites that successfully traverse the nasal cavity next contact the trachea and its mucociliary apparatus (MA). Here, the MA is lined by ciliated epithelial cells, serous cells, and goblet cells. The serous cells secrete an inner thin colloidal solution that permits rhythmic beating of the epithelial cilia, and the goblet cells secrete a luminal mucin glycoprotein layer that traps infectious fomites [90]. The coordinated beating of the ciliated epithelium within the serous layer allows for trapped fomites in the mucous layer to be expelled into the pharynx with subsequent

sternutation, expectoration, or deglutition. Pathogens that escape containment by the nasal cavity and trachea can then progress to the lower respiratory tract bronchioles and alveoli.

Transitional and respiratory zones

The final segments of the respiratory tract include the bronchial-bronchiolar transitional zone and the respiratory zone, where oxygen-carbon dioxide gas exchange occurs. Prior to reaching the alveolar respiratory zone, the branching of the bronchial and bronchiolar trees provides one last opportunity for inhaled particles to be trapped by ciliated bronchial mucosa or to contact microfold cells that overlay bronchial-associated lymphoid tissue (BALT) [82, 90]. While most animals have BALT under normal homeostatic conditions, BALT is absent in cats, dogs, Syrian hamsters, and humans; however, after exposure to allergens or infectious agents, inducible BALT (iBALT) can be formed in these species [11, 69]. Areas of iBALT are only maintained for several months before decreasing in size, but these tertiary lymphoid structures can participate in immune responses that are unrelated to the iBALT-initiating particulate thereby enhancing host defense capabilities [31].

Alveolar epithelium is composed of two types of cells: alveolar type 1 (AT1) cells and alveolar type 2 (AT2) cells. AT1 cells facilitate gas exchange and line approximately 95% of the alveolar surface area; AT2 cells produce surfactant, act as reserve cells for the alveolar epithelium, and line approximately 5% of the alveolar surface area [85]. Surfactant is composed of 90% lipids and 10% proteins, which aid in decreasing surface tension to prevent alveolar collapse during expiration but also contain innate immune defense molecules (i.e., collectins) [10]. Surfactant proteins A and D are collectins; these glycoproteins are secreted pattern-recognition receptors (PRRs) that bind pathogen-associated molecular patterns (PAMPs) [58]. Examples of PAMPs include bacterial components, such as lipopolysaccharide and flagellin, and viral components, such as viral nucleic acid. PRRs and PAMPs are discussed in more detail in the following section.

Respiratory tract innate immunity surveillance and cells

Innate immunity surveillance

Innate immunity takes no longer than minutes to hours to be fully activated after pathogen exposure [59]. Both immune cells and mucosal epithelial cells contribute to innate immune responses in the respiratory tract. Similar to the collectins mentioned above, immune cells and mucosal epithelial cells possess PRRs that detect both PAMPs and host-derived damage-associated molecular patterns (DAMPs). PRRs are proteins classified as secreted, transmembrane, and cytosolic. Collectins are an example of secreted PRRs and act as opsonins that enhance phagocyte engulfment. Transmembrane PRRs, such as toll-like receptors (TLRs), have a restricted cellular distribution of macrophages, natural killer cells, dendritic cells, innate lymphoid cells, mucosal epithelial cells, and endothelial cells [19, 44, 90]. TLRs present on the plasma membrane detect bacterial products, whereas TLRs located on endosomal vesicles commonly detect viral nucleic acids [39]. Cytosolic PRRs relevant to this dissertation are retinoic acid-inducible gene I-like receptors (RLRs) and nucleotide-binding and oligomerization domain-like receptors (NLRs), which can detect cytoplasmic viral nucleic acids and a variety of DAMPs. Activation of PRRs induces signaling pathways that upregulate transcription factors (e.g., interferon regulatory factors), activate the complement system, trigger apoptosis, and initiate type I interferon (IFN) gene transcription signaling [63, 90]. Host-related factors, such as age and sex (discussed in Chapter 2), impact how quickly PRRs are activated, and therefore, can impact immune response outcomes and disease trajectory.

In addition to active surveillance by PRRs, the respiratory tract epithelium engages in important passive defense. Goblet cells and submucosal glands located in the trachea and bronchi constitutively secrete antimicrobial molecules, such as lysozymes, lactoferrin, and defensins, that aid in clearing pathogens [4]. The non-ciliated Club cells within bronchioles secrete surfactant proteins A and D [90]. Lastly, pathogen-induced injured respiratory epithelial cells can

release DAMPs, such as high-mobility group box 1 protein and mitochondrial DNA, that serve as danger signals to activate and recruit immune cells [7].

Innate immune cells

Innate immune cells serve as a critical first-line defense in the respiratory tract. These cells include dendritic cells, natural killer cells, innate lymphoid cells, and macrophages. Collectively, these cells function to recognize pathogens or damaged host cells and activate pro-inflammatory signaling pathways that ultimately eliminate the inciting stimulus. Elaboration of pro-inflammatory cytokines from these cells shapes the microenvironment that pulmonary infectious disease occurs within – examples of how these cytokine responses can be manipulated for pathogen benefit will be discussed in Chapter 2. Only select subtypes of these inflammatory cells are described below as there are several other subpopulations whose functions are irrelevant to this dissertation, such as Langerhans dendritic cells found in the skin and group 2 innate lymphoid cells that protect against helminth parasites.

Conventional dendritic cells (DCs) are specialized, non-phagocytic cells that are the most efficient antigen-presenting cell for activating naïve $CD4^+$ and $CD8^+$ T lymphocyte cells [65]. These cells express high levels of MHCII, have numerous filopodia, and express a variety of PRRs. DCs are present in low numbers in the respiratory tract; however, their interleukin-12, tumor necrosis factor-alpha, and interleukin-6 cytokine production per cell is substantial and dramatically shapes the local inflammatory environment [18]. Upon DAMP or PAMP antigen uptake along with exposure to either endogenous (e.g., tumor necrosis factor-alpha) or exogenous (e.g., TLR ligand) co-stimuli, DCs migrate to naïve T-cells within lymph node paracortical areas to recruit T-cells to affected areas [90].

Type 1 natural killer (NK) cells and group 1 innate lymphoid cells (ICL1) belong to a heterogenous cell group known as the innate lymphoid cell family where they both serve as early defense cells that eliminate stressed cells and detect pathogens [1]. NK cells are not MHC-

restricted, which allows them to eliminate abnormal cells, such as virus-infected cells, without prior exposure to or activation by said pathogen [39]. NK cell cytotoxic mechanism of action is via perforin and granzyme B [1]. NK cells also activate macrophages and DCs via rapid interferon-gamma elaboration [62, 90]. Similar to NK cells, ILC1 monitor host cells for intracellular pathogens and produce high levels of interferon-gamma and tumor necrosis factor-alpha upon stimulation [7, 90]. Unlike NK cells, ILC1 are noncytotoxic and primarily only aid in modulating the immune response [1].

Once within the respiratory zone, alveolar macrophages play an integral role in detecting pathogens. These cells are the most abundant immune cell in the respiratory tract and phagocytose antigens opsonized by antibody, PRRs, or complement components to then present to memory T-cells for T-cell activation and expansion [39, 90]. Macrophages can be classically activated by interferon-gamma to engage in enhanced killing ability, increased MHCII expression, and secrete pro-inflammatory cytokines, such as interleukin-1beta (IL-1β), tumor necrosis factor-alpha (TNFα), and soluble interleukin-6 (sIL-6) [39, 90]. A unique feature of alveolar macrophages is that they co-express M1/M2 activation markers, which bestows a high degree of plasticity and enables them to transition between pro-inflammatory (M1) and reparative (M2) states [49]. It is important to note that alveolar macrophage activity is, in part, regulated by the surrounding surfactant and AT2 cell secretion of anti-inflammatory cytokines thereby making alveolar macrophages more tolerant to inspired air and preventing hyper-responsiveness to innocuous particulate matter [56].

Although not an innate immune surveillance cell, neutrophils are the first leukocyte to be recruited in response to infectious disease. The early preponderance of neutrophils in inflammation is attributed to their rapid response to cytokines and their firm and swift attachment to activated endothelial cells [39]. Neutrophils eliminate pathogens via the phagocytosis-phagolysosome pathway and granule elaboration into the extracellular inflammatory exudate to

enhance acute inflammatory responses [90]. Given their propensity to mitigate pathogen propagation, as with any of the aforementioned cell types, immune cell dysregulation can create an environment that ultimately favors pathogen survival.

Activation and resolution of inflammatory signaling pathways

After PAMPs or DAMPs are successfully detected, and PRRs are appropriately activated, signaling pathways are engaged to ultimately yield the production of cytokines that initiate and propagate inflammation. As it pertains to viral-bacterial pneumonia, important pro-inflammatory pathways that are activated include NOD-like receptor protein 3 (NLRP3) inflammasome, nuclear factor-kappa B (NF-kB), Janus kinase-signal transducer and activator of transcription (JAK/STAT), and prostaglandin E_2 synthesis.

IL-1β, TNFα, and sIL-6 are key cytokines elaborated from macrophages that initiate and amplify acute inflammatory responses. IL-1β is most commonly generated via the cytosolic NLRP3 inflammasome. Detection of PAMPs or DAMPs stimulates formation of the NLRP3 inflammasome, which is a complex composed of NLRP3, procaspase-1, and apoptosis associated speck-like protein [6]. This complex ultimately activates caspase-1 to cleave pro-IL-1β into its active state. Two additional potent cytokine mediators of acute inflammation are TNFα and sIL-6. TNFα and IL-6 are membrane-anchored proteins within monocytes that are cleaved by membrane proteases into their bioactive state [74]. PRR-activated pathways often converge onto the NF-kB and MAPK pathways, leading to increased transcription of TNFα and IL-6 [32, 79]. Together, IL-1β, TNFα, and IL-6 induce systemic acute phase responses, such as fever induction, acute-phase protein synthesis, and leukocyte recruitment.

Once TLRs are bound to their respective antigens, these PRRs can activate the NF-kB pathway. Several proteins are involved in pathway protein complex formations, including myeloid differentiation primary response 88 and TIR-domain-containing adapter-inducing interferon-beta,

followed by phosphorylation of interferon regulatory factor 3 or NFkB subunit 3 that ultimately regulate transcription [32, 35]. Activation of this pathway results in induction of proinflammatory cytokines and chemokines, such as TNFα and type I interferons, the upregulation of co-stimulatory molecules on DCs that are essential for T-cell activation, and adhesion molecules critical for leukocyte recruitment [35, 39]. TLRs important in detecting extracellular bacteria and intracellular viral particles include TLR1, TLR4, TLR7, TLR8, and TLR9.

JAK/STAT pathways are utilized by macrophages to generate interferon-beta (IFNβ; a type I interferon), and by NK cells and ILC1 to elaborate interferon-gamma (IFNγ; a type II interferon) [39]. Under regulation by suppressor of cytokine signaling, JAK proteins dimerize and phosphorylate STAT proteins leading to increased transcription of genes that drive inflammatory processes [90]. Type I IFN activate enzymes that degrade viral nucleic acids and inhibit viral replication, whereas type II IFN induce conventional $CD4^+$ T helper lymphocyte T_H1 and T_H17 responses. Briefly, T_H1 cell-mediated immunity results in potent macrophage activation against intracellular microbes; T_H17 cell-mediated immunity results in neutrophil and monocyte recruitment to destroy extracellular pathogens [39].

Acute inflammation can be further stimulated by arachidonic acid metabolites synthesized from the membrane phospholipids of epithelia, endothelia, platelets, and leukocytes. After these cells incur injury, membrane lipids are rapidly released and converted to create biologically active prostaglandins that exert systemic, pro-inflammatory effects. Injured epithelial cells routinely synthesize prostaglandin E_2 (PGE_2) via cyclooxygenase-2 (COX-2) for immune cell recruitment, vasodilation, and increased vascular permeability of postcapillary venules [90]. Moreover, PGE_2 has been shown to influence IL-6 production in models of human temporomandibular joint disease [36]. These collective changes modify the host state to one that is primed to respond to acute cellular damage.

As important as initiating acute inflammatory responses are, it is equally critical that such processes are appropriately downregulated after the inciting stimulus has been removed. Without such regulation, unchecked pro-inflammatory responses often lead to excessive tissue damage and hemodynamic changes that can be fatal. Active termination of acute pro-inflammatory responses includes a change in the type of arachidonic acid metabolites synthesized and the elaboration of anti-inflammatory cytokines [39].

One of the counterparts to COX-2-PGE_2 synthesis is the generation of anti-inflammatory lipid mediators, Lipoxin A_4 and B_4, via 5-lipoxygenase (5-LOX), 12-lipoxygenase (12-LOX), and 15-lipoxygenase (15-LOX) pathways. PGE_2 gradually induces phospholipids released from the cell membrane of select cells to be shunted away from COX-2 pathways and instead redirected to the LOX pathways [76]. 5-LOX within myeloid cells generate and elaborate leukotriene A_4, which is rapidly taken up by platelets and converted to Lipoxin A_4 via 12-LOX [13, 53]. A second route of endogenous lipoxin formation is via 15-LOX within epithelial cells and monocytes that generate an eicosanoid intermediate that is taken up by neutrophils and converted to Lipoxin A_4 and B_4 via 5-LOX [13, 53]. Lipoxin A_4 and B_4 function to promote homeostasis by limiting neutrophil recruitment, stimulating nonphlogistic monocyte infiltration, and activating tissue remodeling pathways [73, 76].

Canonical regulatory $CD4^+/Foxp3^+/CD25^+$ T lymphocytes (Treg) are essential for modulating acute inflammatory immune responses. Direct Treg activation can occur upon recognition of antigens displayed on MHCII molecules and co-stimulation of interleukin-2 [20]. Activated Tregs secrete the anti-inflammatory molecules interleukin-10 (IL-10), transforming growth factor-beta (TGFβ), and interleukin-35 (IL-35); IL-10 is the most important anti-inflammatory molecule of the three [84]. IL-10 inhibits phagocyte function, antigen presentation, co-stimulatory molecule expression, effector T lymphocyte proliferation, and impairs the production of IL-2 and IFNγ [70].

UPPER RESPIRATORY TRACT MICROBIOME DYSBIOSIS AS A POTENTIAL CONTRIBUTOR TO VBP

Primary bacterial pneumonia often arises when host defenses are impaired or the host is exposed to a highly virulent bacterium or a large inoculum [82]. Bacterial pneumonia has been classically categorized as community-acquired or nosocomial; nosocomial infections are further subclassified as hospital-acquired, ventilator-associated, or procedure-associated. Within the context of VBP, these exogenous sources of bacterial infection classification are still applicable. However, another category that should be considered is endogenous bacterial sources arising from upper respiratory tract microbiome dysbiosis, followed by microaspiration. The term microbiome encompasses all microbial communities and their environment, but this section will only focus on the bacterial microbiota.

Although exogenous bacterial sources can serve as the secondary bacterial infection source point for VBP, a greater emphasis has been placed on endogenous bacterial overgrowth in recent years. The upper respiratory tract mucosal surface requires a constant balance of commensals and non-invasive microbes against immune activation for harmful pathogens [26]. However, viral infections can disrupt the resident microbial compositions such that some commensal bacteria, such as *S. pneumoniae, H. influenzae*, and *Staphylococcus aureus*, engage in opportunistic overgrowth ("pathobionts") [26]. As such, it has been postulated that virus-induced upper respiratory tract microbiome dysbiosis can lead to opportunistic flora overgrowth and subsequent infection [3, 5, 48, 87]. Bacteria most often associated with secondary bacterial pneumonia in humans also diagnosed with viral pneumonia include *S. pneumoniae, H. influenzae*, *S. aureus*, and *Klebsiella pneumoniae*; all of which are members of the respiratory bacterial microbiota [3, 28]. Similar virus-microbiome associations have been postulated in veterinary production animal species diagnosed with VBP [12, 67].

GENERAL PATHOGEN-DERIVED AND HOST-DERIVED DAMAGE THAT SUPPORTS VBP DEVELOPMENT

As previously stated, the most commonly implicated bacteria in VBP are species of low virulence and are typically unable to cause significant destruction on their own. As such, the pathogenesis of VBP usually follows the general trend of virus-induced pathophysiological changes that enable a secondary, opportunistic bacterial species to colonize and infect the host respiratory tract. A major assumption in this generalized overview is that the host has an adequate innate immune response before viral infection. Biological risk factors, such as host age or sex, and co-morbidities, such as diabetes or immunocompromisation, negatively influence basal innate immune responses.

Viruses are obligate intracellular pathogens that can metabolically exhaust or lyse permissive host cells during viral replication. Damage to respiratory epithelial cells translates to loss of cilia, secreted antimicrobial peptides, mucins, and even epithelial cell death leading to surface denudation leaving an exposed basement membrane (Fig. 1A) [54]. When cilia and protective glycoproteins are lost, the mucociliary apparatus can no longer participate in effective pathogen capture and clearance [63]. Exposed extracellular matrix proteins in the denuded basement membrane provide substrates that bacteria, such as *S. pneumoniae*, *S. aureus*, and *H. influenzae*, can bind to, thereby allowing colonization with subsequent translocation into the submucosa (Fig. 1A) [8]. The reported peak susceptibility to most bacterial infections occurs days after viral infection [71].

In addition to pathogen-induced structural damage, bacterial and viral virulence factors further damage the pulmonary microenvironment and derail host immune responses. Regarding bacterial species relevant to VBP, three virulence factor categories are of note. Polysaccharide capsules suppress innate immune cell phagocytosis and reduce the efficacy of antimicrobial proteins [21]. Lipopolysaccharide released from dead Gram-negative bacteria and lipoteichoic acid released from dead Gram-positive bacteria induce pro-inflammatory immune responses that can

propagate host tissue damage [78]. Bacterial spreading factors, such as hyaluronidase, collagenase, and phospholipase, break down mucus layers, cell junctional complexes, and extracellular matrix collagen to aid in infiltrating deeper tissue layers (Fig. 1A) [90]. Viral virulence factors are less complex than bacterial virulence factors and often focus on modulating or evading host immune responses (Fig. 1B). General examples include modulating chemokine signaling networks to favor viral replication, limiting NK cell activation to shift T_H1 responses towards Treg responses, and encoding homologous proteins that dampen pro-inflammatory cytokine production [15, 54].

Lastly, as host innate immune responses are nonspecific, the elaboration of defense molecules into the extracellular space damages both invading pathogens and neighboring host cells (Fig. 1B). Neutrophil release of primary and secondary granules and neutrophil extracellular traps into the extracellular space can further impair lung function via injuring vascular endothelium, inactivating antiproteases, and enhancing cytokine expression [33, 38, 90]. Non-specific $CD8^+$ T-cells near ongoing inflammation can be activated without antigen presentation-T-cell receptor signaling to release perforins and host cell killing that exacerbates tissue damage [86, 89]. Overutilization of the NLRP3 inflammasome, NF-kB, JAK/STAT, and PGE_2 synthesis pathways can also enhance microenvironment damage. If the host can appropriately regulate pro- and anti-inflammatory responses, the contributing damage from host responses is usually minimal. However, excessive tissue damage can occur if the host response is uncontrolled.

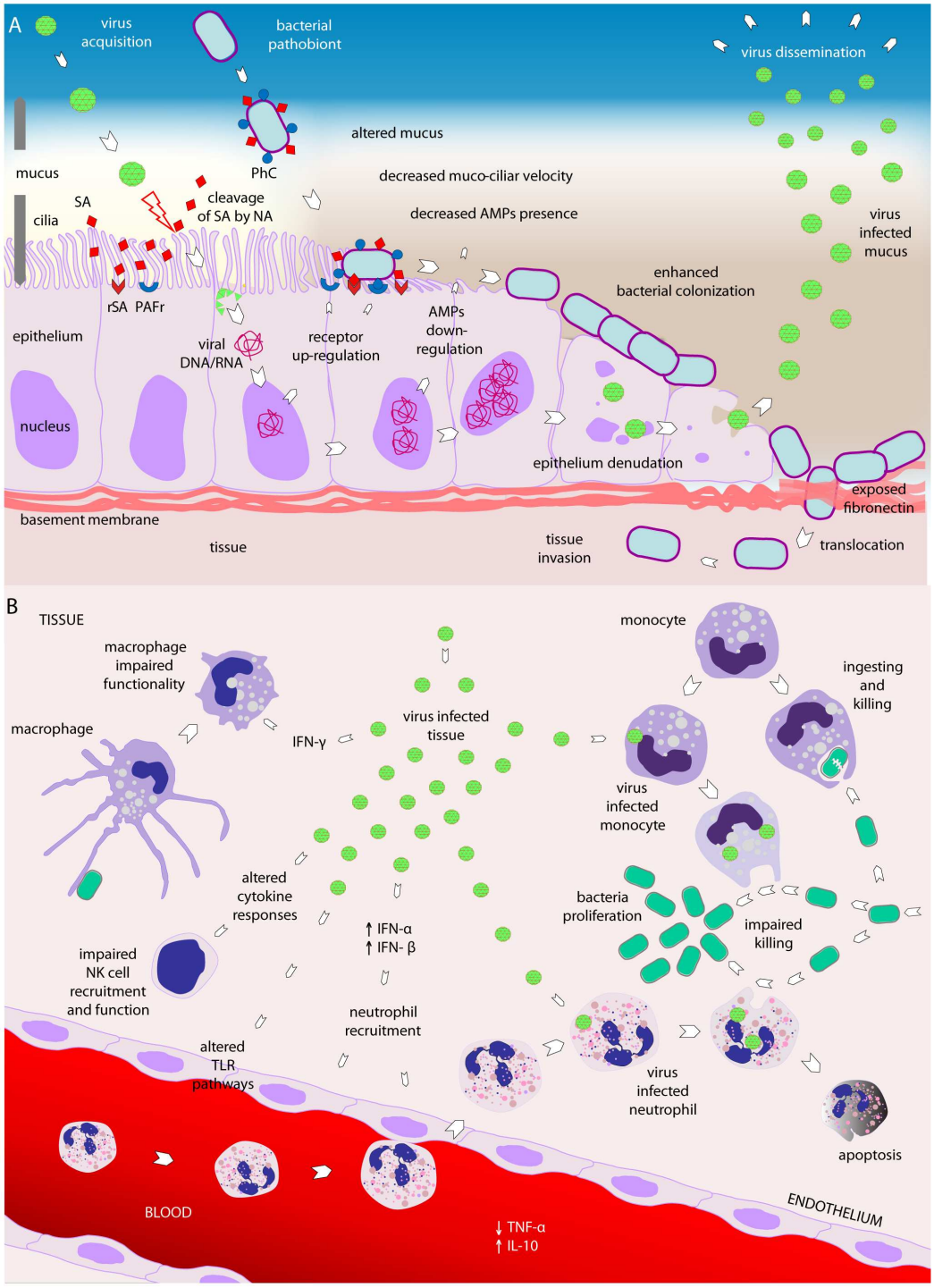

Figure 1. Respiratory viral-bacterial interactions [8].

Reprinted with permission from PLoS Pathogens. Bosch AA, Biesbroek G, Trzcinski K, Sanders EA, Bogaert D. Viral and bacterial interactions in the upper respiratory tract. *PLoS Pathog*. 2013;9:e1003057 [8].

A. Viral–bacterial interaction on the respiratory epithelial surface. Viral presence is thought to predispose the respiratory niche to bacterial colonization by different mechanisms. First, viruses may render the epithelium more susceptible to bacterial colonization by altering the mucosal

surfaces. Ciliae may be damaged, leading to decreased mucociliar function of the respiratory epithelium. Additionally, due to viral-induced damage and loss of integrity of the epithelium layer, bacterial colonization may be enhanced and translocation may be increased. Virus-infected cells may decrease the expression of antimicrobial peptides, as shown for β-defensins, thereby affecting the natural defense of the host epithelium. Influenza viral neuraminidase (NA) activity is able to cleave sialic acids residues, thereby giving access to bacterial receptors that were covered by these residues. Finally, viruses may induce bacterial colonization and replication both directly and indirectly, the latter by inducing upregulation of various receptors required for bacterial adherence, including PAFr, CAECAM-1, P5F, ICAM-1, and G-protein. PAFr, platelet activating factor receptor; ICAM-1, intracellular adhesion molecule 1; P5 fimbriae, outer membrane protein P5-homologous fimbriae; CAECAM-1, carcinoembryonic adhesion molecule-1; PhC, phosphorylcholine; SA, sialic acids; rSA, receptor for sialic acids; NA, neuraminidase; mRNA, messenger RNA, AMPs, antimicrobial peptides. **B.** Viral–bacterial interaction in relation to the host immune system. Viruses may also induce changes in immune function favorable to bacterial invasion: fewer NK cells may be recruited into the tissue and their functionality may be suboptimal as a consequence of viral infection. Virus-induced IFN-α and IFN-β may impair recruitment and functionality of neutrophils, and subsequently induce apoptosis of neutrophils recruited to combat the viral invader. Furthermore, IFN-γ seems to negatively affect the activity of macrophages. Viral-infected monocytes appear less effective in ingesting and killing bacteria, predisposing them to bacterial overgrowth and invasion. Viral infection seems to impair TLR pathways, induce production of the anti-inflammatory cytokine IL-10, and decrease the concentration of the pro-inflammatory cytokine TNF-α, generally affecting adequate immune responses to bacterial infections. Black arrows indicate increased (↑) or decreased (↓) activity or functionality of a cytokine. IFN, interferon; TNF, tumor necrosis factor; TLR, toll like receptor; IL, interleukin; NK cell, natural killer cell [8].

REFERENCES

1. Barlow JL, McKenzie ANJ. Innate Lymphoid Cells of the Lung. *Annu Rev Physiol*. 2019;81:429.
2. Bartleson JM, Radenkovic D, Covarrubias AJ, Furman D, Winer DA, *et al*. SARS-CoV-2, COVID-19 and the Ageing Immune System. *Nat Aging*. 2021;1:769.
3. Belizário J, Garay-Malpartida M, Faintuch J. Lung microbiome and origins of the respiratory diseases. *Curr Res Immunol*. 2023;4:100065.
4. Berry SB, Haack AJ, Theberge AB, Brighenti S, Svensson M. Host and Pathogen Communication in the Respiratory Tract: Mechanisms and Models of a Complex Signaling Microenvironment. *Front Med (Lausanne)*. 2020;7:537.
5. Besteman SB, Bogaert D, Bont L, et al. Interactions between respiratory syncytial virus and Streptococcus pneumoniae in the pathogenesis of childhood respiratory infections: a systematic review. *Lancet Respir Med*. 2024;12(11):915.
6. Blevins HM, Xu Y, Biby S, Zhang S. The NLRP3 Inflammasome Pathway: A Review of Mechanisms and Inhibitors for the Treatment of Inflammatory Diseases. *Front Aging Neurosci*. 2022;14:879021.
7. Borger JG, Lau M, Hibbs ML. The Influence of Innate Lymphoid Cells and Unconventional T Cells in Chronic Inflammatory Lung Disease. *Front Immunol*. 2019;10:1597.
8. Bosch AA, Biesbroek G, Trzcinski K, Sanders EA, Bogaert D. Viral and bacterial interactions in the upper respiratory tract. *PLoS Pathog*. 2013;9:e1003057.
9. Brugger SD, Bomar L, Lemon KP. Commensal-Pathogen Interactions along the Human Nasal Passages. *PLoS Pathog*. 2016;12(7):e1005633.
10. Cañadas O, Olmeda B, Alonso A, Pérez-Gil J. Lipid-Protein and Protein-Protein Interactions in the Pulmonary Surfactant System and Their Role in Lung Homeostasis. *Int J Mol Sci*. 2020;21(10):3708.
11. Cesta MF. Normal structure, function, and histology of mucosa-associated lymphoid tissue. *Toxicol Pathol*. 2006;34(5):599.
12. Chai J, Capik SF, Kegley B, Richeson JT, Powell JG, Zhao J. Bovine respiratory microbiota of feedlot cattle and its association with disease. *Vet Res*. 2022;53:4.
13. Chandrasekharan JA, Sharma-Walia N. Lipoxins: nature's way to resolve inflammation. *J Inflamm Res*. 2015;8:181.
14. Chiu L, Bazin T, Truchetet ME, Schaeverbeke T, Delhaes L, Pradeu T. Protective Microbiota: From Localized to Long-Reaching Co-Immunity. *Front Immunol*. 2017;8:1678.
15. Christiaansen A, Varga SM, Spencer JV. Viral manipulation of the host immune response. *Curr Opin Immunol*. 2015;36:54.
16. Chuaychoo B, Ngamwongwan S, Kaewnaphan B, et al. Clinical manifestations and outcomes of respiratory syncytial virus infection in adult hospitalized patients. *J Clin Virol*. 2019;117:103.
17. Cillóniz C, Ewig S, Menéndez R, et al. Bacterial co-infection with H1N1 infection in patients admitted with community acquired pneumonia. *J Infect*. 2012;65(3):223.
18. Cook PC, MacDonald AS. Dendritic cells in lung immunopathology. *Semin Immunopathol*. 2016;38(4):449.
19. Deravi N, Poudineh M, Pirzadeh M, et al. The Yin and Yang of toll-like receptors in endothelial dysfunction. *Int Immunopharmacol*. 2022;108:108768.
20. Fiyouzi T, Pelaez-Prestel HF, Reyes-Manzanas R, Lafuente EM, Reche PA. Enhancing Regulatory T Cells to Treat Inflammatory and Autoimmune Diseases. *Int J Mol Sci*. 2023;24(9):7797.
21. Gao S, Jin W, Quan Y, et al. Bacterial capsules: Occurrence, mechanism, and function. *NPJ Biofilms Microbiomes*. 2024;10(1):21.

22. Gaudino M, Nagamine B, Ducatez MF, Meyer G. Understanding the mechanisms of viral and bacterial coinfections in bovine respiratory disease: a comprehensive literature review of experimental evidence. *Vet Res*. 2022;53(1):70.
23. Gill JR, Sheng ZM, Ely SF, et al. Pulmonary pathologic findings of fatal 2009 pandemic influenza A/H1N1 viral infections. *Arch Pathol Lab Med*. 2010;134(2):235.
24. Godbole NM, Chowdhury AA, Chataut N, Awasthi S. Tight Junctions, the Epithelial Barrier, and Toll-like Receptor-4 During Lung Injury. *Inflammation*. 2022;45(6):2142.
25. Godefroy R, Giraud-Gatineau A, Jimeno MT, et al. Respiratory Syncytial Virus Infection: Its Propensity for Bacterial Coinfection and Related Mortality in Elderly Adults. *Open Forum Infect Dis*. 2020;7(12):ofaa546.
26. Hanada S, Pirzadeh M, Carver KY, Deng JC. Respiratory Viral Infection-Induced Microbiome Alterations and Secondary Bacterial Pneumonia. *Front Immunol*. 2018;9:2640.
27. Hardy BL, Merrell DS. Friend or Foe: Interbacterial Competition in the Nasal Cavity. *J Bacteriol*. 2021;203(5):e00480.
28. Hernández-Terán A, Mejía-Nepomuceno F, Herrera MT, Barreto O, García E, *et al*. Dysbiosis and structural disruption of the respiratory microbiota in COVID-19 patients with severe and fatal outcomes. *Sci Rep*. 2021;11:21297.
29. Holtkamp DJ, Kliebenstein JB, Neumann EJ, et al. Assessment of the economic impact of porcine reproductive and respiratory syndrome virus on United States pork producers. *J. Swine Heal. Prod*. 2013 (21):72.
30. Hu GN, Liu WL, Chang CH, et al. Microbial dynamics, risk factors and outcomes of secondary pneumonia in critically ill patients with COVID-19: A multicenter retrospective cohort study. *J Formos Med Assoc*. 2024;123(11):1186.
31. Hwang JY, Randall TD, Silva-Sanchez A. Inducible Bronchus-Associated Lymphoid Tissue: Taming Inflammation in the Lung. *Front Immunol*. 2016;7:258.
32. Jiang Y, Zhao T, Zhou X, Xiang Y, Gutierrez-Castrellon P, Ma X. Inflammatory pathways in COVID-19: Mechanism and therapeutic interventions. *MedComm (2020)*. 2022;3(3):e154.
33. Johansson C, Kirsebom FCM. Neutrophils in respiratory viral infections. *Mucosal Immunol*. 2021;14(4):815.
34. Kamel MS, Davidson JL, Verma MS. Strategies for Bovine Respiratory Disease (BRD) Diagnosis and Prognosis: A Comprehensive Overview. *Animals (Basel)*. 2024;14(4):627.
35. Kawai T, Akira S. Signaling to NF-kappaB by Toll-like receptors. *Trends Mol Med*. 2007;13(11):460.
36. Kawashima M, Ogura N, Akutsu M, Ito K, Kondoh T. The anti-inflammatory effect of cyclooxygenase inhibitors in fibroblast-like synoviocytes from the human temporomandibular joint results from the suppression of PGE2 production. *J Oral Pathol Med*. 2013;42(6):499.
37. Khan R, Petersen FC, Shekhar S. Commensal Bacteria: An Emerging Player in Defense Against Respiratory Pathogens. *Front Immunol*. 2019;10:1203.
38. Kumar V. Pulmonary Innate Immune Response Determines the Outcome of Inflammation During Pneumonia and Sepsis-Associated Acute Lung Injury. *Front Immunol*. 2020;11:1722.
39. Kumar V, Abbas A, Aster J. *Robbins and Cotran Pathologic Basis of Diseases*. 10th Edition, Elsevier, Amsterdam.
40. Kumpitsch C, Koskinen K, Schöpf V, Moissl-Eichinger C. The microbiome of the upper respiratory tract in health and disease. *BMC Biol*. 2019;17(1):87.
41. Langford BJ, So M, Simeonova M, Leung V, Lo J, *et al*. Antimicrobial resistance in patients with COVID-19: a systematic review and meta-analysis. *Lancet Microbe*. 2023;4:e179.

42. Lawrence P, Heung M, Nave J, Henkel C, Escudero-Pérez B. The natural virome and pandemic potential: Disease X. *Curr Opin Virol*. 2023;63:101377.
43. Lee N, Lui GC, Wong KT, et al. High morbidity and mortality in adults hospitalized for respiratory syncytial virus infections. *Clin Infect Dis*. 2013;57(8):1069.
44. Leiva-Juárez MM, Kolls JK, Evans SE. Lung epithelial cells: therapeutically inducible effectors of antimicrobial defense. *Mucosal Immunol*. 2018;11(1):21.
45. Lin HC, Liu YC, Hsing TY, et al. RSV pneumonia with or without bacterial co-infection among healthy children. *J Formos Med Assoc*. 2022;121(3):687.
46. MacCallum WG. Pathological anatomy of pneumonia associated with influenza; 23 plates. Johns Hopkins Hosp Rep. 1921;20:149.
47. MacIntyre CR, Chughtai AA, Barnes M, et al. The role of pneumonia and secondary bacterial infection in fatal and serious outcomes of pandemic influenza a(H1N1)pdm09. *BMC Infect Dis*. 2018;18(1):637.
48. Mahmud ASM, Seers CA, Shaikh AA, Taznin T, Uzzaman MS, *et al*. A multicentre study reveals dysbiosis in the microbial co-infection and antimicrobial resistance gene profile in the nasopharynx of COVID-19 patients. *Sci Rep*. 2023;13:4122.
49. Malla S, Sajeevan KA, Acharya B, Chowdhury R, Saha R. Dissecting metabolic landscape of alveolar macrophage. *Sci Rep*. 2024;14(1):30383.
50. Manohar P, Loh B, Nachimuthu R, Hua X, Welburn SC, *et al*. Secondary Bacterial Infections in Patients With Viral Pneumonia. *Front Med*. 2020;7:420.
51. Mazur NI, Caballero MT, Nunes MC. Severe respiratory syncytial virus infection in children: burden, management, and emerging therapies. *Lancet*. 2024;404(10458):1143.
52. McCray PB Jr, Pewe L, Wohlford-Lenane C, et al. Lethal infection of K18-hACE2 mice infected with severe acute respiratory syndrome coronavirus. *J Virol*. 2007;81(2):813.
53. McMahon B, Godson C. Lipoxins: endogenous regulators of inflammation. *Am J Physiol Renal Physiol*. 2004;286(2):F189.
54. Meskill SD, O'Bryant SC. Respiratory Virus Co-infection in Acute Respiratory Infections in Children. *Curr Infect Dis Rep*. 2020;22(1):3.
55. Morens DM, Taubenberger JK, Fauci AS. Predominant role of bacterial pneumonia as a cause of death in pandemic influenza: implications for pandemic influenza preparedness. *J Infect Dis*. 2008;198(7):962.
56. Morgan DJ, Casulli J, Chew C, et al. Innate Immune Cell Suppression and the Link With Secondary Lung Bacterial Pneumonia. *Front Immunol*. 2018;9:2943.
57. Morris DE, Cleary DW, Clarke SC. Secondary Bacterial Infections Associated with Influenza Pandemics. *Front Microbiol*. 2017;8:1041.
58. Murugaiah V, Tsolaki AG, Kishore U. Collectins: Innate Immune Pattern Recognition Molecules. *Adv Exp Med Biol*. 2020;1204:75.
59. Netea MG, Schlitzer A, Placek K, Joosten LAB, Schultze JL. Innate and Adaptive Immune Memory: an Evolutionary Continuum in the Host's Response to Pathogens. *Cell Host Microbe*. 2019;25(1):13.
60. Nguyen C, Kaku S, Tutera D, Kuschner WG, Barr J. Viral Respiratory Infections of Adults in the Intensive Care Unit. *J Intensive Care Med*. 2016;31(7):427.
61. Nidadavolu LS, Walston JD. Underlying Vulnerabilities to the Cytokine Storm and Adverse COVID-19 Outcomes in the Aging Immune System. *J Gerontol A Biol Sci Med Sci*. 2021;76:e13.
62. O'Sullivan TE. Dazed and Confused: NK Cells. *Front Immunol*. 2019;10:2235.
63. Oliva J, Terrier O. Viral and Bacterial Co-Infections in the Lungs: Dangerous Liaisons. *Viruses*. 2021;13(9):1725.
64. Patton MJ, Orihuela CJ, Harrod KS, et al. COVID-19 bacteremic co-infection is a major risk factor for mortality, ICU admission, and mechanical ventilation. *Crit Care*. 2023;27(1):34.

65. Peters M, Peters K, Bufe A. Regulation of lung immunity by dendritic cells: Implications for asthma, chronic obstructive pulmonary disease and infectious disease. *Innate Immun*. 2019;25(6):326.
66. Piret J, Boivin G. Pandemics Throughout History [published correction appears in Front Microbiol. 2022 Sep 27;13:988058. doi: 10.3389/fmicb.2022.988058.]. *Front Microbiol*. 2021;11:631736.
67. Pirolo M, Espinosa-Gongora C, Bogaert D, Guardabassi L. The porcine respiratory microbiome: recent insights and future challenges. *Anim Microbiome*. 2021;3:9.
68. Quinn-Bohmann N, Freixas-Coutin JA, Seo J, Simmons R, Diener C, Gibbons SM. Meta-analysis of the human upper respiratory tract microbiome reveals robust taxonomic associations with health and disease. *BMC Biol*. 2024;22(1):93.
69. Randall TD. Bronchus-associated lymphoid tissue (BALT) structure and function. *Adv Immunol*. 2010;107:187.
70. Rocamora-Reverte L, Melzer FL, Würzner R, Weinberger B. The Complex Role of Regulatory T Cells in Immunity and Aging. *Front Immunol*. 2021;11:616949.
71. Rowe HM, Meliopoulos VA, Iverson A, Bomme P, Schultz-Cherry S, Rosch JW. Direct interactions with influenza promote bacterial adherence during respiratory infections. *Nat Microbiol*. 2019;4(8):1328.
72. Salzano FA, Marino L, Salzano G, et al. Microbiota Composition and the Integration of Exogenous and Endogenous Signals in Reactive Nasal Inflammation. *J Immunol Res*. 2018;2018:2724951.
73. Sánchez-García S, Jaén RI, Fernández-Velasco M, Delgado C, Boscá L, Prieto P. Lipoxin-mediated signaling: ALX/FPR2 interaction and beyond. *Pharmacol Res*. 2023;197:106982.
74. Schumacher N, Rose-John S. ADAM17 orchestrates Interleukin-6, TNFα and EGF-R signaling in inflammation and cancer. *Biochim Biophys Acta Mol Cell Res*. 2022;1869(1):119141.
75. Sellers RS, Clifford CB, Treuting PM, Brayton C. Immunological variation between inbred laboratory mouse strains: points to consider in phenotyping genetically immunomodified mice. *Vet Pathol*. 2012;49:32.
76. Serhan CN. Pro-resolving lipid mediators are leads for resolution physiology. *Nature*. 2014;510(7503):92.
77. Shieh WJ, Blau DM, Denison AM, et al. 2009 pandemic influenza A (H1N1): pathology and pathogenesis of 100 fatal cases in the United States. *Am J Pathol*. 2010;177(1):166.
78. Szentirmai É, Massie AR, Kapás L. Lipoteichoic acid, a cell wall component of Gram-positive bacteria, induces sleep and fever and suppresses feeding. *Brain Behav Immun*. 2021;92:184.
79. Tanaka T, Narazaki M, Kishimoto T. IL-6 in inflammation, immunity, and disease. *Cold Spring Harb Perspect Biol*. 2014;6(10):a016295.
80. Taubenberger JK, Morens DM. The 1918 Influenza Pandemic and Its Legacy. *Cold Spring Harb Perspect Med*. 2020;10(10):a038695.
81. Thorburn K, Harigopal S, Reddy V, Taylor N, van Saene HK. High incidence of pulmonary bacterial co-infection in children with severe respiratory syncytial virus (RSV) bronchiolitis. *Thorax*. 2006;61(7):611.
82. Torres A, Cilloniz C, Niederman MS, et al. Pneumonia. *Nature Reviews Disease Primers*. 2021;7:25.
83. Treuting PM, Dintzis SM, Montine KS, eds. Comparative Anatomy and Histology: A Mouse, Rat, and Human Atlas. 2nd ed. Academic Press; 2018.
84. Veiga-Parga T. Regulatory T Cells and Their Role in Animal Disease. *Vet Pathol*. 2016;53(4):737.

85. Wang Y, Tang Z, Huang H, et al. Pulmonary alveolar type I cell population consists of two distinct subtypes that differ in cell fate. *Proc Natl Acad Sci U S A*. 2018;115(10):2407.
86. Whiteside SK, Snook JP, Williams MA, Weis JJ. Bystander T Cells: A Balancing Act of Friends and Foes. *Trends Immunol*. 2018;39(12):1021.
87. Xie L, Chen L, Li X, Zhou J, Tian H, *et al*. Analysis of Lung Microbiome in COVID-19 Patients during Time of Hospitalization. *Pathogens*. 2023;12:944.
88. Yoon SM, Lee J, Lee SM, Lee HY. Incidence and clinical outcomes of bacterial superinfections in critically ill patients with COVID-19. *Front Med (Lausanne)*. 2023;10:1079721.
89. Yosri M, Dokhan M, Aboagye E, Al Moussawy M, Abdelsamed HA. Mechanisms governing bystander activation of T cells. *Front Immunol*. 2024;15:1465889.
90. Zachary JF, ed. Pathologic Basis of Veterinary Disease**.** 6th ed. St Louis, MO: Elsevier; 2017.

CHAPTER 2 – LITERATURE REVIEW

PURPOSE OF THE DISSERTATION AND RESEARCH QUESTIONS

Primary viral respiratory infection with secondary bacterial pneumonia represents a respiratory disease paradigm that is reported in both humans and veterinary species [13, 20, 89]. The resultant complex lung disease complicates treatment protocol and contributes to poor patient outcomes [34]. The prevalent use of empiric antibiotics in the COVID-19 pandemic highlights the ongoing clinical concern of primary viral-secondary bacterial pneumonia [60, 107]. Despite the well-documented, clinical event of VBP, it remains understudied in pre-translational research and the continued poor outcome of patients with VBP substantiates the need for novel therapeutic approaches. To scientifically address such concerns, nonclinical animal studies can help to bridge basic science knowledge gaps and provide proof-of-concept treatment rationales. Published SARS-CoV-2 VBP small animal studies have exclusively used young, naïve, transgenic lab mice with immunological deficits [7, 110]. Not only do these studies lack translational rigor, but they also have limited practical application within veterinary medicine. Providing translational researchers with a well-designed small animal model that can be effectively interrogated for drug discovery represents a critical unmet need.

To address the identified knowledge gaps, I proposed a comprehensive plan consisting of three aims that provided a structured approach to advancing our understanding of VBP in a model species and explored effective therapeutic interventions. These aims stress host susceptibility to infection, which is a significant area of interest in the medical and research communities, and provide mechanistic insights on the basis of host-directed strategies for VBP.

The first aim was to establish a VBP small animal infection model using male Syrian hamsters, SARS-CoV-2, and a secondary bacterial species. This involved determining critical experimental variables such as the optimal time interval between viral and bacterial challenges,

the appropriate bacterial species to utilize, the dose of bacterial inoculum to administer, the route of bacterial infection that resulted in increased disease severity compared to other pilot study variable combinations, and what timepoints to assess. Additionally, this aim investigated whether the biological variable of host age (i.e., comparing 7-week-old to 39-week-old male Syrian hamsters) significantly impacted the development of VBP.

The second aim focused on integrating various analyses to characterize host responses during VBP in adult male Syrian hamsters using SARS-CoV-2 and *Haemophilus influenzae* as the tool pathogens. By examining clinical signs, relative gene expression, histopathology, and microbial titers, this aim sought to confirm that the sequence of pathogen infection affected disease outcomes (i.e., virus-only, virus followed by bacteria, bacteria-only, and bacteria followed by virus). These antemortem and postmortem analyses substantiated differential gene expression patterns in VBP, which were then targeted in the third aim.

The third aim explored the potential of modulating host response pathways using host-directed therapeutics (HDTs) as a supplemental treatment strategy for VBP. Leveraging the antemortem and postmortem analyses utilized in Aim 2, these experiments examined the effects of manipulating host-pathogen interaction pathways using PT150, meloxicam, cenerimod, baricitinib, and the combination of PT150 and meloxicam in our adult male Syrian hamster VBP model.

This innovative dissertation both expands the concept of HDTs in VBP treatment management strategies and reprioritizes current animal modeling selection criteria to develop a nonclinical model with high translational impact. A translationally relevant animal model is an essential tool in this field as it is important to have a representative infection model when the goal is to identify host targets as intervention points. More specifically, this VBP small animal infection model incorporates the biological variables of host age, immune competency, and natural pathogen susceptibility, which are integral elements needed for understanding human disease

pathogenesis. Relative gene expression patterns of this hamster model reveal mechanistic pathways that can be interrogated for druggable targets that improve VBP treatment for human and veterinary patients. In sum, this dissertation addressed two problems: to create a Syrian hamster VBP infection model that identified patterns of gene expression engaged during VBP, and to modulate these pathways with host-direct therapeutics for the purposes of pre-translational research that expedites bench-to-bedside biomedical advances.

OVERVIEW OF SELECT PATHOGENS: SARS-CoV-2 & HAEMOPHILUS INFLUENZAE

Severe acute respiratory syndrome coronavirus 2 biology and disease

Severe acute respiratory syndrome coronavirus 2 (SARS-CoV-2) is an enveloped, positive-sense, single-stranded RNA virus belonging to the *Betacoronavirus* genera in the *Coronaviridae* family [115]. This virus was first identified in China in late 2019 and, due to its high infectivity and pathogenicity, quickly became a global pandemic virus [45]. Since then, multiple mutated variants and numerous sublineages have also been documented [39, 81]. Transmission occurs primarily via person-to-person contact in the form of respiratory droplets and host age is the primary risk factor associated with developing severe COVID-19 [8]. As of March 2025, over 7 million deaths have occurred worldwide due to SARS-CoV-2 [120].

Coronavirus virions include four structural proteins: membrane (M), nucleocapsid (N), envelope (E), and spike (S). The S protein includes S1 and S2 subunits, which facilitate viral entry into host cells expressing angiotensin-converting enzyme 2 (ACE2), furin, and transmembrane protease serine 2 (TMPRSS2) [48]. The receptor binding domain of the S1 subunit binds to ACE2 on the extracellular plasma membrane surface, thereby exposing the S1/S2 furin cleavage site with subsequent cleavage by TMPRSS2 at the S2 subunit site [69]. Proteolytic cleavage of the S2 subunit site enables membrane fusion and viral entry into the host cell [92]. Cells that express TMPRSS2 and ACE2 include epithelial cells lining the respiratory tract, renal tubules, and intestines, as well as endothelium and cardiomyocytes [66]. In patients with severe COVID-19,

circulating monocytes can be permissive to infection via TLR4/7/8-induced ACE2 translocation with secondary TMPRSS2 translocation [123]. TMPRSS2/ACE2 commonly mediates viral entry in naïve hosts; however, infectious virions can also enter naïve permissive host cells via endocytosis of the virus-ACE2 complex followed by cathepsin L-mediated S2 subunit site cleavage [48].

Once inside the host cell cytoplasm, SARS-CoV-2 utilizes its RNA-dependent RNA polymerase and host ribosomes to translate viral genomic RNA into four structural proteins, two polyproteins, and eleven accessory proteins [67]. Polyproteins are subsequently cleaved into sixteen non-structural proteins (NSPs). NSPs carry out both viral replicative functions as well as host immune evasion functions; accessory proteins primarily modulate host responses [129]. Replication occurs within cytoplasmic double-membrane vesicles, which are then transferred to the endoplasmic reticulum for viral particle assembly [91]. Virions exit the infected host cell by either furin-associated Golgi apparatus exocytosis or deacidified lysosomes that fuse with the cell plasma membrane for release into the extracellular space [115].

SARS-CoV-2 induces disease in several mammalian species, including humans and Syrian hamsters, resulting in various host immunological derangements [50]. Such pathogenicity is accomplished by strategies focused on evading the host immune system, namely interfering with interferon (IFN)-JAK/STAT signaling pathways and impairing myeloid and lymphoid cellular processes [42, 95, 106]. Regarding SARS-CoV-2 infection, dysregulation of type I and III IFNs is of greatest concern. Type I IFNs (IFNα, IFNβ) activate enzymes that degrade viral nucleic acids and inhibit viral replication; IFNβ is produced by most cell types, but IFNα is predominantly produced by hematopoietic cells [128]. Type III IFN (IFNλ) induces IFN-stimulating genes that inhibit viral replication and functions at mucosal barriers localizing antiviral protection to the site of infection [71]. A brief overview of several mechanisms engaged by SARS-CoV-2 to augment the activation of innate immune responses is highlighted below.

The majority of COVID19-related host response impairment has been attributed to virus-induced interferon dysregulation (Fig. 2). Viral non-structural and accessory proteins NSP1, NSP3, NSP13, NSP14, NSP15, ORF3b, and ORF8 reduce IFN production and antagonize IFN signaling throughout the IRF3 formation pathway [106]. Moreover, ORF3c and ORF9b inhibit the adaptor protein MAVS, which is generally activated by RIG-1, to thereby block phosphorylation of IRF3 and subsequent transcription of genes encoding type I and III IFNs [70, 106]. Lastly, ORF3a, ORF6, and ORF7b antagonize IFN production throughout the JAK/STAT1 pathway [106]. Interference with IFN production ultimately disrupts the host immune system from engaging responses needed to combat early stages of viral infection, such as degrading viral RNA via ribonuclease L and inhibiting furin activity via guanylate-binding proteins [71]. These IFN alterations have been used to characterize mild versus severe COVID-19: strong type I IFN response in the early stages of infection effectively limits viral propagation, resulting in mild symptoms, whereas strong type I IFN response at later stages of infection (i.e., delayed onset seen frequently in aged individuals) results in severe symptoms [93]. Delayed type I IFN responses interfere with viral clearance and induce paradoxical hyperinflammation, thereby increasing the risk of immune dysregulation [122].

Several SARS-CoV-2 accessory and non-structural proteins disrupt myeloid and lymphoid cellular processes. ORF8 impairs MHCI molecule antigen presentation, which impedes cytotoxic T-cells from destroying SARS-CoV-2 infected cells [42]. NSP13, NSP14, and NSP16 are involved in capping viral genomic RNA to avoid host detection once in the cytoplasm and ensure ribosomal loading for transcription [74]. ORF3a and ORF7a interfere with autophagosome acidification and autolysosome formation (Fig. 2), antagonizing host cell autophagy but ensuring viral intracellular survival [132]. These alterations collectively hinder host cells' functional capability to detect this viral pathogen.

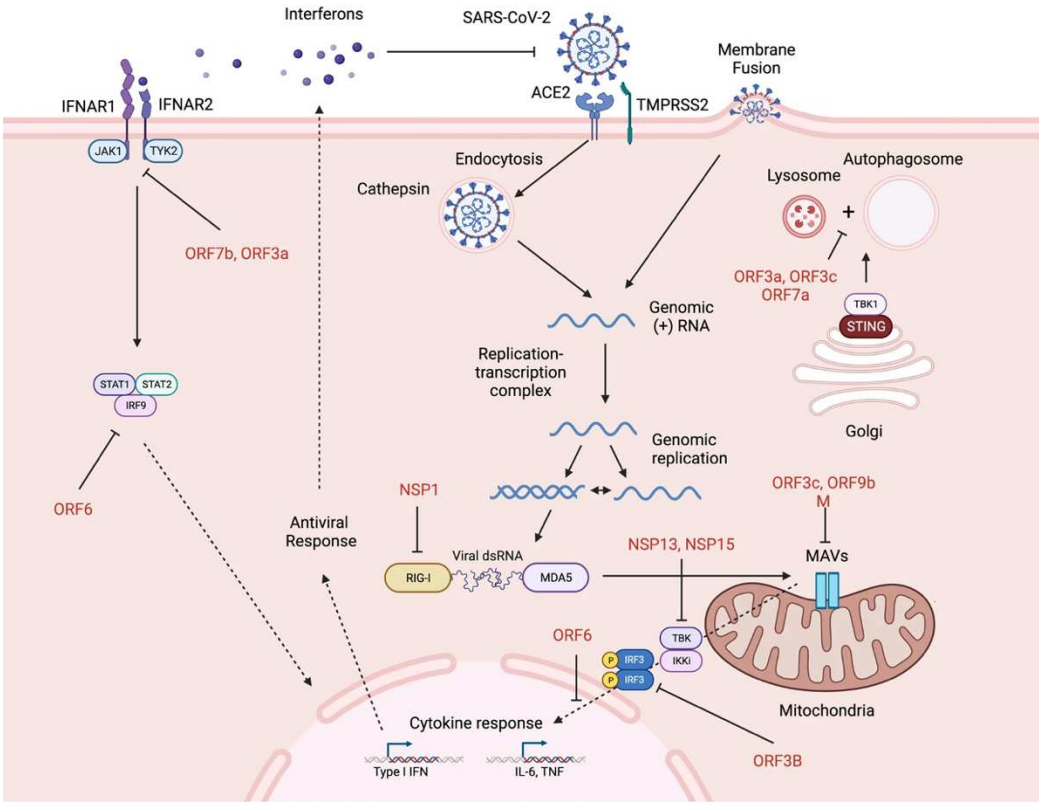

Figure 2. SARS-CoV-2 cell entry and early life cycle, innate immune pathways, and virus-encoded antagonists [106].
Reprinted with permission from Nature Cellular & Molecular Immunology. Sievers BL, Cheng MTK, Csiba K, Meng B, Gupta RK. SARS-CoV-2 and innate immunity: the good, the bad, and the "goldilocks". *Cell Mol Immunol*. 2024;21(2):171 [106].

Haemophilus influenzae biology and disease

Haemophilus influenzae is a small (0.3 – 1.0 micron), nonmotile, Gram-negative, facultatively anaerobic coccobacillus [54]. *H. influenzae* is further classified based on the antigenic structure of the capsular polysaccharide, designated ‘a’ through ‘f’; one subtype remains unencapsulated and is classified as ‘nontypeable’ (NTHi) [54, 79]. All subtypes require hemin (factor X) and nicotinamide adenine dinucleotide (factor V) for propagation, and readily grow on chocolate agar or broth culture supplemented with these factors [79]. *Haemophilus* species colonize the respiratory tract as commensal in various mammalian host species, including humans and Syrian hamsters [10, 98].

Despite being a commensal, *H. influenzae* serotype B (HiB) was historically the most clinically relevant serotype before vaccine development in the 1980s [17, 47]. At that time, HiB was the most common cause of primary bacterial meningitis in children less than two years of age [79]. Affected patients of any age could develop meningitis, bacteremia, epiglottitis, pneumonia, arthritis, or cellulitis [17]. In the post-vaccine era, NTHi is the most likely subtype to cause primary disease in humans – particularly neonates and adults older than 65 years of age – manifesting as otitis media, sinusitis, or pneumonia [17]. Interestingly, *H. influenzae* as a secondary pathogen has had a resurgence during the COVID-19 pandemic.

The transition from commensal microbiota to opportunistic pathogen likely occurs under certain environmental conditions, such as structural barrier defects or immunosuppression. Disease induced specifically by HiB is instigated through the utilization of its virulence factors: polysaccharide capsule, immunoglobulin A (IgA) protease, and lipooligosaccharide (LOS) [51, 94]. Once routine colonization is established through fimbrial adhesions and further aided by its polysaccharide capsule and biofilm formation, HiB can utilize IgA protease to inactivate host IgA1 present on nasopharyngeal mucosal surfaces [94]. LOS next assists with epithelial attachment and subsequent endothelial invasion during infection [94]. LOS is also the primary source of antigenic stimulation, which can activate the innate immune system through engagement with TLR4 to initiate pathogen elimination.

In some instances of gram-negative infections, another outcome that can result is septic shock. Lipopolysaccharide- or LOS-induced endotoxemia stimulates macrophages to overproduce IL-1 and TNFα, which induces nitric oxide production with subsequent neutrophil activation, vasodilation, and endothelial activation [59]. Moreover, these bacterial products disrupt appropriate coagulation by inhibiting tissue factor pathway inhibitor and thrombomodulin, activating clotting factors XII and XIII, and engaging the complement cascade to generate anaphylatoxins C3a and C5a [59, 128]. These endotoxin-activated pathways ultimately result in hemodynamic, leukocyte, and metabolic derangements beyond what the body can compensate

for, leading to death. Although bacterial infections are the most common cause of sepsis, it is important to note that viral infections can also lead to the development of sepsis. Usually in this scenario, a local inflammatory event progresses to systemic inflammation with a massive outpouring of cytokines and activated neutrophils producing vasodilation, vascular leakage, and venous pooling [128]. When the dysregulated inflammatory response is severe, the event is referred to as a cytokine storm. Of note, changes to the innate immune system in older COVID-19 patients, and their increased risk of developing secondary bacterial pneumonia, augment pro-inflammatory responses that can contribute to cytokine storm development [8].

OVERVIEW OF SARS-CoV-2 PNEUMONIA: IMPLICATIONS IN VBP, RISK FACTORS, AND CYTOKINE STORM

Primary SARS-CoV-2-secondary bacterial pneumonia

At the beginning of the pandemic, numerous single-center studies reported risk factors for developing severe COVID-19 with few studies acknowledging the importance of secondary bacterial infection. Since then, several meta-analysis studies have been conducted that provide a more comprehensive insight into the complex topic of VBP [46, 60, 87]. SARS-CoV-2 has disproportionately caused severe disease in select patient demographics, and chronological age is the single greatest risk factor for COVID-19 mortality [8, 19]. Other risk factors include male sex and pre-existing comorbidities, such as hypertension and type II diabetes mellitus [131]. Meta-analyses of COVID-19 patients with bacterial-associated pneumonia occur in approximately 18% of hospitalized patients [6, 60, 105]. The most common pathogens isolated from SARS-CoV-2-associated bacterial pneumonia include *S. aureus*, *S. pneumoniae*, *H. influenzae*, and *Klebsiella pneumoniae* [10, 11, 66, 96]. Moreover, patients with secondary pneumonia are more likely to be classified as severely ill and have longer hospitalization stays with worse clinical outcomes once admitted to intensive care units compared to COVID-19 only patients [26, 46, 87, 103, 125].

Several confounders can mar bacterial detection rates in VBP. There have been criticisms of a low detection rate of positive bacterial cultures in COVID-19 patients; however, this finding is complicated because if empirical antibiotic treatment was administered before obtaining culture samples, the positive detection rate for a secondary bacterial infection would inherently be lower. The gold standard for assessing bacterial pneumonia is tissue culture of an affected lung region. However, studies are often limited to using sputum, bronchiolar alveolar lavage fluid, or peripheral blood cultures to indicate a bacterial infection, thereby minimizing the true positive detection rate of VBP [26, 43, 87]. One meta-analysis specifically omitted the inclusion of secondary pulmonary infections from microorganisms considered to be either colonizers of the respiratory tract or were positive cultures detected post-mortem [22]. Lastly, incidence rates of VBP likely vary due to inconsistent definitions used in published studies, where co-infection, secondary infection, super infection, super imposed infection, community-acquired, hospital-acquired, ventilator-associated pneumonia, and post-viral bacterial pneumonia are either used interchangeably to describe the same event or are used incorrectly and therefore omit or distort the frequency of true VBP cases [125].

Immunity risk factors

Biological variable of host age

Beyond biophysical defense structures found in the mammalian respiratory tract, defense capability differences exist when assessing host biological variables. Respiratory viruses, including SARS-CoV-2, have disproportionately caused severe disease in select individuals, and disease severity has been, in part, related to age and sex [3, 31]. The altered immune function associated with aging is a complex biological process, and the most salient features of inflammaging and immunosenescence and their impact on SARS-CoV-2 pathogenesis are discussed below.

Inflammaging is characterized by low-grade, sterile, chronic inflammation in response to the accumulation of exogenous and endogenous physiological stressors that occur over time [8]. This constitutive, low-level immune activity results in elevated basal activation of innate immune cell elaboration of TNFα, IL-1β, and IL-6. Moreover, during aging, senescent epithelial and hematopoietic cells progressively lose their ability to proliferate and instead secrete senescence-associated secretory phenotype factors, such as pro-inflammatory cytokines [130]. In COVID-19 pathogenesis, the viral-induced inflammation and associated tissue damage are compounded by the aged host's basal pro-inflammatory state, leading to an exaggerated immune response with worse clinical disease.

Inflammaging is suspected to be a primary contributor to immunosenescence, which is defined as age-associated immune response changes that affect an individual's ability to respond to immunological challenges [111]. This chronic pro-inflammatory state can lead to hyporesponsive alterations, including impaired antigen presentation, decreased phagocytic function, delayed type I IFN responses, diminished $CD8^+$ T lymphocyte cell cytotoxic function, and impaired production of effective neutralizing antibodies [8]. Suboptimal antigen presentation and phagocytic function hinder the speed at which the innate immune system can be primed and activated. In the context of acute COVID-19 pathogenesis, delayed type I IFN responses hamper macrophage activation, DC antigen presentation, and effector T cell responses [8]. Adaptive immunity alterations (i.e., diminished cytotoxic T cell function and effective neutralizing antibodies) prevent the host from controlling viral infections, further allowing SARS-CoV-2 to evade the immune system. Immunosenescence-delayed responses may lead to an inappropriate inflammatory state with exaggerated tissue destruction beyond what the host can compensate for.

Biological variable of host sex

Sex (i.e., an individual's chromosome pair designation) as a biological variable impacts immune responses to infection, disease severity, and mortality (Table 1). In general, females

demonstrate more robust innate and adaptive immune responses than males, allowing for better pathogen clearance [28]. Similar to other respiratory infectious disease sex-based mortality findings, males with COVID-19 were reported to die at almost twice the rate of females with COVID-19 [28, 40]. Specific molecular mechanisms for the reported sex differences in SARS-CoV-2 related morbidity and mortality have yet to be confirmed [68, 119]; however, the following section provides a general overview of the impact of biological sex on immune cell function.

Innate immunity is the first line of immunological defense against pathogens, and macrophages and neutrophils are critical contributors to this defense. Female macrophages possess stronger activation, phagocytic capability, and IL-10 production compared to males [57]. Moreover, female antigen-presenting cells demonstrate increased presentation efficiency and TLR7 activity. These characteristics translate to faster activation of innate immune responses, especially in response to single-stranded RNA viruses such as SARS-CoV-2, and greater negative modulation after removing the inciting stimulus. Male neutrophils and macrophages express higher levels of TLR4 and produce more pro-inflammatory cytokines upon stimulation than females [28, 68]. Additionally, males have greater absolute numbers of NK cells [57]. This robust response and increased population of MHC-unrestricted cells may support an exuberant pro-inflammatory state, leading to enhanced tissue damage.

Once adaptive immunity is triggered, well-regulated adaptive responses are required to resolve inflammatory events appropriately. Females possess higher absolute and relative $CD4^+$ T lymphocyte cell numbers and higher CD4/CD8 ratios than males [57]. A higher CD4/CD8 ratio is compatible with a stronger immune system that can confer greater protection. In contrast, males have a higher percentage of $CD8^+$ T cells and are more likely to have weak T cell activation [28, 57, 68]. These findings make immunological sense as $CD4^+$ T cells activate $CD8^+$ effector T cells. Without sufficient $CD4^+$ T cells, many effector T cells remain inactive against invading pathogens, thereby prolonging infection. Finally, females have higher absolute numbers of B lymphocyte cells with greater antibody production compared to males [57]. As B cells are responsible for generating

antibodies that tag pathogens for destruction, increased amounts of antibodies can support faster pathogen clearance.

Although these immunological sex differences presumably contribute to the observed COVID-19 clinical differences between males and females, other sex distinctions may further impact disease development. Adult males have larger airway lumina than females, which increases male susceptibility to lower respiratory tract infections compared to females, who more often develop upper respiratory tract infections [28]. Males are slightly more at risk for being diagnosed with hypertension and type II diabetes mellitus, which are also risk factors for developing severe COVID-19 [24, 53]. Lastly, sociocultural risk behavior differences, such as hand-washing and delayed healthcare seeking, may also contribute to the infectious disease sex disparity [68].

Table 1. Host sex differences in innate and adaptive immune responses.

Host sex differences in innate immunity		
Immune component	**Characteristic**	**Sex difference**
Macrophages	Activation	Higher in females
	Phagocytic capacity	Higher in females
	Pro-inflammatory cytokine elaboration	Higher in males
	IL-10 production	Higher in females
	TLR4 expression	Higher in males
Neutrophils	Pro-inflammatory cytokine elaboration	Higher in males
Antigen presenting cells	APC efficiency	Greater in females
	TLR7 expression and activity	Greater in females
Natural Killer cells	Absolute NK cell numbers	Higher in males
Host sex differences in adaptive immunity		
Immune component	**Characteristic**	**Sex difference**
T lymphocytes	Absolute $CD4^+$ T cell numbers	Higher in females
	CD4/CD8 ratio	Higher in females
	Absolute $CD8^+$ T cell numbers	Higher in males
	T cell activation	Greater in females
B lymphocytes	Absolute B cell numbers	Higher in females
	Antibody production	Higher in females

IL-10: interleukin-10; TLR4: toll-like receptor 4; APC: antigen-presenting cell; TLR7: toll-like receptor 7; NK cell: Natural Killer cell.

Cytokine storm

Cytokine storm (CS) is a severe immune reaction in which the body releases too many cytokines into the blood stream too quickly [80]. CS can lead to fatal multiorgan failure by inducing inappropriate and excessive tissue infiltration of activated immune cells and hypotension with venous pooling. In the context of pulmonary disease, untreated CS leads to the development of acute respiratory distress syndrome (ARDS), a life-threatening syndrome whereby large regions of lung tissue are damaged and prevent effective gas exchange from occurring. Approximately 15% of COVID-19 patients develop CS and ARDS [76]. The most commonly implicated cytokines

in SARS-CoV-2 CS include IL-1β, IL-6, TNFα, and IL-10 [93]. As discussed in Chapter 1, IL-1β, IL-6, and TNFα induce systemic acute phase responses, such as acute-phase protein synthesis and leukocyte recruitment; IL-10 is a potent anti-inflammatory cytokine that inhibits phagocyte function and antigen presentation. Significant upregulation of numerous pro- and anti-inflammatory cytokines supports the idea that the host is in an abnormal, dysregulated state.

SARS-CoV-2 and VBP HISTOPATHOLOGY

SARS-CoV-2 histopathology in humans

Biopsy or autopsy specimens from fatal COVID-19 patients reveal that the lung is the primary organ affected by SARS-CoV-2 infection with or without changes in the heart, kidney, intestines, liver, and central nervous system (CNS). The predominant pulmonary histopathological lesion is diffuse alveolar damage (DAD) with hyaline membrane formation resulting from epithelial and endothelial injury [4]. Other pulmonary lesions include interstitial lymphocytic infiltrate, endothelialitis, microvascular injury, and hemorrhage during the acute phase of DAD; pneumocyte reactive hyperplasia with septal fibroplasia are observed in the organizing phase of DAD [4, 15]. Although lesions compatible with bacterial pneumonia were noted in a subset of patient tissues (e.g., bronchopneumonia, neutrophilic inflammation), these findings were either not further investigated or were questionably considered to be associated with DAD [12, 15]. Commonly reported lesions in other organ systems include myocarditis, renal acute tubular injury, shock lesions in the liver or intestines, and CNS lymphocytic infiltrates [15].

SARS-CoV-2 disease and histopathology in mice, ferrets, and Syrian hamsters

Wild-type C57BL/6 mice are minimally susceptible to SARS-CoV-2, which required the development of B6.Cg-Tg(K18-ACE2)2Prlmn/J transgenic mice (“K18-hACE2 mouse”) [83, 114]. By Day 7 post-viral infection (PVI) in this mouse model, viral replication is detected in alveolar type I

and II pneumocytes resulting in lethal interstitial pneumonia with mixed inflammatory cell alveolar infiltrate, variably severe pneumocyte injury and hyperplasia, and vasculitis [83]. A unique feature of this model is that they often develop fatal encephalitis; however, its pathogenesis is linked to the hACE2 expressional control of cytokeratin 18. This disease mechanism has questionable translational utility to human disease [41]. Two studies have investigated the biological variables of host age and sex in K18-hACE2. These studies found that aged, 4-month-old mice develop slightly higher mortality and viral pulmonary replication than young, 1.5-month-old mice [30]. Ondera et al. demonstrated that female mice experience less weight loss, lower lung histopathology scores, and lower viral replication than males. Given the overall lethality observed in this model, K18-hACE2 mice can be used to investigate the efficacy of COVID-19 preventative and therapeutic drugs.

A few studies have assessed SARS-CoV-2 infection in young ferrets less than one year of age. Regardless of intranasal or intratracheal virus administration, pulmonary lesions are either minimal or not associated with the viral infection [5, 23, 55]. The nasal turbinates exhibited the highest viral titers among all assessed organs and displayed the most substantial histopathological lesion, characterized by mild to moderate rhinitis [5, 23]. As such, authors have suggested that young ferrets can be used as a model for studying asymptomatic SARS-CoV-2 infections.

Syrian hamsters (“hamsters”) represent a third small animal model option that has been integral in elucidating SARS-CoV-2 pathogenesis and assessing antiviral therapeutics. Like humans, hamster nasal, bronchiolar, and alveolar epithelial cells, and alveolar macrophages are permissive to SARS-CoV-2 infection [41, 124, 126]. Hamster pulmonary pathology consists of mild, patchy DAD with interstitial and intraalveolar mixed inflammatory cell infiltrate, endothelialitis, and occasional hemorrhage [41, 124]. Infection and disease are generally limited to the respiratory tract without significant involvement in other organs. This hamster model closely mimics moderate COVID-19 disease in humans without substantial comorbidities [41].

VBP histopathology

The histopathological changes of VBP have been best documented in food animal species – namely cattle and swine. As VBP is bacterial pneumonia superimposed on active viral pneumonia, the corresponding histopathology is generally bronchopneumonia (i.e., bacterial component) superimposed on interstitial pneumonia (i.e., viral component) usually found within the cranioventral lung regions in quadruped animals. High numbers of neutrophils within alveolar spaces increases the suspicion of a bacterial component [97]. It is not uncommon for VBP bronchointerstitial pneumonia to have fibrinous pleuritis as a tertiary lesion [2]. Similar additive histopathological lesions have been observed in laboratory mouse VBP studies [7, 63]. These histopathological pattern differences help to differentiate pneumonia etiologies, as well as help to suggest when dual infections are present.

ESTABLISHED ANIMAL MODELS OF VBP WITH A FOCUS ON SARS-CoV-2

The complex respiratory microenvironment alterations of VBP are difficult to mechanistically study in humans, and therefore, rely on animal modeling. In the realm of animal modeling, researchers should strive to utilize microbes that satisfy both the ability to induce disease within an animal model as well as have translational relevance to human medicine [86]. Several study design challenges are promptly encountered when devising a small animal VBP infection model. Such foundational design parameters include animal signalment, host susceptibility to viral and bacterial agents, dose of infectious inocula to administer, time interval between pathogen exposures, route of pathogen exposure, and study timepoints to assess. Multiple small animal models of VBP have been characterized, most of which have utilized the laboratory mouse.

Of the published mouse VBP models, BALB/c and C57BL/6 substrains have commonly been used [7, 63, 64, 110]. Standard laboratory mouse strains are categorized as immunocompetent animals compared to their SCID and nude immunodeficient mouse counterparts; however, all

standard laboratory mouse strains possess inbred genetic mutations that impact their immune response. Regarding SARS-CoV-2 VBP infection models, mouse studies often use a C57BL/6 substrain [7, 110]. Any C57BL/6 substrain, including the K18-hACE2 mouse used in COVID-19 studies, demonstrates a T_H1 response bias to pathogens [99, 100]. T_H1 T cells are utilized to clear intracellular pathogens; T_H2 T cells are important in responding to extracellular pathogens [100]. The impact of this inbred biological variable is highlighted by intracellular and extracellular pathogen studies performed in BALB/c and C57BL/6 mice. Gingles et al. that found BALB/c mice, which have a T_H2 response bias, are resistant to *S. pneumoniae* serotype 2 intranasal infection, whereas C57BL/6 mice develop bacteremia with 50% mortality. Contrastingly, C57BL/6 mice are more resistant to lethal and sublethal intranasal doses of pneumonia virus of mice compared to BALB/c mice [118]. Using animals with immunodeficits skews study outcomes and interpretations when co-assessing intracellular and extracellular pathogens in the same host.

Despite the lack of translational rigor using the K18-hACE2 mouse to model SARS-CoV-2 VBP, some integral biological knowledge can still be gleaned from such studies. Firstly, Smith et al. demonstrated the importance of time interval between pathogen exposures: *S*. *pneumoniae* infections administered five or seven days PVI resulted in increased lethality, whereas there was no enhanced lethality when the bacterial infection was administered three days PVI [110]. Secondly, Barman et al. discovered that vaccination with the Pfizer mRNA COVID-19 vaccine and Prevnar13 *S*. *pneumoniae* vaccine resulted in 100% protection and no fatalities, whereas 100% of unvaccinated mice succumbed to VBP infection [7]. These studies used different serotypes of *Streptococcus pneumoniae*, serotype 2 and serotype 3; however, the C57BL/6 background T_H1 bias likely negates the importance of this distinction. In sum, conceptual premises from studies using animals with immune deficits still substantiate the key immunological insights of infection time interval and the power of adaptive immunity.

Many mouse-associated limitations for studying VBP are appreciably mitigated with outbred animals with non-biased immune systems, such as ferrets. Ferrets have been utilized to

study primary influenza A virus (H1N1pdm09)-secondary *S. pneumoniae* serotype 19F infection [73, 78]. In these studies, bacterial infections administered at either two or five days PVI resulted in a fatal outcome in up to 83% of ferrets [73, 78]; no fatalities were observed when the bacterial infection occurred 10 or 16 days PVI [73]. Although no studies have assessed SARS-CoV-2 in the context of VBP in ferrets, two studies have assessed SARS-CoV-2 age-related pathology in male and female ferrets. van de Ven et al. showed that young male ferrets less than 10 months old develop more extensive rhinitis as compared to male ferrets older than three years of age; no differences in viral titers were observed. Pulmonary histopathology was difficult to interpret in this study as young ferrets demonstrated prominent BALT hyperplasia on Day 21 PVI, but had also tested positive for systemic and enteric coronaviruses prior to SARS-CoV-2 challenge [112]. Contrastingly, compared to juvenile and young adult female ferrets, aged female ferrets older than three years developed higher viral titers and prolonged viral shedding with demonstrable pulmonary pathology (i.e., lymphocytic interstitial pneumonia) [55]. These ferret studies reinforce the importance of the time interval between viral and bacterial infections and the assessment of host age and sex as biological variables in infectious disease animal modeling.

SYRIAN HAMSTER AS AN ANIMAL MODEL FOR SARS-CoV-2 VBP

No single animal model encompasses all features of human disease, which underscores the need for multiple animal models to comprehensively study human disease in a research setting (Table 2). Syrian hamsters have emerged as a reliable small animal model for studying SARS-CoV-2 because of their natural susceptibility to this virus and increased susceptibility compared to ferrets [56, 75]. Syrian hamsters maintain genetic diversity via closed outbred colony breeding and have qualitatively similar immune responses as humans (i.e., intact, non-biased immune system) [21, 49, 72, 117]. Although increased genetic variation prevents issues such as inbred immunodeficits, genetic diversity can increase the variation of clinical responses observed in

infectious disease animal modeling studies. This issue may necessitate a larger sample size to accurately capture a desired phenotype.

Much of the published COVID-19 research using Syrian hamsters has been based on young animals, 6-12 weeks of age. These studies have established that young hamsters develop self-limiting disease, with resolution of major pathological changes by 14 days PVI [16, 41]. Of the limited COVID-19 research utilizing aged hamsters, several have shown that 8-20-month-old hamsters develop worse clinical signs with slower recovery [82, 85, 101]. Based on these studies, Syrian hamsters demonstrate age-related SARS-CoV-2 disease phenotype differences as observed in humans and can be used as a translational small animal infection model for COVID-19 research.

Studies have also assessed the biological variable of host sex in Syrian hamsters during SARS-CoV-2 infection. Male and female hamsters are equally susceptible to intranasal SARS-CoV-2 infection; however, males demonstrate more severe clinical signs and pulmonary histopathological lesions [16, 35, 127]. Similar lesion severity differences are observed on chest computed tomography [27]. Female hamster lung IgM and IgA neutralizing antibody responses are greater than those in males, supporting that female hamsters mount greater antiviral antibody responses than males during SARS-CoV-2 intranasal infection [27]. There are conflicting results on the impact of sex on viral titers, with some groups demonstrating increased viral titers in males while one group reported no difference [16, 27, 127]. Each of these groups utilized different viral titering methods (plaque assay, TCID50, reverse transcription droplet digital PCR) on different sample types (lung tissue, nasal wash), which likely further confounds this discrepancy. These studies largely underscore the importance of sex as a biological variable when utilizing Syrian hamsters in SARS-CoV-2 infection modeling.

No published studies have assessed hamster VBP infection scenarios, which is vital for understanding host molecular mechanisms for translational research purposes. Although VBP has not been assessed in Syrian hamsters, two studies have assessed bacterial pneumonia

secondary to elastase-induced emphysema in Syrian hamsters. After inducing a COPD-like pulmonary microenvironment with elastase, hamsters were intratracheally inoculated with *S. aureus* or *H. influenzae* [113, 116]. These studies determined that a bacterial infection can delay recovery or decrease survival in emphysematous hamsters. As such, these studies demonstrate that Syrian hamsters are a feasible small animal model option for studying secondary bacterial pneumonia using extracellular bacterial species.

Table 2. Summary comparison of SARS-CoV-2 and bacterial pneumonia small animal infection models in K18-hACE2 mice, ferrets, and Syrian hamsters.

	K18-hACE2 Mouse	Ferret	Syrian Hamster
SARS-CoV-2 respiratory infection			
Infection in URT	Yes	Yes	Yes
Infection in LRT	Yes	Only in adult females.	Yes
Dissemination to brain	Yes. Induces fatal encephalitis.	Transient positive titers in males.	No
Lethality	Yes	No	Not lethal in 6–12-week-old hamsters. Rarely lethal in 8–20-month-old hamsters.
Age differences	Yes. 4-month-old mice develop slightly higher mortality and viral pulmonary replication than 1.5-month-old mice.	Yes. Young males (<10 months old) and adult females (>3 years old) develop more severe respiratory tract histopathologic lesions than their adult male (>3 years old) and young female (<6 months old) counterparts.	Yes. Hamsters older than 8 months of age develop worse clinical signs with slower recovery than 6–12-week-old hamsters.
Sex differences	Yes. Females (8–10-weeks old) experience less weight loss, lower lung histopathology scores, and lower viral replication than males of the same age.		Yes. Males demonstrate more severe clinical signs and pulmonary histopathological lesions than females.
Model utility	Assess efficacy of preventative and therapeutic SARS-CoV-2 treatments.	Studying asymptomatic SARS-CoV-2 infections.	Assess efficacy of preventative and therapeutic SARS-CoV-2 treatments.
Extracellular bacteria respiratory infection			
Susceptibility	Extremely susceptible but may lack translational relevance.	Susceptible	Susceptible
Systemic dissemination	Yes	Yes	Undetermined

URT: upper respiratory tract; LRT: lower respiratory tract.

SARS-COV-2 THERAPEUTICS

FDA-approved SARS-CoV-2 therapeutics

Anti-SARS-CoV-2 drug development has focused primarily on direct acting small molecules, but other drug classes assessed include antibodies, peptide inhibitors, and

macromolecular inhibitors. Hundreds of anti-SARS-CoV-2 agents have been assessed in preclinical and clinical studies, but only a select few have received full FDA approval as of March 2025. This section will focus on the two FDA-approved virus-targeted antiviral therapeutics and the two FDA-approved immunomodulatory therapies, with an emphasis on treating severe COVID-19 disease. Therapeutics approved under emergency use authorization by the FDA are outside the scope of this dissertation.

The two FDA-approved first-line antiviral treatments, nirmatrelvir–ritonavir (Paxlovid [Pfizer]) and remdesivir (Veklury [Gilead Sciences]), both target the SARS-CoV-2 main protease, M^{pro}. Inhibition of M^{pro} prevents polyprotein cleavage, thereby blocking the maturation of key viral non-structural proteins needed for viral replication [65]. Nirmatrelvir–ritonavir is an oral medication approved for adults and children older than 12 years of age, and is particularly effective in unvaccinated, nonhospitalized, high-risk individuals [18, 36]. Among unvaccinated high-risk individuals, such as older patients or those with a cardiovascular disease comorbidity, nirmatrelvir–ritonavir reduced the risk of hospitalization or death by 88% [44]. Remdesivir is approved for adults and children of any age, but is an intravenous therapeutic that requires administration at a health care facility [18, 65]. In addition to M^{pro} inhibition, remdesivir also targets SARS-CoV-2 RNA-dependent RNA polymerase [65]. A double-blind, randomized, placebo-controlled study revealed that hospitalized COVID-19 adult patients receiving remdesivir had a shortened time to recovery as compared to individuals receiving a placebo, 10 days versus 15 days [9]. An obvious gap that remains with SARS-CoV-2 virus-targeted antiviral therapeutics is developing an oral medication that provides efficacy in standard-risk patients (i.e., vaccinated individuals without an underlying medical condition) that will decrease the duration of symptoms. Moreover, nirmatrelvir–ritonavir has been reported to have negative drug-drug interactions with a variety of medications [88]. Developing therapeutics with a wider safety profile remains a high priority.

Virus-targeted antiviral drugs have limited clinical utility in COVID-19 patients once severe disease develops because viral replication is significantly diminished at that point [108]. During this stage of disease, patients are in a hyperinflammatory state and can readily progress to acute respiratory distress and multiorgan failure. To mitigate such progression and associated tissue damage, host-directed immunomodulators can be used alone or in conjunction with remdesivir for patients hospitalized with COVID-19. Two FDA-approved immunomodulators are baricitinib (Olumiant [Eli Lilly]) and tocilizumab (Actemra [Genentech]). Impressively, a meta-analysis found that immunocompromised patients (e.g., patients with malignant neoplasia, organ transplant, auto-immune disorders) administered these immunomodulators receive a benefit of similar magnitude when compared to the general population of hospitalized COVID-19 patients [104].

Baricitinib is approved for treating severe COVID-19 in hospitalized, adult patients requiring either supplemental oxygen, mechanical ventilation, or extracorporeal membrane oxygenation [32]. It can be administered as a monotherapy or with antiviral drugs [29]. Baricitinib is an oral medication that preferentially inhibits JAK1/JAK2 to block IL-6, IL-2, and IFNγ signaling pathways [102]. Modulating the dysregulated production of pro-inflammatory cytokines can mitigate the hyperinflammatory phase during severe COVID-19. Meta-analysis revealed that baricitinib used with standard-of-care treatments resulted in a statistically significant reduction in 28-day mortality [102]. It has also been postulated that baricitinib possesses antiviral properties by inhibiting host-derived kinases, AP2-associated protein kinase-1 and cyclin G-associated kinase, which are required for viral internalization via clathrin-mediated endocytosis [52]. Baricitinib for COVID-19 treatment is contraindicated in patients with end-stage renal disease and has not been assessed in pregnant or breastfeeding patients [109].

Tocilizumab is approved for treating severe COVID-19 in hospitalized, adult patients receiving systemic corticosteroids and require either supplemental oxygen, mechanical ventilation, or extracorporeal membrane oxygenation [33]. Tocilizumab is an anti-IL-6 receptor monoclonal antibody that is intravenously administrated. Meta-analysis revealed that tocilizumab

used with standard-of-care treatment reduced mortality, need for mechanical ventilation, and length of stay in hospitalized COVID-19 patients [90]. Tocilizumab for COVID-19 treatment is contraindicated in neutropenic patients and there is insufficient data to conclude the safety profile in COVID-19 positive pregnant women [1].

One additional recommendation that has been issued for adults hospitalized with severe COVID-19 receiving supplemental oxygen or mechanical ventilation is the incorporation of dexamethasone into the treatment plan. Canonically, dexamethasone impairs T- and B-lymphocyte function [14]. Researchers recently found that dexamethasone administration in this patient population also results in immunomodulation and reversal of circulating and pulmonary monocyte dysregulation, namely via downregulation of *IL-1β* and *CCL3*, and upregulation of *IL1R2*, the decoy receptor for IL-1 [58]. Furthermore, a national US cohort study found that early administration of dexamethasone resulted in a statistically significant reduction of in-hospital mortality or discharge to hospice in this patient population [77]. It is important to note that dexamethasone administration to patients not requiring supplemental oxygen is contraindicated [25].

Considerations for including antibacterial therapies for COVID-19 patients

The administration of antibiotics to moderate to critically ill COVID-19 patients remains controversial. Up to 75% of COVID-19 patients received empiric antibiotics at the time of hospitalization [62, 107]. Antibiotics do not impede viral replication; however, this patient population is at an increased risk of developing a secondary bacterial infection. Fluoroquinolones, macrolides, β-lactam/β-lactamase inhibitors, and cephalosporins are the most empirically prescribed drug classes to COVID-19 patients [61]. The World Health Organization stated that there has been extensive antibiotic over-prescription in hospitalized COVID-19 patients during this pandemic, and they raised concerns of antimicrobial resistance (AMR) [121]. While AMR development is a legitimate concern, there has been significant methodology heterogeneity in

published studies, different AMR metrics used, and inconsistent adjustment of confounding factors [62]. As such, direct comparisons among studies assessing the impact of antibiotic use during COVID-19 remain challenging. Despite the varying conclusions of AMR development, two studies have found that multi-drug resistant organism (MDRO) secondary bacterial pneumonia manifests approximately 27 days into the hospitalization period, especially in those receiving mechanical ventilation. In contrast, non-MDRO secondary bacterial pneumonia appears approximately eight days into the hospitalization period [37, 46]. Physicians must maintain a high index of suspicion for VBP and utilize their professional discretion to empirically treat this patient population with antibiotics. However, a balance should be identified that appropriately supports antibiotic utilization for critically ill patients while observing antimicrobial stewardship practices.

CONCLUSION

Based on the review of the literature, experimental reports addressing SARS-CoV-2 with susceptibility to secondary infections are sparse, as is the assessment of host-directed therapeutics as a treatment strategy for VBP patients not on supplemental oxygen. Before starting this dissertation, no VBP Syrian hamster model existed and no immunomodulatory drug investigative studies in murine VBP SARS-CoV-2 infections had been assessed. This dissertation is an opportunity to characterize how biological variables of immune competency and host age impact nonclinical VBP animal modeling in an unvaccinated host. Furthermore, we assessed the effects of both antiviral and immunomodulatory host-directed therapeutics to determine if hosts could overcome secondary bacterial infections without the need for antibiotics. This dissertation contributes basic science information that advances biomedical research to establish more efficacious therapeutic standards of care in humans and veterinary species diagnosed with VBP.

REFERENCES

1. Actemra. Important Safety Information & Indications. https://www.actemrahcp.com/coronavirus/safety.html. Accessed 3 March 2025.
2. Arenales A, Santana CH, Rolim ACR, Pereira EMMS, Nascimento EF, et al. Histopathologic patterns and etiologic diagnosis of porcine respiratory disease complex in Brazil. *Arq Bras Med Vet Zootec*. 2022;74(3):497.
3. Arnold CG, Libby A, Vest A, Hopkinson A, Monte AA. Immune mechanisms associated with sex-based differences in severe COVID-19 clinical outcomes. *Biol Sex Differ*. 2022;13(1):7.
4. Arrossi AV,Farver C. The pulmonary pathology of COVID-19. *Cleve Clin J Med*. Published online September 23, 2020.
5. Au GG, Marsh GA, McAuley AJ, et al. Characterisation and natural progression of SARS-CoV-2 infection in ferrets. *Sci Rep*. 2022;12(1):5680.
6. Baghdadi JD, Coffey KC, Adediran T, et al. Antibiotic Use and Bacterial Infection among Inpatients in the First Wave of COVID-19: a Retrospective Cohort Study of 64,691 Patients. *Antimicrob Agents Chemother*. 2021;65(11):e0134121.
7. Barman TK, Singh AK, Bonin JL, Nafiz TN, Salmon SL, Metzger DW. Lethal synergy between SARS-CoV-2 and Streptococcus pneumoniae in hACE2 mice and protective efficacy of vaccination. *JCI Insight*. 2022;7(11):e159422.
8. Bartleson JM, Radenkovic D, Covarrubias AJ, Furman D, Winer DA, *et al*. SARS-CoV-2, COVID-19 and the Ageing Immune System. *Nat Aging*. 2021;1:769.
9. Beigel JH, Tomashek KM, Dodd LE, et al. Remdesivir for the Treatment of Covid-19 - Final Report. *N Engl J Med*. 2020;383(19):1813.
10. Belizário J, Garay-Malpartida M, Faintuch J. Lung microbiome and origins of the respiratory diseases. *Curr Res Immunol*. 2023;4:100065.
11. Bogdan I, Gadela T, Bratosin F, et al. The Assessment of Multiplex PCR in Identifying Bacterial Infections in Patients Hospitalized with SARS-CoV-2 Infection: A Systematic Review. *Antibiotics (Basel)*. 2023;12(3):465.
12. Borczuk AC, Salvatore SP, Seshan SV, et al. COVID-19 pulmonary pathology: a multi-institutional autopsy cohort from Italy and New York City. *Mod Pathol*. 2020;33(11):2156.
13. Bosch AA, Biesbroek G, Trzcinski K, Sanders EA, Bogaert D. Viral and bacterial interactions in the upper respiratory tract. *PLoS Pathog*. 2013;9:e1003057.
14. Cain DW, Cidlowski JA. After 62 years of regulating immunity, dexamethasone meets COVID-19. *Nat Rev Immunol*. 2020;20(10):587.
15. Caramaschi S, Kapp ME, Miller SE, et al. Histopathological findings and clinicopathologic correlation in COVID-19: a systematic review. *Mod Pathol*. 2021;34(9):1614.
16. Castellan M, Zamperin G, Franzoni G, Foiani G, Zorzan M, *et al*. Host Response of Syrian Hamster to SARS-CoV-2 Infection including Differences with Humans and between Sexes. *Viruses*. 2023;15:428.
17. Centers for Disease Control and Prevention. Epidemiology and Prevention of Vaccine-Preventable Diseases. Hall E., Wodi A.P., Hamborsky J., et al., eds. 14th ed. Washington, D.C. Public Health Foundation, 2021.
18. Centers for Disease Control and Prevention. Types of COVID-19 Treatment. https://www.cdc.gov/covid/treatment/index.html. Accessed 3 March 2025.
19. Centers for Disease Control and Prevention. Underlying Conditions and the Higher Risk for Severe COVID-19. https://www.cdc.gov/covid/hcp/clinical-care/underlying-conditions.html. Accessed 6 March 2025.
20. Chai J, Capik SF, Kegley B, Richeson JT, Powell JG, Zhao J. Bovine respiratory microbiota of feedlot cattle and its association with disease. *Vet Res*. 2022;53:4.

21. Charles River Laboratories. LVG Golden Syrian Hamster, https://www.criver.com/products-services/find-model/lvg-golden-syrian-hamster?region=3611. Accessed 25 March 2024.
22. Chong WH, Saha BK, Ananthakrishnan Ramani, Chopra A. State-of-the-art review of secondary pulmonary infections in patients with COVID-19 pneumonia. *Infection*. 2021;49(4):591.
23. Ciurkiewicz M, Armando F, Schreiner T, et al. Ferrets are valuable models for SARS-CoV-2 research. *Vet Pathol*. 2022;59(4):661.
24. Connelly PJ, Currie G, Delles C. Sex Differences in the Prevalence, Outcomes and Management of Hypertension. *Curr Hypertens Rep*. 2022;24(6):185.
25. Crothers K, DeFaccio R, Tate J, et al. Dexamethasone in hospitalised COVID-19 patients not on intensive respiratory support. *Eur Respir J*. 2022;60(1):2102532.
26. De Francesco MA, Signorini L, Piva S, et al. Bacterial and fungal superinfections are detected at higher frequency in critically ill patients affected by SARS CoV-2 infection than negative patients and are associated to a worse outcome. *J Med Virol*. 2023;95(7):e28892.
27. Dhakal S, Ruiz-Bedoya CA, Zhou R, et al. Sex Differences in Lung Imaging and SARS-CoV-2 Antibody Responses in a COVID-19 Golden Syrian Hamster Model. *mBio*. 2021;12(4):e0097421.
28. Dias SP, Brouwer MC, van de Beek D. Sex and Gender Differences in Bacterial Infections. *Infect Immun*. 2022;90(10):e0028322.
29. Dupuis D, Fritz K, Ike E, et al. Current Use of Baricitinib in COVID-19 Treatment and Its Future: An Updated Literature Review. *Cureus*. 2022;14(9):e28680.
30. Dwivedi V, Shivanna V, Gautam S, et al. Age associated susceptibility to SARS-CoV-2 infection in the K18-hACE2 transgenic mouse model. *Geroscience*. 2024;46(3):2901.
31. Farshbafnadi M, Kamali Zonouzi S, Sabahi M, Dolatshahi M, Aarabi MH. Aging & COVID-19 susceptibility, disease severity, and clinical outcomes: The role of entangled risk factors. *Exp Gerontol*. 2021;154:111507.
32. FDA US Food & Drug Administration. Frequently Asked Questions on Olumiant (Baricitinib) for the Treatment of COVID-19. Published 10 May 2022. https://www.google.com/url?sa=t&source=web&rct=j&opi=89978449&url=https://www.fda.gov/media/143825/download&ved=2ahUKEwjh_a6wx-6LAxXdNzQIHXnvAD8QFnoECBUQAw&usg=AOvVaw3hBDaIblZ_CdqR7xzOC0s6. Accessed 25 March 2025.
33. FDA US Food & Drug Administration. Frequently Asked Questions on the Emergency Use Authorization for Actemra (Tocilizumab) for Treatment of COVID-19. Published 21 December 2022. https://www.google.com/url?sa=t&source=web&rct=j&opi=89978449&url=https://www.fda.gov/media/150345/download&ved=2ahUKEwi0v4La0e6LAxUNDzQIHT7IAeYQFnoECBUQAw&usg=AOvVaw2RixPQ9M9pNFWozNqV77Bl. Accessed 25 March 2025.
34. Feldman C, Anderson R. The role of co-infections and secondary infections in patients with COVID-19. *Pneumonia (Nathan)*. 2021;13(1):5.
35. Foiani G, Castellan M, Leopardi S, de Benedictis P, Monetti G, Vascellari M. Sex differences and histopathological patterns of lung damage in Syrian hamsters induced by SARS-CoV-2 experimental infection. *J Comp Pathol*. 2023;203:46.
36. Gandhi RT, Hirsch M. Treating Acute Covid-19 - Final Chapters Still Unwritten. *N Engl J Med*. 2024;390(13):1234.
37. Garcia-Vidal C, Sanjuan G, Moreno-García E, et al. Incidence of co-infections and superinfections in hospitalized patients with COVID-19: a retrospective cohort study. *Clin Microbiol Infect*. 2021;27(1):83.

38. Gingles NA, Alexander JE, Kadioglu A, et al. Role of genetic resistance in invasive pneumococcal infection: identification and study of susceptibility and resistance in inbred mouse strains. *Infect Immun*. 2001;69(1):426.
39. GISAID. Tracking of hCoV-19 Variants. https://gisaid.org/hcov19-variants/. Accessed 26 March 2025.
40. Green MS, Nitzan D, Schwartz N, Niv Y, Peer V. Sex differences in the case-fatality rates for COVID-19-A comparison of the age-related differences and consistency over seven countries. *PLoS One*. 2021;16(4):e0250523.
41. Gruber AD, Firsching TC, Trimpert J, Dietert K. Hamster models of COVID-19 pneumonia reviewed: How human can they be?. *Vet Pathol*. 2022;59:528.
42. Gu W, Gan H, Ma Y, et al. The molecular mechanism of SARS-CoV-2 evading host antiviral innate immunity. *Virol J*. 2022;19(1):49.
43. Guisado-Gil AB, Infante-Domínguez C, Peñalva G, et al. Impact of the COVID-19 Pandemic on Antimicrobial Consumption and Hospital-Acquired Candidemia and Multidrug-Resistant Bloodstream Infections. *Antibiotics (Basel)*. 2020;9(11):816.
44. Hammond J, Leister-Tebbe H, Gardner A, et al. Oral Nirmatrelvir for High-Risk, Nonhospitalized Adults with Covid-19. *N Engl J Med*. 2022;386(15):1397-1408.
45. Hao YJ, Wang YL, Wang MY, et al. The origins of COVID-19 pandemic: A brief overview. *Transbound Emerg Dis*. 2022;69(6):3181.
46. Hu GN, Liu WL, Chang CH, et al. Microbial dynamics, risk factors and outcomes of secondary pneumonia in critically ill patients with COVID-19: A multicenter retrospective cohort study. *J Formos Med Assoc*. 2024;123(11):1186.
47. Institute of Medicine (US) Vaccine Safety Committee; Stratton KR, Howe CJ, Johnston RB Jr., editors. Adverse Events Associated with Childhood Vaccines: Evidence Bearing on Causality. Washington (DC): National Academies Press (US); 1994. 9, Haemophilus influenzae Type b Vaccines. https://www.ncbi.nlm.nih.gov/books/NBK236299/. Accessed 13 March 2025.
48. Jackson CB, Farzan M, Chen B, Choe H. Mechanisms of SARS-CoV-2 entry into cells. *Nat Rev Mol Cell Biol*. 2022;23(1):3.
49. Jia Y, Wang Y, Dunmall LSC, Lemoine NR, Wang P, *et al*. Syrian hamster as an ideal animal model for evaluation of cancer immunotherapy. *Front Immunol*. 2023;14:1126969.
50. Johansen MD, Irving A, Montagutelli X, et al. Animal and translational models of SARS-CoV-2 infection and COVID-19. *Mucosal Immunol*. 2020;13(6):877.
51. Johnston JW, Apicella MA. (2009). Haemophilus influenzae. In *Encyclopedia of Microbiology* (pp. 153–162). Academic Press.
52. Jorgensen SCJ, Tse CLY, Burry L, Dresser LD. Baricitinib: A Review of Pharmacology, Safety, and Emerging Clinical Experience in COVID-19. *Pharmacotherapy*. 2020;40(8):843.
53. Kautzky-Willer A, Leutner M, Harreiter J. Sex differences in type 2 diabetes [published correction appears in Diabetologia. 2023 Jun;66(6):1165.]. *Diabetologia*. 2023;66(6):986.
54. Khattak ZE, Anjum F. Haemophilus influenzae Infection. [Updated 2023 Apr 27]. In: StatPearls [Internet]. Treasure Island (FL): StatPearls Publishing; 2024 Jan-. Available from: https://www.ncbi.nlm.nih.gov/books/NBK562176/
55. Kim YI, Yu KM, Koh JY, et al. Age-dependent pathogenic characteristics of SARS-CoV-2 infection in ferrets. *Nat Commun*. 2022;13(1):21.
56. Kinoshita T, Watanabe K, Sakurai Y, Nishi K, Yoshikawa R, Yasuda J. Co-infection of SARS-CoV-2 and influenza virus causes more severe and prolonged pneumonia in hamsters. *Sci Rep*. 2021;11(1):21259.
57. Klein SL, Flanagan KL. Sex differences in immune responses. *Nat Rev Immunol*. 2016;16(10):626.

58. Knoll R, Helbig ET, Dahm K, et al. The life-saving benefit of dexamethasone in severe COVID-19 is linked to a reversal of monocyte dysregulation. *Cell*. 2024;187(16):4318.
59. Kumar V, Abbas A, Aster J. (2020) Robbins and Cotran Pathologic Basis of Diseases. 10th Edition, Elsevier, Amsterdam.
60. Langford BJ, So M, Raybardhan S, et al. Bacterial co-infection and secondary infection in patients with COVID-19: a living rapid review and meta-analysis. *Clin Microbiol Infect*. 2020;26(12):1622.
61. Langford BJ, So M, Raybardhan S, et al. Antibiotic prescribing in patients with COVID-19: rapid review and meta-analysis. *Clin Microbiol Infect*. 2021;27(4):520.
62. Langford BJ, So M, Simeonova M, Leung V, Lo J, *et al*. Antimicrobial resistance in patients with COVID-19: a systematic review and meta-analysis. *Lancet Microbe*. 2023;4:e179.
63. Lee LN, Dias P, Han D, et al. A mouse model of lethal synergism between influenza virus and Haemophilus influenzae. *Am J Pathol*. 2010;176(2):800.
64. Lee MH, et al. A postinfluenza model of Staphylococcus aureus pneumonia. *J Infect Dis*. 2010;201(4):508.
65. Li G, Hilgenfeld R, Whitley R, De Clercq E. Therapeutic strategies for COVID-19: progress and lessons learned. *Nat Rev Drug Discov*. 2023;22(6):449.
66. Liu J, Li Y, Liu Q, et al. SARS-CoV-2 cell tropism and multiorgan infection. *Cell Discov*. 2021;7(1):17.
67. López-Ayllón BD, de Lucas-Rius A, Mendoza-García L, et al. SARS-CoV-2 accessory proteins involvement in inflammatory and profibrotic processes through IL11 signaling. *Front Immunol*. 2023;14:1220306.
68. Lott N, Gebhard CE, Bengs S, et al. Sex hormones in SARS-CoV-2 susceptibility: key players or confounders?. *Nat Rev Endocrinol*. 2023;19(4):217.
69. Lu Y, Zhu Q, Fox DM, Gao C, Stanley SA, Luo K. SARS-CoV-2 down-regulates ACE2 through lysosomal degradation. *Mol Biol Cell*. 2022;33(14):ar147.
70. Maison DP, Deng Y, Gerschenson M. SARS-CoV-2 and the host-immune response. *Front Immunol*. 2023;14:1195871.
71. Mertowska P, Smolak K, Mertowski S, Grywalska E. Immunomodulatory Role of Interferons in Viral and Bacterial Infections. *Int J Mol Sci*. 2023;24(12):10115.
72. Miao J, Chard LS, Wang Z, Wang Y. Syrian Hamster as an Animal Model for the Study on Infectious Diseases. *Front Immunol*. 2019;10:2329.
73. Mifsud EJ, Farrukee R, Hurt AC, Reading PC, Barr IG. Infection with different human influenza A subtypes affects the period of susceptibility to secondary bacterial infections in ferrets. *FEMS Microbes*. 2022;3:xtac011.
74. Minkoff JM, tenOever B. Innate immune evasion strategies of SARS-CoV-2. *Nat Rev Microbiol*. 2023;21(3):178.
75. Monchatre-Leroy E, Lesellier S, Wasniewski M, et al. Hamster and ferret experimental infection with intranasal low dose of a single strain of SARS-CoV-2. *J Gen Virol*. 2021;102(3):001567.
76. Montazersaheb S, Hosseiniyan Khatibi SM, Hejazi MS, et al. COVID-19 infection: an overview on cytokine storm and related interventions. *Virol J*. 2022;19(1):92.
77. Mourad A, Thibault D, Holland TL, et al. Dexamethasone for Inpatients With COVID-19 in a National Cohort. *JAMA Netw Open*. 2023;6(4):e238516.
78. Mueller Brown K, Le Sage V, French AJ, et al. Secondary infection with *Streptococcus pneumoniae* decreases influenza virus replication and is linked to severe disease. *FEMS Microbes*. 2022;3:xtac007.
79. Musher DM. Haemophilus Species. In: Baron S, editor. Medical Microbiology. 4th edition. Galveston (TX): University of Texas Medical Branch at Galveston; 1996. Chapter 30. https://www.ncbi.nlm.nih.gov/books/NBK8458/. Accessed 16 March 2025.

80. National Institutes of Health. National Cancer Institute Dictionary of Cancer Terms. https://www.cancer.gov/publications/dictionaries/cancer-terms/def/cytokine-storm. Accessed 8 March 2025.
81. Nextstrain. Genomic epidemiology of SARS-CoV-2 with subsampling focused globally since pandemic start. https://nextstrain.org/ncov/gisaid/global/all-time. Accessed 26 March 2025.
82. Oishi K, Horiuchi S, Frere J, Schwartz RE, tenOever BR. A diminished immune response underlies age-related SARS-CoV-2 pathologies. *Cell Rep*. 2022;39:111002.
83. Oladunni FS, Park JG, Pino PA, et al. Lethality of SARS-CoV-2 infection in K18 human angiotensin-converting enzyme 2 transgenic mice. *Nat Commun*. 2020;11(1):6122.
84. Onodera Y, Liang J, Li Y, et al. Inhalation of ACE2 as a therapeutic target on sex-bias differences in SARS-CoV-2 infection and variant of concern. *iScience*. 2023;26(8):107470.
85. Osterrieder N, Bertzbach LD, Dietert K, Abdelgawad A, Vladimirova D, *et al*. Age-Dependent Progression of SARS-CoV-2 Infection in Syrian Hamsters. *Viruses*. 2020;12:779.
86. Osuchowski MF, Ayala A, Bahrami S, Bauer M, Boros M, *et al*. Minimum Quality Threshold in Pre-Clinical Sepsis Studies (MQTiPSS): An International Expert Consensus Initiative for Improvement of Animal Modeling in Sepsis. *Shock*. 2018;50:377.
87. Patton MJ, Orihuela CJ, Harrod KS, et al. COVID-19 bacteremic co-infection is a major risk factor for mortality, ICU admission, and mechanical ventilation. *Crit Care*. 2023;27(1):34.
88. Paxlovid. Drug interactions. https://www.paxlovidhcp.com/drug-interactions. Accessed 3 March 2025.
89. Pirolo M, Espinosa-Gongora C, Bogaert D, Guardabassi L. The porcine respiratory microbiome: recent insights and future challenges. *Anim Microbiome*. 2021;3:9.
90. Piscoya A, Parra Del Riego A, Cerna-Viacava R, et al. Efficacy and harms of tocilizumab for the treatment of COVID-19 patients: A systematic review and meta-analysis. *PLoS One*. 2022;17(6):e0269368.
91. Pizzato M, Baraldi, Sopetto GB, Finozzi D, Gentile C, et al. SARS-CoV-2 and the Host Cell: A Tale of Interactions. Front. Virol. 2022;11(1):815388.
92. Qiao Y, Wang XM, Mannan R, et al. Targeting transcriptional regulation of SARS-CoV-2 entry factors ACE2 and TMPRSS2. *Proc Natl Acad Sci USA*. 2021;118(1):e2021450118.
93. Ramasamy S, Subbian S. Critical Determinants of Cytokine Storm and Type I Interferon Response in COVID-19 Pathogenesis [published correction appears in Clin Microbiol Rev. 2021 Dec 15;34(4):e0016321]. *Clin Microbiol Rev*. 2021;34(3):e00299.
94. Retchless AC, Topaz N, Marjuki H et al. (2024). Haemophilus influenzae. In *Molecular Medical Microbiology, Third Edition* (pp. 1399-1421). Academic Press.
95. Rubio-Casillas A, Redwan EM, Uversky VN. SARS-CoV-2: A Master of Immune Evasion. *Biomedicines*. 2022;10(6):1339.
96. Russell CD, Fairfield CJ, Drake TM, et al. Co-infections, secondary infections, and antimicrobial use in patients hospitalised with COVID-19 during the first pandemic wave from the ISARIC WHO CCP-UK study: a multicentre, prospective cohort study. *Lancet Microbe*. 2021;2(8):e354.
97. Sarli G, D'Annunzio G, Gobbo F, Benazzi C, Ostanello F. The Role of Pathology in the Diagnosis of Swine Respiratory Disease. *Vet Sci*. 2021;8(11):256.
98. Seibert B, Cáceres CJ, Carnaccini S, Cardenas-Garcia S, Gay LC, *et al*. Pathobiology and dysbiosis of the respiratory and intestinal microbiota in 14 months old Golden Syrian hamsters infected with SARS-CoV-2. *PLoS Pathog*. 2022;18:e1010734.
99. Sellers RS. Translating Mouse Models. *Toxicol Pathol*. 2017;45:134.

100. Sellers RS, Clifford CB, Treuting PM, Brayton C. Immunological variation between inbred laboratory mouse strains: points to consider in phenotyping genetically immunomodified mice. *Vet Pathol*. 2012;49:32.
101. Selvaraj P, Lien CZ, Liu S, Stauft CB, Nunez IA, *et al*. SARS-CoV-2 infection induces protective immunity and limits transmission in Syrian hamsters. *Life Sci Alliance*. 2021;4:e202000886.
102. Selvaraj V, Finn A, Lal A, Khan MS, Dapaah-Afriyie K, Carino GP. Baricitinib in hospitalised patients with COVID-19: A meta-analysis of randomised controlled trials. *EClinicalMedicine*. 2022;49:101489.
103. Shafran N, Shafran I, Ben-Zvi H, et al. Secondary bacterial infection in COVID-19 patients is a stronger predictor for death compared to influenza patients. *Sci Rep*. 2021;11(1):12703.
104. Siempos II, Kalil AC, Belhadi D, et al. Immunomodulators for immunocompromised patients hospitalized for COVID-19: a meta-analysis of randomized controlled trials. *EClinicalMedicine*. 2024;69:102472.
105. Sieswerda E, de Boer MGJ, Bonten MMJ, et al. Recommendations for antibacterial therapy in adults with COVID-19 - an evidence based guideline. *Clin Microbiol Infect*. 2021;27(1):61.
106. Sievers BL, Cheng MTK, Csiba K, Meng B, Gupta RK. SARS-CoV-2 and innate immunity: the good, the bad, and the "goldilocks". *Cell Mol Immunol*. 2024;21(2):171.
107. Sili U, Tekin A, Bilgin H, Khan SA, Domecq JP, *et al*. Early empiric antibiotic use in COVID-19 patients: results from the international VIRUS registry. *Int J Infect Dis*. 2024;140:39.
108. Singh M, de Wit E. Antiviral agents for the treatment of COVID-19: Progress and challenges. *Cell Rep Med*. 2022;3(3):100549.
109. Sinha A, Deshwal H, Vashisht R. Safe and Effective Use of Baricitinib and Remdesivir in Hospitalized Patients With Coronavirus (COVID-19) [Updated 2023 Mar 6]. In: StatPearls [Internet]. Treasure Island (FL): StatPearls Publishing; 2025 Jan-. https://www.ncbi.nlm.nih.gov/books/NBK589640/. Accessed 10 March 2025.
110. Smith AP, Williams EP, Plunkett TR, et al. Time-Dependent Increase in Susceptibility and Severity of Secondary Bacterial Infections During SARS-CoV-2. *Front Immunol*. 2022;13:894534.
111. Tizazu AM, Mengist HM, Demeke G. Aging, inflammaging and immunosenescence as risk factors of severe COVID-19. *Immun Ageing*. 2022;19(1):53.
112. van de Ven K, van Dijken H, Wijsman L, et al. Pathology and Immunity After SARS-CoV-2 Infection in Male Ferrets Is Affected by Age and Inoculation Route. *Front Immunol*. 2021;12:750229.
113. Verghese A, Catanese A, Arbeit RD. Staphylococcus aureus pneumonia in hamsters with elastase-induced emphysema--the virulence enhancing activity of mucin. *Proc Soc Exp Biol Med*. 1988;188(1):1.
114. Vidal E, López-Figueroa C, Rodon J, et al. Chronological brain lesions after SARS-CoV-2 infection in hACE2-transgenic mice. *Vet Pathol*. 2022;59(4):613.
115. V'kovski P, Kratzel A, Steiner S, Stalder H, Thiel V. Coronavirus biology and replication: implications for SARS-CoV-2. *Nat Rev Microbiol*. 2021;19(3):155.
116. Wang D, Wang Y, Liu YN. Experimental pulmonary infection and colonization of Haemophilus influenzae in emphysematous hamsters. *Pulm Pharmacol Ther*. 2010;23(4):292.
117. Warner BM, Safronetz D, Kobinger GP. Syrian Hamsters as a Small Animal Model for Emerging Infectious Diseases: Advances in Immunologic Methods. *Adv Exp Med Biol*. 2017;972:87.

118. Watkiss ER, Shrivastava P, Arsic N, Gomis S, van Drunen Littel-van den Hurk S. Innate and adaptive immune response to pneumonia virus of mice in a resistant and a susceptible mouse strain. *Viruses*. 2013;5(1):295.
119. Wilkinson NM, Chen HC, Lechner MG, Su MA. Sex Differences in Immunity. *Annu Rev Immunol*. 2022;40:75.
120. World Health Organization. Coronavirus disease (COVID-19) pandemic. https://www.who.int/emergencies/diseases/novel-coronavirus-2019 (2025). Accessed 05 March 2025.
121. World Health Organization. WHO reports widespread overuse of antibiotics in patients hospitalized with COVID-19. https://www.who.int/news/item/26-04-2024-who-reports-widespread-overuse-of-antibiotics-in-patients--hospitalized-with-covid-19 (2024). Accessed 4 March 2025.
122. Yang L, Xie X, Tu Z, Fu J, Xu D, Zhou Y. The signal pathways and treatment of cytokine storm in COVID-19 [published correction appears in Signal Transduct Target Ther. 2021 Aug 31;6(1):326.]. *Signal Transduct Target Ther*. 2021;6(1):255.
123. Yao Y, Subedi K, Liu T, et al. Surface translocation of ACE2 and TMPRSS2 upon TLR4/7/8 activation is required for SARS-CoV-2 infection in circulating monocytes. *Cell Discov*. 2022;8(1):89.
124. Yen HL, Valkenburg S, Sia SF, et al. Cellular tropism of SARS-CoV-2 in the respiratory tract of Syrian hamsters and B6.Cg-Tg(K18-ACE2)2Prlmn/J transgenic mice. *Vet Pathol*. 2022;59(4):639.
125. Yoon SM, Lee J, Lee SM, Lee HY. Incidence and clinical outcomes of bacterial superinfections in critically ill patients with COVID-19. *Front Med (Lausanne)*. 2023;10:1079721.
126. Yu P, Deng W, Bao L, et al. Comparative pathology of the nasal epithelium in K18-hACE2 Tg mice, hACE2 Tg mice, and hamsters infected with SARS-CoV-2. *Vet Pathol*. 2022;59(4):602.
127. Yuan L, Zhu H, Zhou M, et al. Gender associates with both susceptibility to infection and pathogenesis of SARS-CoV-2 in Syrian hamster. *Signal Transduct Target Ther*. 2021;6(1):136.
128. Zachary JF, McGavin MD. (2017) *Pathologic Basis* of Veterinary *Disease*. 6th Edition, Elsevier, Amsterdam.
129. Zawilska JB, Lagodzinski A, Berezinska M. COVID-19: from the structure and replication cycle of SARS-CoV-2 to its disease symptoms and treatment. *J Physiol Pharmacol*. 2021;72(4):479.
130. Zazzara MB, Bellieni A, Calvani R, Coelho-Junior HJ, Picca A, Marzetti E. Inflammaging at the Time of COVID-19. *Clin Geriatr Med*. 2022;38(3):473.
131. Zhang JJ, Dong X, Liu GH, Gao YD. Risk and Protective Factors for COVID-19 Morbidity, Severity, and Mortality. *Clin Rev Allergy Immunol*. 2023;64(1):90.
132. Zhou H, Hu Z, Castro-Gonzalez S. Bidirectional interplay between SARS-CoV-2 and autophagy. *mBio*. 2023;14(4):e0102023.

CHAPTER 3 – SYRIAN HAMSTER VBP MODEL DEVELOPMENT AND CONFIRMATION THAT PATHOGEN INFECTION SEQUENCE IMPACTS DISEASE PHENOTYPE

Respiratory viral infections complicated by secondary bacterial pneumonia represent a significant and well-documented disease complex in human and veterinary medicine [8, 14, 32, 41]. Although specific viral and bacterial combinations vary by host and context, they follow a common pathological trajectory of virus-induced alterations in the respiratory microenvironment to facilitate bacterial colonization and subsequent infection. This phenomenon has been widely recognized in viral infections, such as influenza A virus and respiratory syncytial virus, with SARS-CoV-2 as the most recent and notable example [7, 8]. Meta-analyses indicate secondary bacterial infections occur in approximately 18% of hospitalized COVID-19 patients [28], yet up to 75% receive empiric antibiotics at the time of hospitalization [49]. This discrepancy emphasizes the pressing need to further investigate primary viral-secondary bacterial pneumonia (VBP) pathogenesis.

Nonclinical animal models are essential for elucidating host-pathogen interactions and evaluating therapeutic interventions. Historically, mouse models have been foundational in understanding mechanisms of human diseases; however, only 10% of the drug targets and therapeutic interventions from these studies successfully translate into human medicine [19, 56]. The translational utility of murine models is limited by inherent genetic deficits in standard laboratory mice, such as T-helper cell immune response biases [46]. The high mortality rate of 80-100% among virus followed by bacteria (VB)-infected mice, independent of mouse strain or virus-bacteria combination, highlights these immunological deficits [4, 29, 30, 50]. In humans, the mortality rate of secondary bacterial pneumonia ranges from 11-34%, depending on the inciting virus [32]. SARS-CoV-2 VBP studies have utilized the K18-hACE2 mouse strain (B6.Cg-Tg(K18-ACE2)2Prlmn/J transgenic mouse), which exhibits immune response skewing that may not accurately reflect human VBP dynamics. Many mouse-associated limitations for studying intracellular and extracellular pathogens in the same host are appreciably mitigated by using Syrian hamsters

("hamsters"). Wild-type laboratory-bred Syrian hamsters maintain genetic diversity via closed outbred colony breeding, have qualitatively similar immune responses as humans, and are naturally susceptible to SARS-CoV-2 [23, 31, 33, 55]. As no single animal model encompasses all features of human disease, generating alternative models to study human disease in a research setting comprehensively is critical to advancing bench-to-bedside biomedical innovations.

Aging is a critical determinant of disease severity, necessitating the development and characterization of an "aged model" to better understand host responses in older individuals. However, much of the published COVID-19 research using Syrian hamsters has been based on young animals 6-12 weeks of age. Through these studies, it has become well established that young hamsters develop self-limiting disease, with resolution of major pathological changes by 14 days post-infection [13, 17]. Of the limited COVID-19 research utilizing adult and aged hamsters, many have shown that 8-20-month-old hamsters develop worse clinical signs with slower recovery [37, 40, 47]. Besides one study that assessed post-SARS-CoV-2 bacterial infections in 6- to 7-week-old male Syrian hamsters [39], no published studies have assessed true VBP infection scenarios in Syrian hamsters. This knowledge gap is vital for understanding host molecular mechanisms for translational research. It reiterates the need for multiple animal models to comprehensively study human disease in a research setting. This age-dependent variation is particularly relevant, as older individuals in clinical settings experience worsened outcomes and higher mortality rates from COVID-19, particularly when complicated by secondary bacterial infections [22]. Age-associated immune dysregulation, increased inflammatory signaling, and reduced tissue repair capacity likely contribute to the exacerbated disease severity observed in these cases.

Secondary bacterial infections compound disease severity by amplifying inflammation, worsening lung injury, and increasing the risk of systemic complications. Bacterial pathogens such as *Haemophilus influenzae* exploit virus-induced epithelial damage and immune dysregulation to establish infection, often resulting in a hyperinflammatory state and impaired lung function.

Despite the recognized clinical impact of secondary bacterial infections, there remains a critical gap in experimental studies addressing the interplay between SARS-CoV-2 and secondary bacterial pneumonia in immunocompetent animal models. Understanding the role of secondary bacterial infections in exacerbating the consequences of COVID-19 is vital for developing novel therapeutic strategies.

To address these gaps, we established an adult Syrian hamster model of VBP using SARS-CoV-2 and *Haemophilus influenzae* serotype B. This study demonstrates that sequential intranasal viral infection followed by intratracheal bacterial infection induces moderate to severe pneumonia, leading to a dysregulated immune state in a subset of adult male hamsters. Moreover, we show that the pathogen exposure sequence significantly influences disease phenotype and progression.

MATERIALS & METHODS

Virus and cell culture procedures

All *in vitro* and *in vivo* infectious virus work was performed in a biosafety level 3 (BSL-3) facility at Colorado State University. SARS-CoV-2 virus strain WA1/2020WY96 was graciously donated by Dr. Angela Bosco-Lauth. The virus was passaged four times in Vero E6 cells using Dulbecco's Modified Eagle Medium supplemented with 8% heat-inactivated fetal bovine serum and 1% penicillin-streptomycin. Clarified viral stocks were supplemented with 10% heat-inactivated fetal bovine serum and frozen at −70°C. Virus stock and lung homogenate titrations were performed using a double-overlay plaque assay as previously described [27]. Briefly, 6-well plates with 85% confluent monolayers of cells were inoculated with 100 uL of serial 10-fold dilutions of samples, incubated for 1 hour at 37°C, and overlaid with a 0.55% noble agar in Temin's Modified Eagle Medium containing 2.5% heat-inactivated fetal bovine serum and 1% penicillin-streptomycin. Plates were wrapped in parafilm to minimize desiccation. A second overlay

containing 4% neutral red dye was added at 69 hours and plaques were counted at 72 hours. Plaque formation was confirmed by microscopic quantification.

Bacteria and agar/broth culture procedures

Frozen glycerol stocks of *Streptococcus pneumoniae* serotype 19A (BEI HM-145) were streaked onto blood agar plates (BAP) consisting of tryptic soy broth, tryptic soy agar, and 5% defibrinated sheep blood. Bacterial colonies were incubated for 18 hours in 5% CO2 at 37°C. Isolated colonies were selected and inoculated into Todd Hewitt broth supplemented with yeast extract. Liquid culture bio-reaction conical tubes were incubated in 5% CO2 at 37°C for 10 hours and then passaged and incubated again for an additional four hours. For hamster infections, bacterial broth suspensions were centrifuged three times at 3,400 RPM for 5 minutes. Centrifuged bacterial pellets were resuspended in PBS. Inocula and organ homogenate bacterial titers were confirmed via serial 10-fold dilution and plating onto BAP, followed by incubation for 13-20 hours in 5% CO2 at 37°C.

Frozen glycerol stocks of *Haemophilus influenzae* serotype B (ATCC 10211) were streaked onto supplemented chocolate agar plates (sCAP) consisting of gonococcal agar base, 1% bovine hemoglobin, and 2% IsoVitaleX. Bacterial colonies were incubated for 17 hours in 5% CO2 at 37°C. Isolated colonies were selected and inoculated into supplemented Brain Heart Infusion broth (sBHI) consisting of BHI liquid culture, hemin (10 ug/mL), and nicotinamide (10 ug/mL) to a starting optical density (OD600) of 0.05. Liquid culture flasks were loosely capped and grown in a shaking incubator at 200 RPM, 37°C until bacteria reached mid-log growth at approximately 4.5 hours. For hamster infections, bacterial broth suspensions were centrifuged three times at 3,400 RPM for 5 minutes. Centrifuged bacterial pellets were resuspended in 5% sBHI. Infection inoculum contained 5% sBHI because *H. influenzae* suspended in plain PBS rapidly loses viability [42]. Inocula and organ homogenate bacterial titers were confirmed via serial 10-fold dilution and plating onto sCAP, followed by incubation for 13-18 hours in 5% CO2 at 37°C.

Nontypeable *Haemophilus influenzae* (ATCC 49766) and hamster-passaged *Haemophilus influenzae* were propagated using a similar protocol as outlined for *H. influenzae* serotype B (ATCC 10211).

Animals

For all pilot, repeat, and infection sequence studies, a total of 20 young male Syrian hamsters (7-week-old) and 127 adult male Syrian hamsters (39–44-week-old) were obtained from Charles River Laboratory (Kingston, NY). Studies were performed in male hamsters due to their increased susceptibility and associated pathology to SARS-CoV-2 infection compared to female hamsters [13]. Additionally, it was financially infeasible to house female hamsters until the required adult age for study parameters. Animals were housed individually and maintained on a 12:12 light-dark cycle at 20-25°C in an Animal Biosafety Level-3 facility at Colorado State University. Hamsters had access to food and water *ad libitum* and were acclimated for at least seven days before infection.

Animal anesthetic procedures and pathogen challenge

For viral intranasal infection, hamsters were anesthetized by inhalation with isoflurane gas, placed in dorsal recumbency, and intranasally inoculated with 2.8×10^4 plaque-forming units (PFU) SARS-CoV-2 for a total volume of 100 uL. Post-viral infection, hamsters were manually restrained in a 60-degree position until conscious to promote the distal migration of viral inoculum into the lower respiratory tract.

For bacterial non-surgical intratracheal infection, hamsters were lightly anesthetized by inhalation with isoflurane gas followed by intraperitoneal injection of ketamine and xylazine (90 mg/kg and 9 mg/kg, respectively). Our non-surgical intratracheal approach was adapted from Sudhadevi et al. Briefly, hamsters were placed in dorsal recumbency, restrained on a 60-degree inclined board, and an otoscope light source was used to visualize the rima glottidis. Inocula were

administered into the trachea via a 200 uL gel-loading pipette tip affixed to a 1 mL syringe. The base of the pipette was trimmed to ensure a secure fit onto the syringe. Before loading the syringe with bacteria, 0.5 mL of room air was aspirated into the syringe hub to facilitate distal instillation of bacterial inoculum into the lower respiratory tract. Bacterial inoculum was approximately 4.0×10^9 colony-forming units (CFU) HiB for a total volume of 160 uL.

This study's intranasal viral infection with nonsurgical intratracheal bacterial infection is termed "IN/IT infection model". The IN/IT infection model was performed for virus-only (VO), virus followed by bacteria (VB), bacteria-only (BO), and bacteria followed by virus (BV) infection scenarios. All hamsters were infected with a viral or bacterial pathogen on Day 0; VB and BV infection groups received the second pathogen infection on Day 2.5. Control and single-pathogen infected hamsters were given sham PBS inoculations of equivalent volume on Day 2.5 post-primary infection (PPI). This ensured that all animals underwent one intranasal anesthetic and one intratracheal anesthetic procedure. Animals were observed until fully recovered from all anesthetic procedures. Hamsters were monitored daily for signs of infection (e.g., weight changes, activity level, respiratory effort) and were removed from the study if showing signs of severe disease (i.e., moribund presentation).

Of the eight hamsters in each group, the four hamsters with the most significant weight loss and lowest activity level on Day 7 PPI were selected for the Day 7 study endpoint. The remaining four hamsters in each group were terminated at the Day 14 study endpoint.

Necropsy and histopathology

On Days 7 and 14 PPI, four hamsters per group were sacrificed via lethal overdose of ketamine and xylazine (500 mg/kg and 20 mg/kg, respectively), followed by terminal intracardiac blood collection and cervical dislocation. A board-certified veterinary anatomic pathologist performed tissue harvesting and complete post-mortem examinations. Lung, kidney, and spleen tissues were collected for bacterial culture; these tissues were used instead of blood to assess

for bacterial dissemination. Fresh lung tissue was also obtained for viral titers and qRT-PCR. Tissues collected for microbial and qRT-PCR analyses were homogenized using a Precellys Evolution Touch Homogenizer (Bertin Instruments). The corresponding bronchioles were ligated with a string after fresh lung tissue specimens were obtained from the right cranial and middle lobes. The remaining lung lobes were inflated by tracheal instillation of 10% neutral-buffered formalin using a 5 mL syringe attached to 30 cm IV tubing until the lung lobes were fully expanded. Standard diagnostic tissue collection for formalin fixation was performed, and select organs were reviewed for histopathology. Harvested organs were fixed in 10% neutral-buffered formalin under BSL-3 containment for three days.

Trimmed histopathological tissues were processed routinely, paraffin-embedded, and stained with hematoxylin and eosin on an automated staining system (Bond-Max; Leica). Immunohistochemistry (IHC) detection for the SARS-CoV-2 nucleocapsid was also performed in all virus-infected hamster groups using a monoclonal antibody generated by Terry et al. The initial histopathology slide review was performed as a partially masked review by a board-certified veterinary anatomic pathologist. Histopathological analysis was performed on four transverse lung sections (two left lobe [cranial and middle regions], one accessory lobe, and one right caudal lobe) using lung-specific scoring parameters. Our VBP scoring scheme was adapted from those developed for Syrian hamster SARS-CoV-2 respiratory infections [2, 18], and further modified based on assessment of our VBP pilot study hamster histopathological findings. Lesions were semiquantitatively scored for each of the four lung tissue sections obtained from each animal in each group, and the predominant lesion feature was used to calculate the score. Anatomic lesion categories assessed in this scoring scheme included bronchiolar, alveolar, alveolar space contents, pleural, vascular/perivascular, and overall percent of tissue affected. An additional point was awarded for the presence of hyaline membranes, intra-alveolar organizing fibrin, foci of pulmonary necrosis, or pericarditis (see Table 3 for complete scoring scheme). Lesion features, but not points, were cumulative within each category. For example, if an animal was awarded a

“2” for alveolar lesions, interstitial inflammation was the predominant lesion, but alveolar type 2 (AT2) cell hyperplasia was also present. Pulmonary findings noted but not included in scoring were atypical or multinucleated epithelial cells (i.e., syncytia) and degree of pulmonary hemorrhage.

Table 3. Histopathology scoring criteria.

Percent of tissue affected (0 - 5)	(0) 0% (1) 1-5% (2) 6-20% (3) 21-50% (4) 51-75% (5) 76-100%
Bronchiolar lesions (0 - 3)	(0) None (1) Epithelial hyperplasia with empty lumen (2) Inflammatory cells marginating through bronchiolar epithelium (3) Luminal exudate
Alveolar lesions (0 - 3)	(0) None (1) Alveolar type 2 cell hyperplasia (2) Interstitial inflammation (3) Alveolar type 1 or 2 cell degeneration
Alveolar space contents (0 - 3)	(0) None (1) Foamy macrophages and/or lymphocytes with few neutrophils (2) Proteinaceous edema (3) Neutrophils with or without macrophages
Pleural lesions (0 - 2)	(0) None (1) Mesothelial hypertrophy (2) Inflammatory infiltrate with or without fibroplasia
Vascular and perivascular lesions (0 - 3)	(0) None (1) Edema and/or low numbers of loosely arranged mixed inflammatory cells (2) Densely packed mixed inflammatory cells (3) Endothelialitis
Hyaline membranes (0 - 1)	(0) Absent (1) Present
Intra-alveolar organizing fibrin (0 - 1)	(0) Absent (1) Present
Foci of necrosis (0 - 1)	(0) Absent (1) Present
Pericarditis (0 - 1)	(0) Absent (1) Present
Total score per tissue section	0 - 23

Additional microscopically examined organs included the heart, kidney, liver, and spleen; three decalcified, transverse sections of the nasal cavity were also assessed from VO and VB infection groups. Lesions in non-scored organs that were interpreted to be related to VBP and/or sepsis (e.g., acute passive hepatic congestion, splenic contraction) aided in characterizing systemic histopathological changes observed in this hamster infection model.

Lung tissue relative gene expression profiling using quantitative real-time PCR

Select genes were interrogated to quantify relative gene abundance on Day 7 PPI. The following genes assessed various host response parameters to our infection scenarios. *Tmprss2* and *Ace2* encode for host proteins that SARS-CoV-2 utilizes for host cell entry, while *Lbp* and *Tlr4* encode for proteins that detect bacterial and host-damage-associated products that activate innate immune responses. Host pro-inflammatory marker genes (*Ifng*, *Cxcl10*, *Ifnb1*, *Il6*, *Ptgs2*) and anti-inflammatory marker gene (*Il10*) generally assess the host's overall inflammatory state. *Icam1*, largely associated with endothelial cells, and *Nr4a3*, commonly associated with tumor necrosis factor-activated myeloid cells [58], provide an overview of the relationship between inflammatory cells and their ability to marginate through vessels into affected tissues. Finally, *Mki67* gene expression can be used to assess for epithelial hyperplasia, a supporting indicator of the recovery stage in hamsters infected with SARS-CoV-2 [40].

For measurement of host relative gene expression, total RNA was extracted from lung homogenate with TRIzol Reagent, 5 mm stainless steel beads, and a Precellys Evolution Touch Homogenizer (Bertin Instruments) under BSL-3 conditions. Total RNA was then isolated from individual samples by TRIzol/phenol-chloroform extraction as previously described [3]. RNA purity and concentration were confirmed using a NanoDrop One C (Thermo Scientific) and Qubit 4 Fluorometer (Invitrogen). Primer pairs were developed using NCBI Primer-BLAST with PCR efficiency values of 1.95-2.1. *Actb* (Beta-actin) was used as the internal standard reference gene. Primer pairs used in qRT-PCR are listed in Table 4. cDNA was prepared from total RNA samples

using RevertAid First Strand cDNA Synthesis kit (Thermo Scientific). Both the generated cDNA used in qRT-PCR assays on a Roche LightCycler 480 and the resultant Cp values used to calculate relative gene expression were performed as previously described by Rocha et al. All biological samples (n = 3/group) were quantified independently in technical duplicate.

Table 4. Primer sequences used in qRT-PCR study.

Gene Name	Forward Primer 5'-3'	Reverse Primer 5'-3'
Actb	CGCAGCGATATCGTCATCCA	CTAGTGGCCCGCGTTGAC
Tmprss2	CTCCAGGAATCGGGCCTTAC	GCACTGGAGGTGGGTAGTTC
Ace2	TGGACTTCAGATGCTCAGGTG	CACGAGATGGGACACATCCAA
Nr4a3	CGAGGGCTTGAAGTGGAAGA	CTGGACCCGCAGATGAAGG
Icam1	CCTGACAGTGCTTCGTGAGT	ACAATGATGATGACGGCCCA
Lbp	TCGCCGTTATCAACACATCTCT	GAACCCACTGACCTTGTGGAT
Mki67	ACCAGTGGAAGAGCAGATTAGC	TTCCCAACAAGCACCCACTA
Tlr4	CTCCTCCCCAAAGGCAAGTAA	ATGACTGAATGGGTAGGTGGG
Il10	GTGCTAGAGCCTGGAGTGAAA	CTTCTGCCTGGGTGTTCAAG
Ifng	GTCCCCTCCATTCACGACAT	GGTTGGGAAGGAAATCAGCG
Cxcl10	GATGTAGCCCACCGTGTCAT	ATGCCTCCCTACCTAAGCCT
Ifnb1	CGAGCAGCAGTCTCAAGGAA	CCAGTCTCAGAGGCATCAGC
Ptgs2	CTGTCCGAGTACAGTCGCAT	GAGGATGACAAGAGTGACTGACA
Il6	AGTGGATGGAAGTCTCCTGTG	AGCTACTGAGCCTGTGTGAGA

Statistical analysis

All data is presented as mean ± standard deviation (SD). Differences between two variables were identified using a two-way ANOVA statistical test followed by Tukey's *post hoc* test for multiple comparisons. Significance is denoted as *p < 0.05, **p < 0.01, ***p < 0.001, ****p < 0.0001. All statistical analyses were conducted in Prism.

Study assumptions

The primary assumption in this study is that hamster and human phenotypes are controlled by similar pathways. A second assumption is that all study hamsters are healthy, with no underlying comorbidities (e.g., no overt metabolic abnormalities, structural anomalies, or neoplasia), prior to the start of experimentation.

Study scope, delimitations, and limitations

The scope of this research was to assess the ancestral SARS-CoV-2 strain and four bacteria (*Streptococcus pneumoniae* serotype 19A, *Haemophilus influenzae* serotype B, Nontypeable *Haemophilus influenzae*, and hamster-passaged *Haemophilus influenzae*) in male Syrian hamsters. The infection time course focused on the subacute to early chronic stages, emphasizing the first seven days after primary pathogen infection. Assessing adaptive immune responses was outside the scope of this study. Combinations of other bacterial respiratory pathogens or SARS-CoV-2 variants, assessing VBP in female Syrian hamsters, and evaluating chronic stages of infection (i.e., greater than 14 days post-viral infection) were also beyond the scope of this study.

This study offers valuable insights into infection modeling using an immunocompetent laboratory animal but has certain limitations. Due to the absence of prior research on hamster VBP, the bacterial species assessed had to be highly selective. Secondly, geriatric male Syrian hamsters would have served as the optimal disease model; however, aging male hamsters in individual cages to 16 months of age was resource-intensive and intractable.

RESULTS

VBP model development through pilot studies.

Multiple pilot studies were performed to determine the optimal VBP hamster modeling infection scenario. The following variables were assessed over eight separate studies: age of male hamsters at time of viral infection (7-weeks-old, 39 to 44-weeks-old), time interval between primary viral infection and secondary bacterial exposure (2, 2.5, 3.5, 6 days post-viral infection [PVI]), bacterial species to administer (*Streptococcus pneumoniae* serotype 19A [BEI HM-145], *Haemophilus influenzae* serotype B [ATCC 10211], Nontypeable *Haemophilus influenzae* [ATCC 49766], hamster-passaged *Haemophilus influenzae*), dose of viral inoculum (10^4, 10^5 plaque-

forming units [PFU]), dose of bacterial inoculum (10^7, 10^8, 10^9, 10^{10} colony-forming units [CFU]), route of bacterial infection (intranasal, non-surgical intratracheal), and on which day post-viral infection the first study endpoint would occur (Day 6 PVI, Day 7 PVI). See Table 5 for specific pilot study parameters.

Table 5. Specific pilot study parameters assessed to create VBP model.

SARS-CoV-2 Dose (PFU)	Age	Bacterial species	Bacteria on Day PVI	Bacteria Route	CFU	First euthanasia endpoint on Day PVI	Outcome
10^5	9 mo	S. pneumoniae serotype 19A	3.5	IN	10^7	6	2° bacterial infection delays histo recovery in aged males but can have a protective effect in young males
	7 wk						
	9 mo	S. pneumoniae serotype 19A	6			6	10^7 S. pneumoniae on D6 PVI does not delay progression of histo recovery in aged males
10^4	9 mo	S. pneumoniae serotype 19A	3.5	IN	10^9	6	Similar trend as D3.5 10^7 CFU age male study
	9 mo	H. influenzae serotype B	3.5		10^8	6	HiB induces greater weight loss than NTHi
		Nontypeable H. influenzae					
	10 mo	S. pneumoniae serotype 19A	2.5		10^9	6	Bacterial infection at 2.5 DPVI induces greater weight loss compared to infection at 3.5 DPVI HiB induces more consistent weight loss than S. pneumoniae
		H. influenzae serotype B					
	9 mo	Hamster-passaged H. influenzae	2.5		10^8	7	Not as pathogenic as compared to ATCC HiB
	9 mo	H. influenzae serotype B	2		10^9	7	Bacterial infection at 2 days PVI is too early
			2.5				
	10 mo	H. influenzae serotype B	2.5	IN	10^{10}	7	IT induces more consistent weight loss than IN IT 10^9 induces sustained, significant weight loss compared to IN or 10^7 IT bacterial infections
				IT	10^7		
				IT	10^9		

VBP: primary viral-secondary bacterial pneumonia; PFU: plaque-forming units; PVI: post-viral infection; CFU: colony-forming units; mo: month; wk: week; S. pneumoniae serotype 19A: Streptococcus pneumoniae serotype 19A; H. influenzae serotype B: Haemophilus influenzae serotype B; Nontypeable H. influenzae: Nontypeable Haemophilus influenzae; DPVI: days post-viral infection; IN: intranasal; IT: intra-tracheal.

The first pilot study assessed host age to determine if this biological variable could impact disease phenotype when comparing virus-only (VO) and virus followed by bacteria (VB) infection groups (Fig. 3). We found that 7-week-old and ≥39-week-old hamster VO groups demonstrated similar histopathological lesions on Day 6 PVI: regionally extensive AT2 cell hyperplasia (Figs. 3A and 3D). AT2 cell hyperplasia is indicative of recovery in the Syrian hamster SARS-CoV-2 infection model [40]. The predominant lesion in the adult male VB group was interstitial pneumonia

with patchy AT2 cell hyperplasia and pulmonary edema (Fig. 3E). This finding supports that the bacterial infection delayed histopathological recovery. Surprisingly, in three of the four young male VB group hamsters, the predominant lesion was multifocal AT2 cell hyperplasia (i.e., distinctively less structural damage than the young male VO group; Fig. 3B). We hypothesize that this finding is linked to innate immune priming [15], an immunological event that contrasts with the infection model we aimed to establish. These data directly showed that the biological variable of host age impacts disease pathology under similar infection conditions: a secondary bacterial infection delays recovery in adult male hamsters but can have a protective effect in young male hamsters.

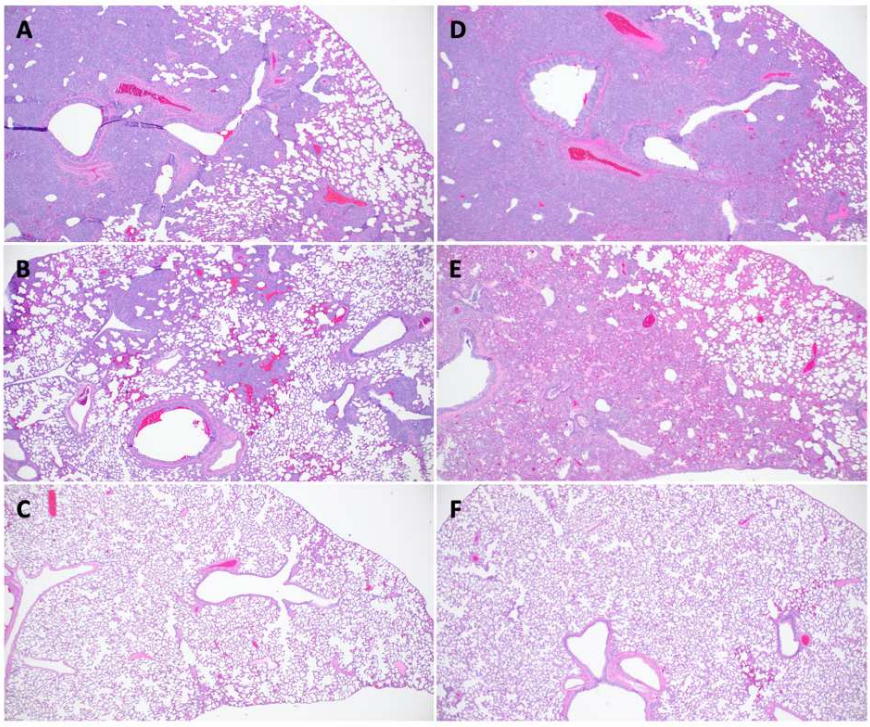

Figure 3. Lung histopathology of 7- and ≥39-week-old male Syrian hamsters at 6 days post-CoV2 intranasal infection ± 2.5 days post-*S. pneumoniae* intranasal infection. Young male hamsters (A-C); adult male hamsters (D-F). **A** and **D.** Virus only infection. Primary lung lesion in both age groups is regional epithelial hyperplasia indicative of recovery. HE. 4×. **B.** Young male hamster with virus followed by bacteria infection. Primary lung lesion is multifocal epithelial hyperplasia. The multifocal hemorrhage is interpreted to be a perimortem, xylazine overdose-induced artifact. HE. 4×. **E.** Adult male hamster with virus followed by bacteria infection. Primary lung lesion is regional bronchointerstitial pneumonia with pulmonary edema. HE. 4×. **C** and **F.** Normal lungs from mock-infected, control hamsters. HE. 4×. CoV2: SARS-CoV-2. *S. pneumoniae*: *Streptococcus pneumoniae* serotype 19A; HE: hematoxylin and eosin.

The VBP findings in adult male hamsters aligned more closely with our research goal of developing a feasible Syrian hamster infection model. Consequently, all subsequent pilot studies were conducted exclusively in adult male Syrian hamsters. As weight loss is a key indicator of infectious disease severity in animal models [38, 40], our ideal model was one in which animals continued losing weight and exhibited prolonged decreased activity beyond that seen in virus-only infected hamsters or other pilot study hamsters (Fig. 4). Biologically, this correlated with sustained and excessive inflammation in the lung with or without detectable bacteria in the lungs, kidney, or spleen by tissue culture.

The remainder of the pilot studies focused on determining the optimal conditions for a secondary bacterial infection. Li et al. found that mucociliary transport function of COVID-19 infected hamsters is diminished through Day 6 PVI. As such, the Day 6 PVI was assessed as a time point for secondary bacterial infection. With Day 8 PVI as the first study endpoint, the primary lung lesion of these hamsters was epithelial hyperplasia – supporting that bacterial infection on Day 6 PVI does not impact pulmonary pathology in COVID-19 infected adult male Syrian hamsters.

Next, we explored the impact of utilizing different bacterial species for the secondary infection. Geriatric female hamsters infected with SARS-CoV-2 exhibit respiratory tract dysbiosis on Day 3 PVI, with genera *Haemophilus*, *Provetella*, and *Streptococcus* showing the greatest percent increase in relative abundance [60]. Relatedly, respiratory tract bacterial microbiota in human males and females is not statistically different, but males have a greater absolute abundance of bacterial microbiota [61]. Moreover, bacteria most often associated with secondary bacterial pneumonia in humans also diagnosed with viral pneumonia include *S. pneumoniae, H. influenzae*, *S. aureus*, and *Klebsiella pneumoniae* [63, 64]. To maintain a translationally-relevant infection model, *Haemophilus influenzae* serotype B (HiB) and Nontypeable *H. influenzae* (NTHi) were assessed in our VBP hamster infection scenarios; HiB induced greater weight loss than NTHi (Fig. 4).

We then compared HiB against *S. pneumoniae* serotype 19A and altered the secondary infection timing to Day 2.5 PVI instead of Day 3.5 PVI. HiB induced more consistent weight loss compared to *S. pneumoniae* serotype 19A (Fig. 4). As pathogens can be host adapted via lung-to-lung animal passage to enhance a pathogen's virulence in a particular animal species [62], we also evaluated whether hamster-passaged HiB would induce increased pulmonary pathology. The results indicated that hamster-passaged HiB did not increase pulmonary damage, thereby confirming HiB as the preferred species for our secondary bacterial infection.

Finally, given HiB's low virulence, we evaluated the role of the infection route in overcoming the high relative surface area of the rodent nasal turbinates [21]. Intra-tracheal administration of HiB at 10^9 CFU was able to bypass the nasal cavity structural defense barrier to induce the greatest reduction in body weight and the most pronounced pulmonary pathology (Fig. 4). The CFU doses assessed in this study were adapted from previous Syrian hamster studies that used intratracheal administration of 10^7 and 10^8 CFU for assessing bacterial pneumonia models in Syrian hamsters [1, 20, 54].

Based on these pilot studies, we concluded that a suitable hamster VBP model consisted of: male Syrian hamsters older than 39 weeks of age; intranasal SARS-CoV-2 10^4 PFU administered on Day 0; non-surgical intratracheal *H. influenzae* serotype B (HiB) 10^9 CFU administered on Day 2.5 PVI (the "IN/IT infection model"). The IN/IT infection model for virus followed by bacteria infection sequence was performed in triplicate: pilot study, repeat study, and in a model comparison against virus-only (VO), bacteria-only (BO), and bacteria followed by virus (BV) infection scenarios. From these studies, 17 adult male hamsters were used for the virus followed by bacteria (VB) infection. Five out of the 17 hamsters (29%) developed severe to fatal VBP by Days 6 or 7 PVI; one hamster was euthanized on Day 6 PVI, and four hamsters were prioritized to be euthanized first on the Day 7 PVI study endpoint in their respective studies due to their clinical presentation. As such, the Day 7 PVI time point using the IN/IT infection model was interpreted to be the critical point for assessing the maximal effects of VBP. Findings from

the VO-, VB-, BO-, and BV-infected hamster study are discussed in greater detail in the following sections.

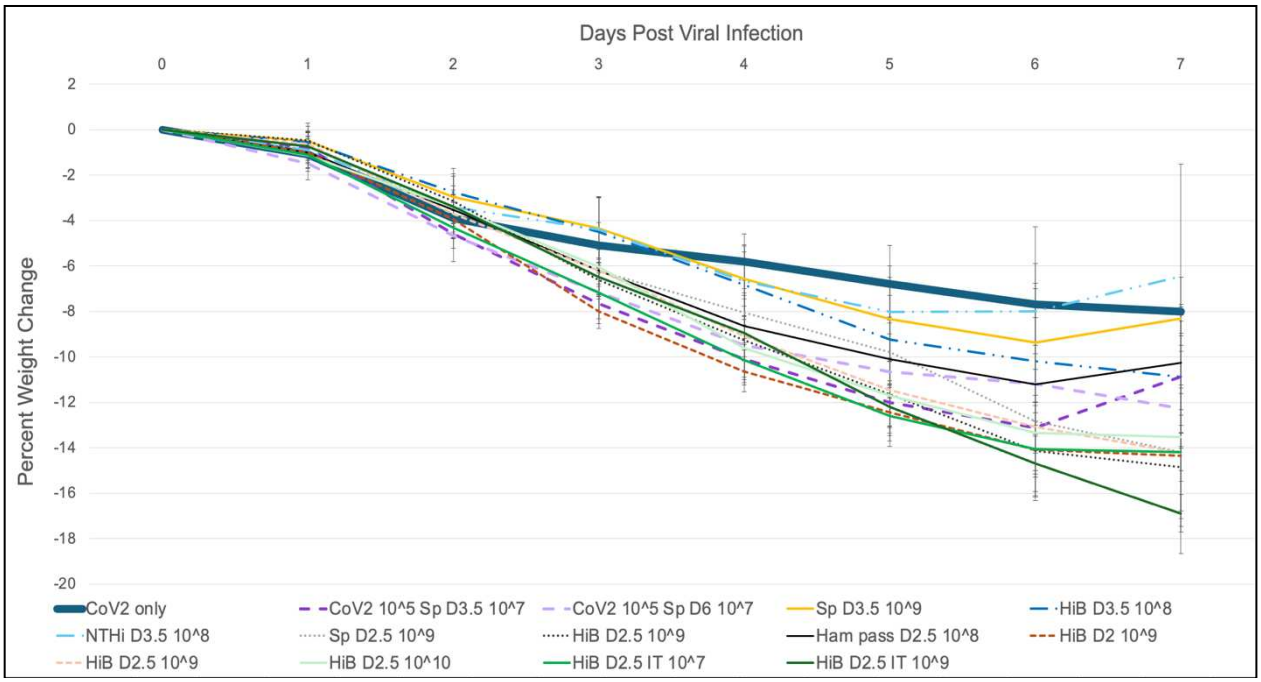

Figure 4. Group average body weight changes in 39-44-week-old male Syrian hamsters intranasally infected with CoV2 followed by bacterial respiratory infection at varying intervals post-viral infection with different bacterial species and different routes of infection. Group average body weight changes through Day 7 PVI with group sizes ranging from 3 to 8 hamsters per infection group. Mean percent body weight change at Day 0 ± SD is shown at each consecutive day. Unless indicated by "CoV2 10^5" (SARS-CoV-2 10^5 PFU), virus inoculum was 10^4 PFU. Unless indicated by "IT" (non-surgical intratracheal), bacterial species were administered intranasally. CoV2: SARS-CoV-2; PVI: post-viral infection; Sp: *Streptococcus pneumoniae* serotype 19A; HiB: *Haemophilus influenzae* serotype B; NTHi: Nontypeable *Haemophilus influenzae*; Ham pass: hamster-passaged *Haemophilus influenzae*; D#: day PVI that bacterial infection occurred on; PFU: plaque-forming units; CFU: colony-forming units; 10^#: bacterial CFU administered for bacterial infection.

Determining the time interval between pathogen exposures was critical in this study. The 60-hour time point was derived from COVID-19 transmission electron microscopy studies performed in hamsters demonstrating that infected cells of the lower respiratory tract exhibit degenerative changes by Day 2 PVI [57]. Moreover, neutrophil recruitment and viral burden in the

hamster lung peaks 2-3 days PVI [25, 36]. These respiratory tract changes represent a compromised host state, providing an excellent susceptibility window for introducing a secondary bacterial pathogen. Despite this plan, an emergency BSL-3 shut down necessitated that the bacterial infection for the first pilot study (i.e., host age study), and several subsequent studies, occur on Day 3.5 PVI instead of Day 2.5 PVI.

Primary viral infection followed 60 hours later by secondary bacterial infection results in moderate to severe pneumonia in adult male Syrian hamsters.

To establish a translationally relevant model of primary SARS-CoV2 with secondary bacterial pneumonia, adult male Syrian hamsters (≥39 weeks old) were sequentially infected with SARS-CoV-2 (CoV2) intranasally on Day 0, followed by *Haemophilus influenzae* serotype B (HiB) administered non-surgically via intratracheal instillation on Day 2.5 post-viral infection (PVI). This pathogen sequence was found to be a key determinant of disease severity. Weight loss, a primary clinical indicator of disease severity [38], was most pronounced in VB-infected hamsters, with significant reductions observed by Day 7 post-primary infection (PPI) compared to all other groups (Fig. 5). This trend correlated with reduced physical activity, which was lowest in the VB group. Although a subset of hamsters in each infection group was maintained until Day 14 PPI, these hamsters recovered unremarkably despite their relatively plateaued weight loss. As such, this study focuses on the Day 7 PPI time point, which assesses the most susceptible hamsters in each infection group and emphasizes the critical disease window at Day 3-7 PPI.

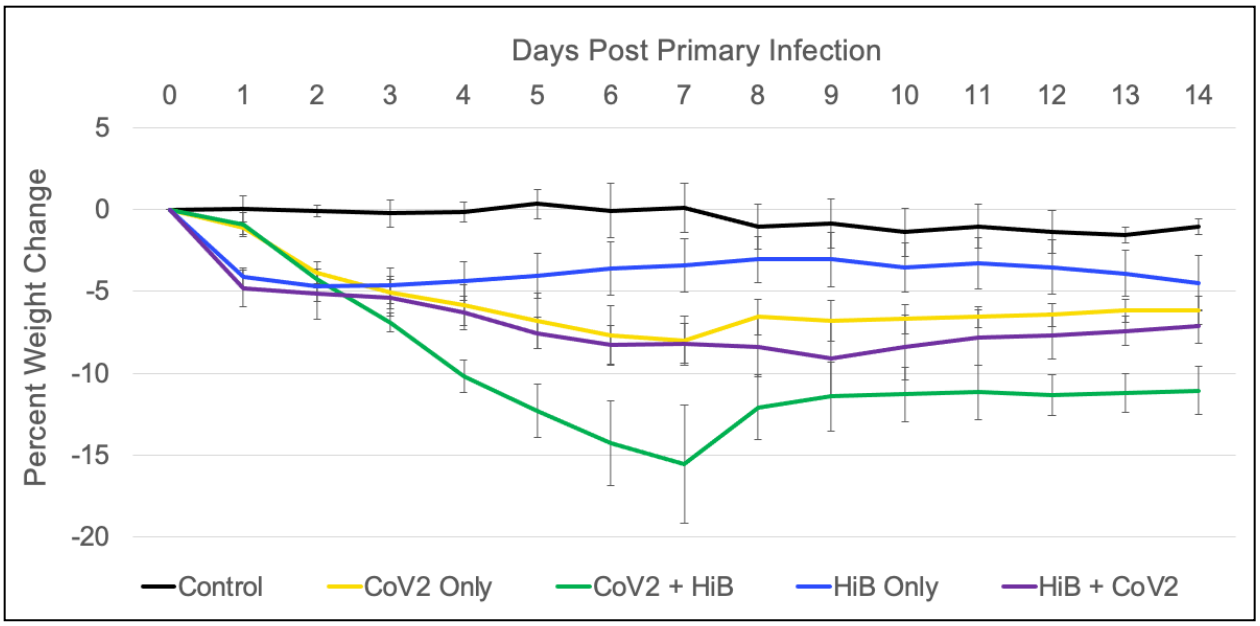

Figure 5. Effect of single- and dual-pathogen infections on body weight in 39-44-week-old male Syrian hamsters. Body weight changes in hamsters (*n* = 8/group through Day 7; *n* = 4/group Days 8-14) infected either singly or sequentially with 10^4 PFU of CoV2 intranasally and/or 10^9 CFU of HiB intratracheally on Day 0 ± Day 2.5. Cov2 + HiB induces the greatest amount of weight loss as compared to CoV2 only, HiB only, or HiB + CoV2 infected hamsters. Control hamsters were administered intranasal (Day 0) and intratracheal (Day 2.5) PBS. Mean percent body weight change at Day 0 ± SD is shown at each consecutive day. PFU: plaque-forming units; CoV2: SARS-CoV-2; CFU: colony-forming units; HiB: *Haemophilus influenzae* serotype B.

Gross pathology and histopathological analysis of IN/IT infection model at Day 7 PPI.

Gross lung evaluation and scored histopathology sections showed semiquantitative differences between all infection groups at Day 7 PPI (Fig. 6 and Fig. 7E, respectively). At necropsy, VB-infected hamsters displayed extensive pulmonary consolidation, coalescing to widespread regions of congestion and hemorrhage, and non-collapsing lung lobes (Fig. 6 B1-B4). Histopathologically, VB hamsters exhibited moderate to severe bronchointerstitial pneumonia with moderate intra-alveolar neutrophils, macrophages, cellular debris, hyaline membrane formation (HMF), and patchy organizing fibrin plugging alveolar spaces (Fig. 7B). Hyaline membranes are a defining feature of diffuse alveolar damage, which is the pathological correlate of the clinical syndrome known as acute respiratory distress syndrome (ARDS) [12]. Notably, severe COVID-19 patients can develop ARDS [9]. Additional pathologic findings observed in the severely

affected VB hamsters included splenic contraction, mild hepatic sinusoidal congestion, rare foci of pulmonary necrosis, and rare regionally extensive pericarditis (Figs. 8-11). Acute pulmonary hemorrhage was a feature observed exclusively in the VB infection group.

On gross examination of VO-infected hamsters, all lung lobes were minimally non-collapsing and included small, multifocal regions of congestion (Fig. 6 A1-A4). The primary histopathologic lesion in this group was moderate AT2 cell hyperplasia with mild lymphohistiocytic interstitial pneumonia and mild mononuclear cell infiltrate within alveolar spaces (Fig. 7A). These findings are compatible with those previously reported in Syrian hamsters intranasally infected with SARS-CoV-2 [2, 40].

BV-infected hamsters demonstrated similar gross lesions as VO-infected hamsters, albeit more extensive (Fig. 6 D1-D4). Histopathologically, these hamsters exhibited mild to moderate interstitial pneumonia with mild alveolar mononuclear cell infiltrate and infrequent HMF (Fig. 7D). HMF was primarily observed within alveoli abutting vascular spaces.

BO-infected hamster lung lobes had rare multifocal regions of congestion grossly (Fig. 6 C1-C4). These hamster lungs demonstrated microscopic scant clusters of foamy macrophages within low numbers of alveolar spaces and rare vessels surrounded by perivascular mononuclear cells (Fig. 7C).

No significant gross or microscopic extrapulmonary lesions were observed in any organ system of VO-, BO-, or BV-infected hamsters.

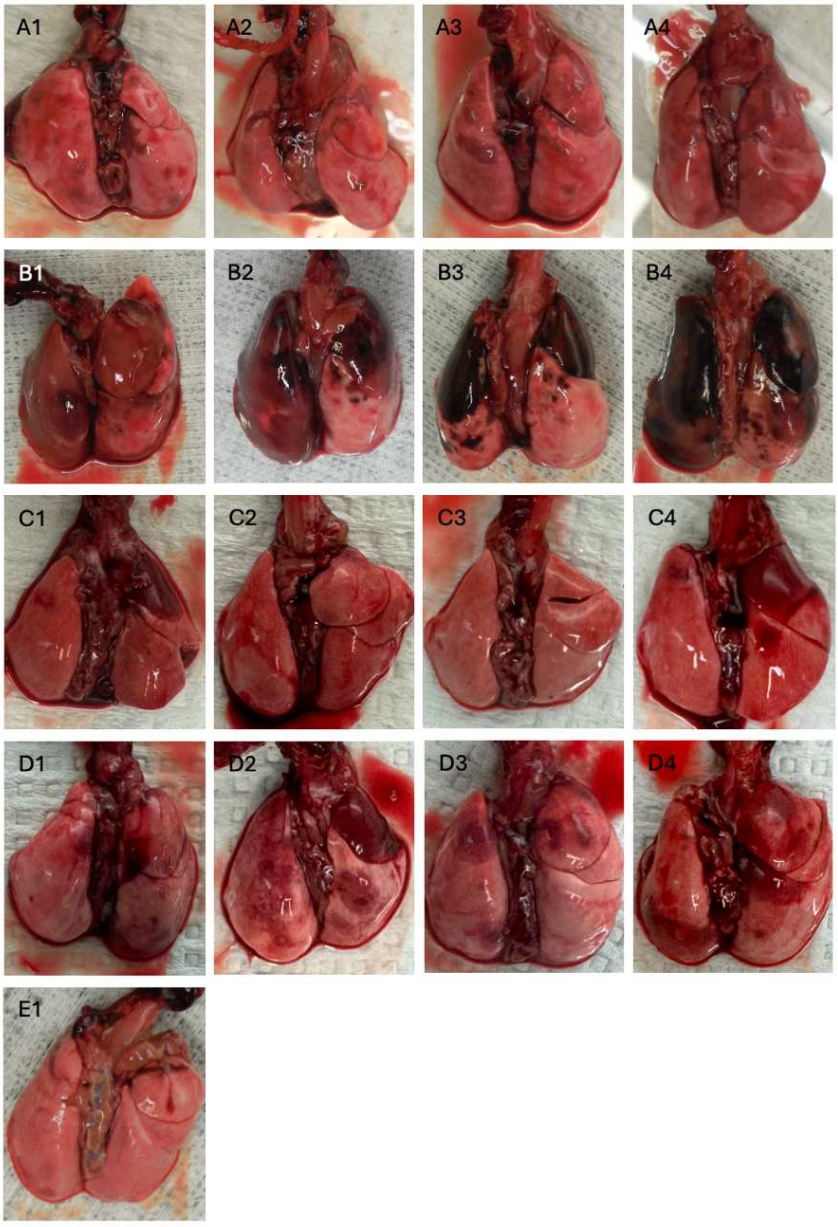

Figure 6. Gross lung pathology on Day 7 PPI of CoV2 only, CoV2 + HiB, HiB only, HiB + CoV2, and Negative Control adult male Syrian hamster infection groups infected on Day 0 ± Day 2.5 PPI. A1-A4. CoV2 only infected lungs are minimally non-collapsing and included small, multifocal regions of congestion. **B1-B4**. CoV2 + HiB infected lungs are moderately non-collapsing and include coalescing to widespread regions of congestion and hemorrhage. **C1-C4**. HiB only infected lungs include rare foci of congestion. **D1-D4**. HiB + CoV2 infected lungs are mildly non-collapsing and included small, multifocal regions of congestion. **E1**. Normal lungs from a Negative Control hamster. PPI: post-primary infection. CoV2: SARS-CoV-2; HiB: *Haemophilus influenzae* serotype B; Negative Control: mock-infected, control hamster.

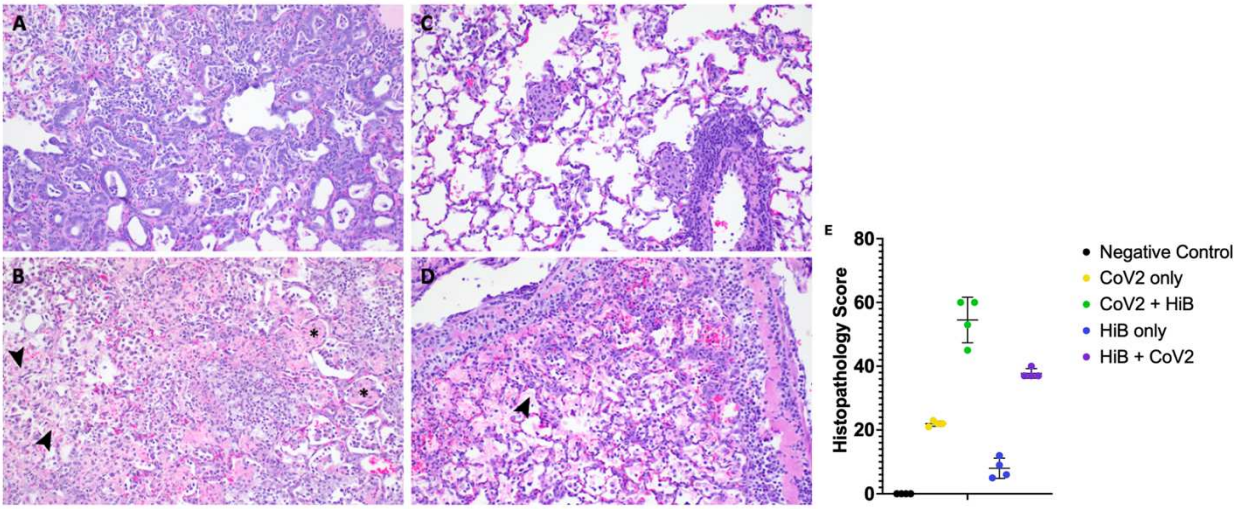

Figure 7. Combined lung histopathology photomicrographs and histopathology score summary of 39-44-week-old male Syrian hamsters at Day 7 PPI. A. Hamster intranasally infected with CoV2 only on Day 0. Alveolar spaces are lined by hypertrophied and hyperplastic epithelium and interstitial spaces are mildly expanded by mononuclear cells. Multifocally, alveolar spaces contain increased numbers of foamy alveolar macrophages. HE. 10×. **B.** Hamster intranasally infected with CoV2 on Day 0 and intratracheally infected with HiB on Day 2.5. Alveolar epithelium is minimally hypertrophied with low numbers of mixed inflammatory cells within interstitial spaces. Alveolar spaces are variably filled with either foamy macrophages, neutrophils, hyaline membranes (arrowheads) or intra-alveolar organizing fibrin (asterisks). HE. 10×. **C.** Hamster intratracheally infected with HiB only on Day 0. Several alveolar spaces include clusters of foamy macrophages. There is moderate mononuclear perivascular cuffing around a pulmonary arteriole. HE. 10×. **D.** Hamster intratracheally infected with HiB on Day 0 and intranasally infected with CoV2 on Day 2.5. Alveolar epithelium is mildly hypertrophied and alveolar spaces contain low numbers of mononuclear cells. Alveoli abutting perivascular spaces are multifocally lined by delicate hyaline membranes (arrowhead). Vessels include mild endothelialitis and mild mononuclear perivascular cuffing. HE. 10×. **E.** Histopathology score summary of each hamster infection group on Day 7 PPI. Single pathogen infection groups were sham infected with PBS on Day 2.5. PPI: post-primary infection; CoV2: SARS-CoV-2; HiB: *Haemophilus influenzae* serotype B.

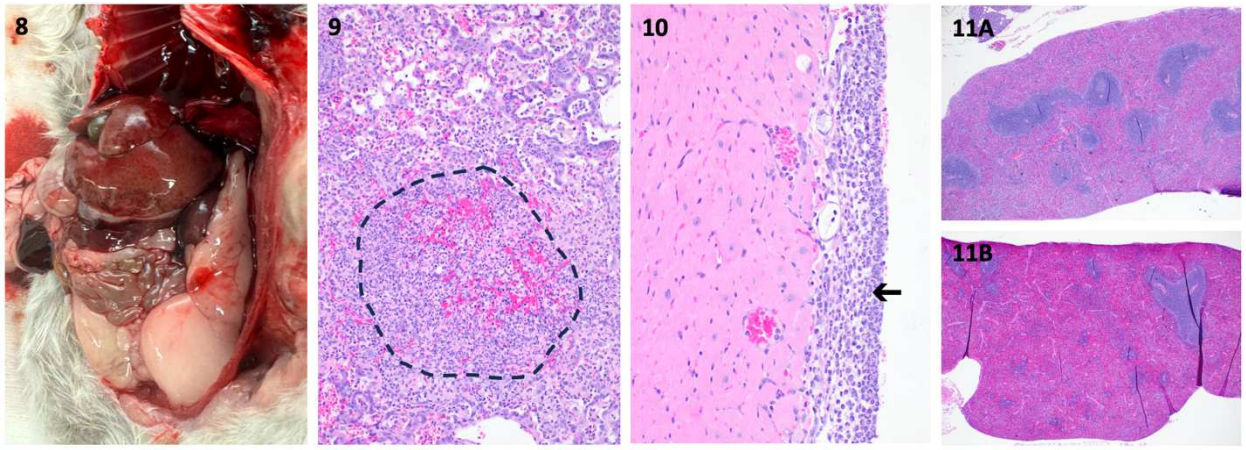

Figures 8-11. Miscellaneous pathology findings on Day 7 PPI in adult male Syrian hamsters infected with intranasal CoV2 on Day 0 and non-surgical intratracheal HiB on Day 2.5. Fig 8. All hepatic lobes demonstrate an enhanced reticular pattern and mildly rounded lobe margins. **Fig 9**. Small foci of alveolar septal loss with replacement by hemorrhage, variably degenerate neutrophils, mononuclear cells, fibrin, and cellular debris (encircled by dashed line). HE. 20×. **Fig 10**. Arrow points to neutrophils and mononuclear cells expanding the pericardial space and superficially interdigitating between epicardial myocyte fibrils. Overlaying pericardial cells are hypertrophied. HE. 20×. **Fig 11A**. VB-infected hamster with splenic red pulp vascular spaces that are modestly depleted of erythrocytes. HE. 4×. **Fig 11B**. Negative Control hamster with numerous erythrocytes expanding splenic red pulp vascular spaces. HE. 4×. PPI: post-primary infection; CoV2: SARS-CoV-2; HiB: *Haemophilus influenzae* serotype B; HE: hematoxylin and eosin; Negative Control: mock-infected, control hamster.

Bacterial dissemination and viral persistence.

Bacterial cultures from lung, kidney, and spleen tissues were performed to assess for bacterial dissemination. Among VB-infected hamsters, two of four had positive lung cultures (2.0×10^7 CFU/g lung tissue and 1.1×10^4 CFU/g lung tissue), with one animal also exhibiting bacterial dissemination to the kidney (5.7×10^4 CFU/g) and spleen (5.2×10^5 CFU/g) (Table 6). In contrast, no bacteria were detected in BO or BV groups at any time point (Table 6), indicating that viral infection before bacterial infection contributed to bacterial dissemination is some cases. SARS-CoV-2 viral titers were evaluated at Day 7 PPI exhibiting detectable viral loads (4.1×10^4 PFU/g lung tissue and 5.8×10^4 PFU/g lung tissue) in the VB-infected hamster group (Table 7). Notably, this persistence suggests that secondary bacterial pneumonia may prolong viral replication within lung tissues as SARS-CoV-2 lung viral titers in Syrian hamsters are

undetectable by Day 7 PVI [37]. All VO-infected hamsters had cleared detectable virus by Day 7 PPI, whereas all BV-infected hamsters still exhibited viral titers at this time point, consistent with their more recent viral exposure (3.3×10^3 PFU/g to 1.4×10^5 PFU/g lung tissue) (Table 7; Figs. 12A-12C). No virus was detected in extrapulmonary tissues by IHC. The findings from this VBP model underscore the importance of pathogen sequence in disease progression and severity.

Table 6. Bacterial tissue cultures of lung, kidney, and spleen on Day 7 PPI of CoV2 + HiB, HiB only, and HiB + CoV2 adult male Syrian hamster infection groups infected on Day 0 ± Day 2.5 PPI.

Group	Animal	Lung (CFU/g)	Kidney (CFU/g)	Spleen (CFU/g)
SARS-CoV-2 + HiB	Mr24 AM 2.9	0	0	0
	Mr24 AM 2.10	2.0×10^7	5.7×10^4	5.2×10^5
	Mr24 AM 2.12	0	0	0
	Mr24 AM 2.14	1.1×10^4	0	0
HiB only	Mr24 AM 3.17	0	0	0
	Mr24 AM 3.18	0	0	0
	Mr24 AM 3.19	0	0	0
	Mr24 AM 3.20	0	0	0
HiB + SARS-CoV-2	Mr24 AM 4.25	0	0	0
	Mr24 AM 4.26	0	0	0
	Mr24 AM 4.27	0	0	0
	Mr24 AM 4.28	0	0	0

PPI: post-primary infection; CoV2: SARS-CoV-2; HiB: *Haemophilus influenzae* serotype B; CFU: colony-forming units.

Table 7. Plaque assay lung viral titers on Day 7 PPI of CoV2 only, CoV2 + HiB, and HiB + CoV2 adult male Syrian hamster infection groups infected on Day 0 ± Day 2.5 PPI.

Group	Animal	Lung (PFU/g)
SARS-CoV-2 only	Mr24 AM 1.1	0
	Mr24 AM 1.2	0
	Mr24 AM 1.3	0
	Mr24 AM 1.4	0
SARS-CoV-2 + HiB	Mr24 AM 2.9	0
	Mr24 AM 2.10	4.1×10^{4}
	Mr24 AM 2.12	0
	Mr24 AM 2.14	5.8×10^{4}
HiB + SARS-CoV-2	Mr24 AM 4.25	8.3×10^{3}
	Mr24 AM 4.26	3.3×10^{3}
	Mr24 AM 4.27	1.4×10^{5}
	Mr24 AM 4.28	7.5×10^{3}

PPI: post-primary infection; CoV2: SARS-CoV-2; HiB: *Haemophilus influenzae* serotype B; PFU: plaque-forming units.

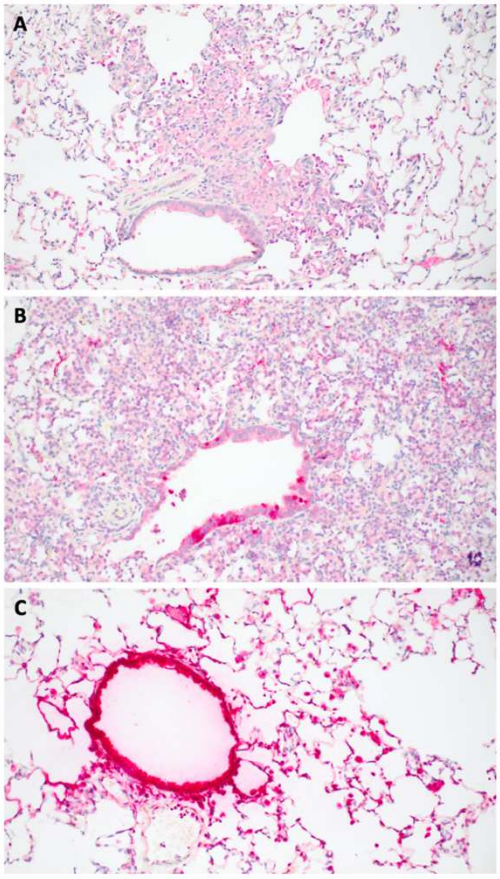

Figure 12. CoV2 immunohistochemistry findings on Day 7 PPI of CoV2 only, CoV2 + HiB, and HiB + CoV2 adult male Syrian hamster infection groups infected on Day 0 ± Day 2.5 PPI. A. Lung tissue section from a CoV2 only infected hamster is diffusely immunonegative for CoV2 within epithelial cells; the weak, diffuse, cytoplasmic blushing was interpreted to be negative. Low numbers of alveolar macrophages demonstrate mild, diffuse, cytoplasmic immunoreactivity for CoV2. CoV2 IHC. 20×. **B**. Lung tissue section from a CoV2 + HiB infected hamster reveals patchy bronchiolar epithelial cells, alveolar epithelial cells, and alveolar mononuclear cells that demonstrate moderate, diffuse, cytoplasmic immunoreactivity for CoV2. CoV2 IHC. 20×. **C**. Lung tissue section from an HiB + CoV2 infected hamster reveals regionally extensive bronchiolar epithelial cells, alveolar epithelial cells, and alveolar mononuclear cells with strong, diffuse, cytoplasmic immunoreactivity for CoV2. CoV2 IHC. 20×. PPI: post-primary infection; IHC: immunohistochemistry; CoV2: SARS-CoV-2; HiB: *Haemophilus influenzae* serotype B.

VBP induces relative differential expression of genes involved in immune signaling leading to a dysregulated host state at Day 7 PPI.

Relative gene expression analysis was performed in each infection group to evaluate host immune responses at Day 7 PPI. Compared to VO-infected hamsters, VB-infected hamsters

exhibited statistically significant elevated expression of inflammatory markers *Il6, Cxcl10, Ifng, Ifnb1,* and *Ptgs2*, as well as endothelial activation marker *Icam1* and bacterial-sensing molecules *Lbp* and *Tlr4* (Fig. 13). Notably, VB hamsters also displayed increased expression of *Ace2* and *Tmprss2*, suggesting that host-virus-bacteria interactions modulate receptor availability. Despite an increase in *Il10*, a key anti-inflammatory cytokine, the overwhelming pro-inflammatory response likely contributed to a dysregulated host state consistent with clinical reports [5, 43]. There were also statistically significant relative gene expression differences between Negative Control and VB hamsters (*Lbp*, *Mki67*, *Ifng*, *Cxcl10*, *Ifnb1*, *Il6*, *Il10*; $p < 0.05$) – further supporting a dysregulated host state when compared to naïve animals.

No statistically significant relative gene expression differences were observed between the Negative Control, VO, BO, or BV hamsters.

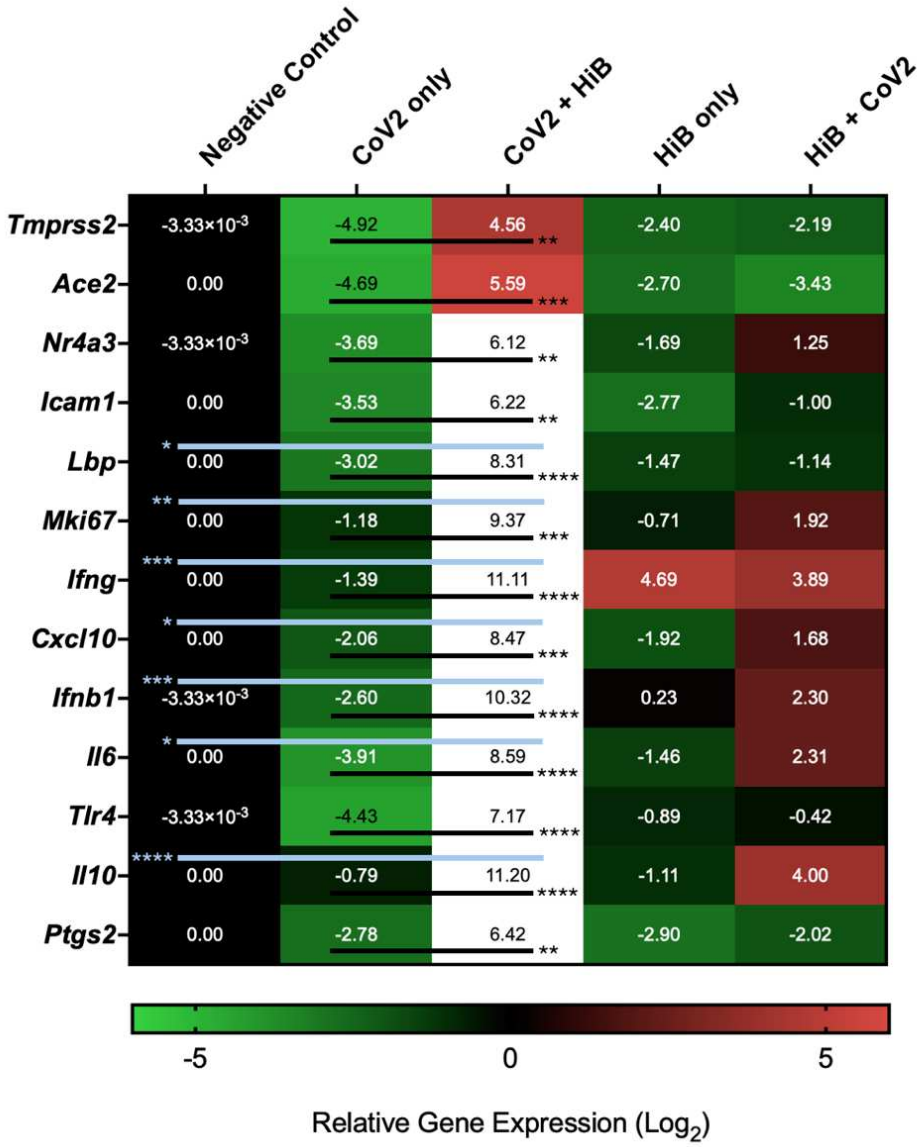

Figure 13. Relative gene expression at Day 7 PPI of Negative Control, CoV2 only, CoV2 + HiB, HiB only, and HiB + CoV2 adult male Syrian hamster infection groups infected on Day 0 ± Day 2.5 PPI. Gene expression was normalized to the *Actb* housekeeping gene. Fold-change of relative gene expression was calculated using delta-delta Ct against Negative Control hamsters (n = 3/group). White boxes represent relative gene expression (Log_2) changes greater than 5. Significance is denoted as *p < 0.05, **p < 0.01, ***p < 0.001, ****p < 0.0001. Black line indicates statistically significant differences between CoV2 only and CoV2 + HiB groups. Light blue line indicates statistically significant differences between Negative Control and CoV2 + HiB groups. PPI: post-primary infection; Negative Control: mock-infected, control hamsters; CoV2: SARS-CoV-2; HiB: *Haemophilus influenzae* serotype B.

DISCUSSION

The prevalent use of empiric antibiotics in the COVID-19 pandemic highlights the ongoing clinical concern of primary viral-secondary bacterial pneumonia. To scientifically address such concerns, nonclinical animal studies help to bridge basic science knowledge gaps and provide proof-of-concept treatment rationales. Published VBP small animal studies have often used young, naïve lab mice with various immunological deficits. Not only do these studies lack translational rigor, but they also have limited practical application within veterinary medicine. Providing translational researchers with alternative small animal models that can be effectively manipulated for drug discovery represents a critical unmet need. Our adult Syrian hamster model accurately reflects severe COVID-19 disease progression compounded by a secondary bacterial infection, particularly in older populations, where immune dysregulation and prolonged inflammation are well-documented. In addition, the findings of this study provide critical insights into the pathogenesis of VBP.

Comparative analysis of relative gene expression and histopathological findings highlight important insights between negative control, VO-, and VB-infected hamsters. There were no statistically significant gene expression differences between negative control and VO hamsters, which supports that adult male hamsters receiving intranasal 2.8×10^4 PFU SARS-CoV-2 are within a recovery state at Day 7 post-viral infection. This finding is further supported by the degree of AT2 cell hyperplasia observed on histopathology. Contrastingly, the statistically significant relative gene expression findings of the VB group suggests that these hamsters are in an immunologically dysregulated host state when compared to the “recovery state” VO hamsters. The VB hamster dysregulated state is consistent with severe COVID-19 patient reports with respiratory infection comorbidities [43]. *Ace2* relative gene expression was increased in our VB hamsters and it is reported that ACE2 expression levels are elevated in patients with severe COVID-19 as an attempt to exert an innate anti-inflammatory function in the lungs [16]. Relative increased expression of *Icam1* and *Nr4a3* can be interpreted as increased inflammatory cell

margination into inflamed lung regions. The increased relative expression of pro-inflammatory gene markers *Lbp*, *Tlr4*, *Ifng*, *Cxcl10*, *Ifnb1*, *Il6*, and *Ptgs2* further supports this finding. Relatedly, inflammatory cytokines can directly upregulate TMPRSS2 expression [44]; as is suspected in our VB hamsters. Overproduction of IL-10 can modulate an overactive immune system; however, its anti-inflammatory function is limited in a state of massive secretion of pro-inflammatory mediators [24], and a similar phenomenon is suspected in our VB hamsters. These collective relative gene expression findings support that the addition of a secondary bacterial infection can lead to a dysregulated host state compared to virus alone in adult male Syrian hamsters using our IN/IT infection model.

The order of pathogen exposure is an important determinant of disease outcomes. One of the most striking findings of this study is the impact of infection sequence on disease severity. When SARS-CoV-2 precedes a bacterial infection, the resulting pathology is significantly more severe than when the infection order is reversed. This aligns with clinical reports indicating that viral respiratory infections prime the lungs for secondary bacterial infection, worsening disease outcomes. Mechanistically, viral infections compromise epithelial integrity, disrupt mucociliary clearance, and impair host antiviral innate responses, creating an environment conducive to bacterial colonization and proliferation [11, 48]. Our findings that viral infection increases susceptibility to bacterial infection and exacerbates bacterial pneumonia align with clinical observations in hospitalized patients, where those with preexisting viral infections often experience more severe bacterial complications [8, 32].

Lesions and findings associated with fatal COVID-19 in humans include diffuse alveolar damage with HMF, AT2 cell hyperplasia, variably complicated by secondary infections with or without organizing fibrin in alveolar spaces [6, 9]. HMF is not documented in Syrian hamsters infected with SARS-CoV-2 alone – barring controversial reports [17]. Our VB-infected adult hamsters at Day 7 PPI demonstrated HMF with or without organizing fibrin plugging alveolar spaces, which was not observed in the young hamster model. These findings support that our

IN/IT model can replicate severe polymicrobial COVID-19-associated lesions documented in humans. Scant HMF was also observed in all BV hamsters on Day 7 PPI. This finding suggests that the primary bacterial infection might have caused enough structural injury to the microenvironment, such that the secondary viral infection induced additional damage that resulted in infrequent HMF. BO hamster lungs demonstrated minimal changes consistent with infection by a low virulent pathogen. The striking histopathological differences between the VO, VB, BO, and BV groups support that a secondary bacterial infection worsens the structural microenvironment when preceded by a viral infection and that the pathogen infection sequence impacts the disease severity phenotype.

Additional findings unique to our adult hamster VBP model were pulmonary hemorrhage, splenic contraction, and hepatic sinusoidal congestion. There was no erythrophagocytosis or hemosiderophages present within the regions of hemorrhage, both of which are findings that support ante-mortem pathophysiological hemorrhage. We hypothesize that given the decreased structural integrity of the pulmonary microenvironment secondary to inflammation in VB-infected hamsters, agonal and/or xylazine-induced perimortem hemorrhage occurred more readily as compared to the other infection groups on Day 7 PPI [34]. Splenic contraction observed in a subset of our VB-infected hamsters is of note because humans with severe sepsis can have a decreased splenic volume and an increased odds ratio for mortality [26, 35]. Mild acute sinusoidal congestion in the liver can be a secondary lesion associated with sepsis-induced, acute right heart failure, which is suspected in our VB hamsters that developed this lesion. By leveraging an adult hamster model, our study addresses the need for nonclinical models that better mirror high-risk patient populations.

The microbial analyses performed on the VB hamsters yielded mixed results at the Day 7 PPI timepoint, with some hamsters demonstrating positive microbial titers while others did not. One possible explanation for negative lung cultures is the patchy distribution of bacterial pneumonia. Since fresh lung tissue was only sampled from the right cranial and middle lobes,

bacteria may have been present in unsampled lobes. Alternatively, given the significant histopathological damage observed in all VB-infected hamster lungs, culture-negative cases might represent a state where an active bacterial infection had resolved, but the pathological damage incurred maintained the moderate-severe histopathologic phenotype. Additionally, it is important to note that wild-type Syrian hamsters are outbred, unlike inbred laboratory mice, which are genetically identical to one another. This increased genetic variation increases the variation of clinical responses observed in animal modeling studies [10], and may be a contributing factor to the variability observed in our VB-infected hamsters. The presence of positive viral titers in two VB hamsters is also noteworthy, as VBP studies in mice suggest that bacterial infection does not affect viral infection [30, 45, 50]. This finding may represent another key immunocompetency difference between outbred Syrian hamsters and inbred laboratory mice used for VBP studies.

This study provides critical insights into the pathogenesis of viral-bacterial pneumonia and underscores the translational value of this standardized adult Syrian hamster model in studying severe COVID-19 and secondary bacterial infections. The combined clinical findings, qRT-PCR results, and histopathology support that our VBP model induces a disease phenotype significantly distinct from the SARS-CoV-2 only infection model. Moreover, it establishes that adult hamsters more closely mimic the immune response of older human patients, which is consistent with immunosenescence and a dysregulated inflammatory response, both of which contribute to severe disease outcomes in COVID-19 [5, 53]. The built-in disease phenotype heterogeneity of this model will allow future researchers to compare molecular pathways of severely- and mildly-affected animals simultaneously to discern unique molecular signatures between these disease phenotypes and leverage novel interventional strategies. This VBP infection model incorporates the biological variables of host age and immune competency to serve as a supplemental model amenable to mechanistic and therapeutic interrogations with potential translational value to human populations.

REFERENCES

1. Arai S, Gohara Y, Akashi A, et al. Effects of new quinolones on Mycoplasma pneumoniae-infected hamsters. *Antimicrob Agents Chemother*. 1993;37(2):287.
2. Ball EE, Weiss CM, Liu H, et al. Severe Acute Respiratory Syndrome Coronavirus 2 Vasculopathy in a Syrian Golden Hamster Model. *Am J Pathol*. 2023;193(6):690.
3. Bantle CM, French CT, Cummings JE, et al. Manganese exposure in juvenile C57BL/6 mice increases glial inflammatory responses in the substantia nigra following infection with H1N1 influenza virus. *PLoS One*. 2021;16(1):e0245171.
4. Barman TK, Singh AK, Bonin JL, Nafiz TN, Salmon SL, *et al*. Lethal synergy between SARS-CoV-2 and Streptococcus pneumoniae in hACE2 mice and protective efficacy of vaccination. *JCI Insight*. 2022;7:e159422.
5. Bartleson JM, Radenkovic D, Covarrubias AJ, Furman D, Winer DA, Verdin E. SARS-CoV-2, COVID-19 and the Ageing Immune System. *Nat Aging*. 2021;1(9):769.
6. Beasley MB. Acute lung injury-from cannabis to COVID. *Mod Pathol*. 2022;35(Suppl 1):1.
7. Bogdan I, Gadela T, Bratosin F, et al. The Assessment of Multiplex PCR in Identifying Bacterial Infections in Patients Hospitalized with SARS-CoV-2 Infection: A Systematic Review. *Antibiotics (Basel)*. 2023;12(3):465.
8. Bosch AA, Biesbroek G, Trzcinski K, Sanders EA, Bogaert D. Viral and bacterial interactions in the upper respiratory tract. *PLoS Pathog*. 2013;9:e1003057.
9. Bösmüller H, Matter M, Fend F, Tzankov A. The pulmonary pathology of COVID-19. *Virchows Arch*. 2021;478(1):137.
10. Brekke TD, Steele KA, Mulley JF. Inbred or Outbred? Genetic Diversity in Laboratory Rodent Colonies. *G3 (Bethesda)*. 2018;8(2):679.
11. Bridges JP, Vladar EK, Huang H, Mason RJ. Respiratory epithelial cell responses to SARS-CoV-2 in COVID-19. *Thorax*. 2022;77(2):203.
12. Cardinal-Fernández P, Lorente JA, Ballén-Barragán A, Matute-Bello G. Acute Respiratory Distress Syndrome and Diffuse Alveolar Damage. New Insights on a Complex Relationship. *Ann Am Thorac Soc*. 2017;14(6):844.
13. Castellan M, Zamperin G, Franzoni G, Foiani G, Zorzan M, *et al*. Host Response of Syrian Hamster to SARS-CoV-2 Infection including Differences with Humans and between Sexes. *Viruses*. 2023;15:428.
14. Chai J, Capik SF, Kegley B, Richeson JT, Powell JG, Zhao J. Bovine respiratory microbiota of feedlot cattle and its association with disease. *Vet Res*. 2022;53:4.
15. Divangahi M, Aaby P, Khader SA, et al. Trained immunity, tolerance, priming and differentiation: distinct immunological processes [published correction appears in Nat Immunol. 2021 Jul;22(7):928.]. *Nat Immunol*. 2021;22(1):2.
16. Gheware A, Ray A, Rana D, et al. ACE2 protein expression in lung tissues of severe COVID-19 infection. *Sci Rep*. 2022;12(1):4058.
17. Gruber AD, Firsching TC, Trimpert J, Dietert K. Hamster models of COVID-19 pneumonia reviewed: How human can they be?. *Vet Pathol*. 2022;59:528.
18. Gruber AD, Osterrieder N, Bertzbach LD, et al. Standardization of Reporting Criteria for Lung Pathology in SARS-CoV-2-infected Hamsters: What Matters?. *Am J Respir Cell Mol Biol*. 2020;63(6):856.
19. Hackam DG, Redelmeier DA. Translation of research evidence from animals to humans. *JAMA*. 2006;296:1731.
20. Hagio T, Kishikawa K, Kawabata K, et al. Inhibition of neutrophil elastase reduces lung injury and bacterial count in hamsters. *Pulm Pharmacol Ther*. 2008;21(6):884.
21. Harkema JR, et al. “Chapter 6: Nose, Sinus, Pharynx, and Larynx.” *Comparative Anatomy and Histology - A Mouse, Rat, and Human Atlas*. 2nd ed. Academic Press, Cambridge, MA, 2018, pp. 89-114.

22. Hu GN, Liu WL, Chang CH, et al. Microbial dynamics, risk factors and outcomes of secondary pneumonia in critically ill patients with COVID-19: A multicenter retrospective cohort study. *J Formos Med Assoc*. 2024;123(11):1186.
23. Jia Y, Wang Y, Dunmall LSC, Lemoine NR, Wang P, *et al*. Syrian hamster as an ideal animal model for evaluation of cancer immunotherapy. *Front Immunol*. 2023;14:1126969.
24. Jiang Y, Zhao T, Zhou X, Xiang Y, Gutierrez-Castrellon P, Ma X. Inflammatory pathways in COVID-19: Mechanism and therapeutic interventions. *MedComm (2020)*. 2022;3(3):e154.
25. Kinoshita T, Watanabe K, Sakurai Y, Nishi K, Yoshikawa R, *et al*. Co-infection of SARS-CoV-2 and influenza virus causes more severe and prolonged pneumonia in hamsters. *Sci Rep*. 2021;11:21259.
26. Koga Y, Fujita M, Nakahara T, et al. Splenic volume in severe sepsis is associated with disease severity and pneumococcal infection. *Acute Med Surg*. 2016;3(4):339.
27. Kropinski AM, Mazzocco A, Waddell TE, Lingohr E, Johnson RP, "Enumeration of bacteriophages by double agar overlay plaque assay" in Bacteriophages, Clokie M. R. J., Kropinski A. M., Eds. (Methods in Molecular Biology, Humana Press, Totowa, NJ, 2009), Vol. 501, pp. 69–76.
28. Langford BJ, So M, Simeonova M, Leung V, Lo J, *et al*. Antimicrobial resistance in patients with COVID-19: a systematic review and meta-analysis. *Lancet Microbe*. 2023;4:e179.
29. Lee MH, Arrecubieta C, Martin FJ, Prince A, Borczuk AC, Lowy FD. A postinfluenza model of Staphylococcus aureus pneumonia. *J Infect Dis*. 2010;201(4):508.
30. Lee LN, Dias P, Han D, Yoon S, Shea A, *et al*. A mouse model of lethal synergism between influenza virus and Haemophilus influenzae. *Am J Pathol*. 2010;176:800.
31. LVG Golden Syrian Hamster, https://www.criver.com/products-services/find-model/lvg-golden-syrian-hamster?region=3611. Accessed 25 March 2024.
32. Manohar P, Loh B, Nachimuthu R, Hua X, Welburn SC, *et al*. Secondary Bacterial Infections in Patients With Viral Pneumonia. *Front Med*. 2020;7:420.
33. Miao J, Chard LS, Wang Z, Wang Y. Syrian Hamster as an Animal Model for the Study on Infectious Diseases. *Front Immunol*. 2019;10:2329.
34. Miller DL, Dou C, Raghavendran K. Anesthetic techniques influence the induction of pulmonary capillary hemorrhage during diagnostic ultrasound scanning in rats. *J Ultrasound Med*. 2015;34(2):289.
35. Mitsuyama Y, Shimizu K, Hirayama A, et al. Splenic volume on computed tomography scans is associated with mortality in patients with sepsis. *Int J Infect Dis*. 2021;104:624.
36. Nouailles G, Wyler E, Pennitz P, Postmus D, Vladimirova D, *et al*. Temporal omics analysis in Syrian hamsters unravel cellular effector responses to moderate COVID-19. *Nat Commun*. 2021;12:4869.
37. Oishi K, Horiuchi S, Frere J, Schwartz RE, tenOever BR. A diminished immune response underlies age-related SARS-CoV-2 pathologies. *Cell Rep*. 2022;39:111002.
38. Olfert ED, Godson DL. Humane endpoints for infectious disease animal models. *ILAR J*. 2000;41:99.
39. Ordonez AA, Wintaco LM, Mota F, et al. Imaging *Enterobacterales* infections in patients using pathogen-specific positron emission tomography. *Sci Transl Med*. 2021;13(589):eabe9805.
40. Osterrieder N, Bertzbach LD, Dietert K, Abdelgawad A, Vladimirova D, *et al*. Age-Dependent Progression of SARS-CoV-2 Infection in Syrian Hamsters. *Viruses*. 2020;12:779.
41. Pirolo M, Espinosa-Gongora C, Bogaert D, Guardabassi L. The porcine respiratory microbiome: recent insights and future challenges. *Anim Microbiome*. 2021;3:9.

42. Poje, G, Redfield, R. (2003). General Methods for Culturing *Haemophilus influenzae* . In: Herbert, M.A., Hood, D.W., Moxon, E.R. (eds) Haemophilus influenzae Protocols. Methods in Molecular Medicine, vol 71. Humana Press.
43. Ramasamy S, Subbian S. Critical Determinants of Cytokine Storm and Type I Interferon Response in COVID-19 Pathogenesis [published correction appears in Clin Microbiol Rev. 2021 Dec 15;34(4):e0016321.]. *Clin Microbiol Rev*. 2021;34(3):e00299.
44. Rocha SM, Fagre AC, Latham AS, et al. A Novel Glucocorticoid and Androgen Receptor Modulator Reduces Viral Entry and Innate Immune Inflammatory Responses in the Syrian Hamster Model of SARS-CoV-2 Infection. *Front Immunol*. 2022;13:811430.
45. Seki M, Yanagihara K, Higashiyama Y, Fukuda Y, Kaneko Y, *et al*. Immunokinetics in severe pneumonia due to influenza virus and bacteria coinfection in mice. *Eur Respir J*. 2004;24:143.
46. Sellers RS. Translating Mouse Models. *Toxicol Pathol*. 2017;45:134.
47. Selvaraj P, Lien CZ, Liu S, Stauft CB, Nunez IA, *et al*. SARS-CoV-2 infection induces protective immunity and limits transmission in Syrian hamsters. *Life Sci Alliance*. 2021;4:e202000886.
48. Sievers BL, Cheng MTK, Csiba K, Meng B, Gupta RK. SARS-CoV-2 and innate immunity: the good, the bad, and the "goldilocks". *Cell Mol Immunol*. 2024;21(2):171.
49. Sili U, Tekin A, Bilgin H, Khan SA, Domecq JP, *et al*. Early empiric antibiotic use in COVID-19 patients: results from the international VIRUS registry. *Int J Infect Dis*. 2024;140:39.
50. Smith AP, Williams EP, Plunkett TR, Selvaraj M, Lane LC, *et al*. Time-Dependent Increase in Susceptibility and Severity of Secondary Bacterial Infections During SARS-CoV-2. *Front Immunol*. 2022;13:894534.
51. Sudhadevi T, Ha AW, Harijith A. A Minimally Invasive Method for Intratracheal Instillation of Drugs in Neonatal Rodents to Treat Lung Disease. *J Vis Exp*. 2021;(174):10.3791/61729.
52. Terry JS, Anderson LB, Scherman MS, et al. Development of a SARS-CoV-2 nucleocapsid specific monoclonal antibody. *Virology*. 2021;558:28.
53. Tizazu AM, Mengist HM, Demeke G. Aging, inflammaging and immunosenescence as risk factors of severe COVID-19. *Immun Ageing*. 2022;19(1):53.
54. Verghese A, Catanese A, Arbeit RD. Staphylococcus aureus pneumonia in hamsters with elastase-induced emphysema--the virulence enhancing activity of mucin. *Proc Soc Exp Biol Med*. 1988;188(1):1.
55. Warner BM, Safronetz D, Kobinger GP. Syrian Hamsters as a Small Animal Model for Emerging Infectious Diseases: Advances in Immunologic Methods. *Adv Exp Med Biol*. 2017;972:87.
56. Wilson E, Ramage FJ, Wever KE, Sena ES, Macleod MR, *et al*. Designing, conducting, and reporting reproducible animal experiments. *J Endocrinol*. 2023;258:e220330.
57. Yen HL, Valkenburg S, Sia SF, Choy KT, Peiris JSM, *et al*. Cellular tropism of SARS-CoV-2 in the respiratory tract of Syrian hamsters and B6.Cg-Tg(K18-ACE2)2Prlmn/J transgenic mice. *Vet Pathol*. 2022;59:639.
58. Zhao Y, Howatt DA, Gizard F, et al. Deficiency of the NR4A orphan nuclear receptor NOR1 decreases monocyte adhesion and atherosclerosis. *Circ Res*. 2010;107(4):501.
59. Li Q, Vijaykumar K, Phillips SE, et al. Mucociliary transport deficiency and disease progression in Syrian hamsters with SARS-CoV-2 infection. *JCI Insight*. 2023;8(1):e163962.
60. Seibert B, Cáceres CJ, Carnaccini S, et al. Pathobiology and dysbiosis of the respiratory and intestinal microbiota in 14 months old Golden Syrian hamsters infected with SARS-CoV-2. *PLoS Pathog*. 2022;18(10):e1010734.

61. Shah V. Letter to the Editor: Microbiota in the Respiratory System-A Possible Explanation to Age and Sex Variability in Susceptibility to SARS-CoV-2. *Microbiol Insights*. 2021;14:1178636120988604.
62. Ueki H, Kiso M, Furusawa Y, et al. Development of a Mouse-Adapted Reporter SARS-CoV-2 as a Tool for Two-Photon In Vivo Imaging. *Viruses*. 2024;16(4):537.
63. Hernández-Terán A, Mejía-Nepomuceno F, Herrera MT, Barreto O, García E, *et al*. Dysbiosis and structural disruption of the respiratory microbiota in COVID-19 patients with severe and fatal outcomes. *Sci Rep*. 2021;11:21297.
64. Belizário J, Garay-Malpartida M, Faintuch J. Lung microbiome and origins of the respiratory diseases. *Curr Res Immunol*. 2023;4:100065.

CHAPTER 4 – ASSESSMENT OF MODULATING HOST PATHWAY RESPONSES WITH HOST-DIRECTED THERAPEUTICS AS A TREATMENT STRATEGY IN THE VBP MODEL

INTRODUCTION

Current FDA-approved anti-SARS-CoV-2 drugs target the SARS-CoV-2 main protease (M^{pro}) and RNA-dependent RNA polymerase (NSP12); however, numerous investigative drugs have attempted other viral targets such as spike proteins, spike-ACE2 interactions, and helicase [18]. Alternatively, antiviral agents can also target host structures to minimize viral replication. Clinical trial anti-SARS-CoV-2 drugs primarily targeting either ACE2 or TMPRSS2 have received the most research in this scenario. An issue with these drugs has been that SARS-CoV-2 can enter host cells in ways other than through ACE2 or TMPRSS2. As such, targeting ACE2 or TMPRSS2 individually still allows other pathways for SARS-CoV-2 to enter host cells.

Severe COVID-19 can result in hyperinflammation that leads to cytokine storm. This stage tends to occur once viral titers are in decline. As such, numerous therapeutic investigations have targeted the host immune response to mitigate hyperinflammation. Two immunomodulating drugs have been approved by the FDA for the treatment of COVID-19, as well as several immunomodulators that have been granted emergency use authorization such as vilobelimab (GOHIBIC [InflaRx]) – a recombinant chimeric monoclonal antibody against C5a [10]. Dexamethasone has also been recommended as an adjunctive therapy in patients receiving supplemental oxygen.

Three studies have assessed combinatorial treatment of antiviral and corticosteroid therapeutics in 5-8-week-old Syrian hamsters infected with SARS-CoV-2 that showed synergistic effects in overcoming infection [27, 34, 35]; however, no studies have been performed in aged hamsters or under VBP experimental conditions. Given the hyperinflammatory state that a subset of adult male Syrian hamsters develop in our VBP infection model, we investigated the application of one host-directed antiviral therapeutic with immunomodulatory properties, PT150, and three

immunomodulators: meloxicam, cenerimod, and baricitinib. These tool compounds disrupt different host cellular and pro-inflammatory pathways, allowing us to evaluate if these selected pathway modulations could serve as potential therapeutic targets.

PT150 is a clinical-stage synthetic glucocorticoid receptor modulator that can also decrease the expression of androgen receptor-related genes [26, 30]. Although PT150 is classified as an androgen receptor (AR) and glucocorticoid receptor (GR) antagonist, PT150 may possess minor GR agonist activity [30]. GR agonist activity promotes the induction of anti-inflammatory proteins, such as annexin I, while inhibiting pro-inflammatory pathways, such as prostaglandin production [25]. ACE2 and TMPRSS2 are transcriptionally regulated by the androgen receptor [24], and both proteins are utilized by SARS-CoV-2 for host cell entry. As such, PT-150 mediated downregulation of ACE2 and TMPRSS2 could decrease SARS-CoV-2 viral entry by limiting two commonly utilized entry points for infection. PT150 has been assessed in 8-week-old, male and female Syrian hamsters infected with intranasal SARS-CoV-2, which resulted in decreased replication of SARS-CoV-2 in the lung as well as decreased ACE2 and TMPRSS2 pulmonary expression [26]. PT150 treatment in this study was started on the day of the virus challenge and administered daily until the final study endpoint 7 days post-viral infection (PVI).

IL-6 is an important pro-inflammatory cytokine contributing to the induction of systemic acute-phase responses. Older adults who develop severe COVID-19 are likelier to exhibit an imbalanced cytokine response during infection that results in a dysregulated pro-inflammatory state, and IL-6 is commonly implicated in this cytokine storm development [21]. Therefore, modulating IL-6 production is an attractive target to mitigate this hyperinflammatory response. Macrophages and bronchial epithelium can synthesize IL-6 via prostaglandin PGE_2 stimulation, and inhibition of COX-2 partly attenuates PGE_2 and IL-6 release [5, 9, 32, 37]. One such therapeutic mechanism to down-modulate IL-6 production is via non-steroidal anti-inflammatory drugs (NSAID). Meta-analyses revealed that the use of NSAIDs during COVID-19 treatment did not worsen patient outcomes and warrants further assessment of NSAIDs for patients hospitalized

with COVID-19 [17, 36]. Meloxicam is an NSAID that preferentially inhibits pro-inflammatory COX-2 more than constitutively expressed COX-1 [33]. It has been well-studied in both human and veterinary species. By negatively modulating COX-2, we anticipated a reduction in prostaglandin-mediated inflammation and subsequent lung damage caused by excessive immune activation secondary to VBP.

Innate lymphoid cells (ILCs) and lymphocytes are critical in elaborating cytokines that initiate innate immunity and direct T helper cell responses. Modulating this subset of cells may mitigate immune cell overactivation and subsequent cytokine overproduction. The $S1P_1$ receptor is highly expressed in endothelial cells and is the predominant S1P receptor subtype expressed in lymphocytes, including ILCs, and is also expressed on dendritic cells (DCs) [14, 16, 23]. Given the hyperinflammation and pulmonary edema associated with SARS-CoV-2 infection, modulating immune cell activity and maintaining endothelial integrity may be accomplished with the selective $S1P_1$ receptor antagonist, cenerimod. Cenerimod is an investigational drug being evaluated for use in autoimmune diseases to inhibit the egress of lymphocytes from lymphoid organs, reduce circulating antigen-presenting cells, and reduce plasma IFNα levels [15, 29]. When administered at a low dosage, we hypothesized that the predominant therapeutic features would be an anti-inflammatory effect on lymphocytes, ILCs, and DCs, as well as maintained vascular integrity.

Acute phase response cytokines, such as IL-6 and IL-1β, can signal through the JAK/STAT pathway to promote systemic innate immune responses. These cytokines are also commonly implicated in the development of cytokine storms. Baricitinib is a selective JAK1/JAK2 inhibitor and is labeled for the treatment of COVID-19 as a monotherapy or adjunctive therapy in patients with severe COVID-19 [2 ,7, 28]. It has also been postulated that baricitinib may possess antiviral properties by inhibiting host AP2-associated protein kinase-1 and cyclin G-associated kinase that facilitate SARS-CoV-2 internalization via clathrin-mediated endocytosis [14]. Moreover, it reduced neutrophil recruitment and pulmonary macrophage inflammation in the lungs of SARS-

CoV-2 infected rhesus macaques [13]. Given the predominance of neutrophils and macrophages observed in our VB-infected hamster lungs, and that baricitinib is labeled as a monotherapy, we hypothesized that this JAK1/JAK2 inhibitor would serve as an effective modulating arm in our VBP hamster model.

Despite the hundreds of clinical trials assessing antiviral and immunomodulating agents for the treatment of COVID-19, only four drugs have received full FDA approval. Recognizing the need for innovative treatment strategies, we investigated the utility of several host-directed therapeutics in our adult male hamster VBP infection model. Assessment of these host-directed tool compounds provides foundational insights toward filling the knowledge gap of HDTs as a therapeutic strategy for polymicrobial pneumonia treatment.

METHODS & MATERIALS

Virus and cell culture procedures

All *in vitro* and *in vivo* infectious virus work was performed in a biosafety level 3 (BSL-3) facility at Colorado State University. SARS-CoV-2 virus strain WA1/2020WY96 was graciously donated by Dr. Angela Bosco-Lauth. The virus was passaged four times in Vero E6 cells using Dulbecco's Modified Eagle Medium supplemented with 8% heat-inactivated fetal bovine serum and 1% penicillin-streptomycin. Clarified viral stocks were supplemented with 10% heat-inactivated fetal bovine serum and frozen at −70°C. Virus stock and lung homogenate titrations were performed using a double-overlay plaque assay as previously described [27]. Briefly, 6-well plates with 85% confluent monolayers of cells were inoculated with 100 uL of serial 10-fold dilutions of samples, incubated for 1 hour at 37°C, and overlaid with a 0.55% noble agar in Temin's Modified Eagle Medium containing 2.5% heat-inactivated fetal bovine serum and 1% penicillin-streptomycin. Plates were wrapped in parafilm to minimize desiccation. A second overlay containing 4% neutral red dye was added at 69 hours and plaques were counted at 72 hours. Plaque formation was confirmed by microscopic quantification.

Bacteria and agar/broth culture procedures

Frozen glycerol stocks of *Haemophilus influenzae* serotype B (ATCC 10211) were streaked onto supplemented chocolate agar plates (sCAP) consisting of gonococcal agar base, 1% bovine hemoglobin, and 2% IsoVitaleX. Bacterial colonies were incubated for 17 hours in 5% CO2 at 37°C. Isolated colonies were selected and inoculated into supplemented Brain Heart Infusion broth (sBHI) consisting of BHI liquid culture, hemin (10 ug/mL), and nicotinamide (10 ug/mL) to a starting optical density (OD600) of 0.05. Liquid culture flasks were loosely capped and grown in a shaking incubator at 200 RPM, 37°C until bacteria reached mid-log growth at approximately 4.5 hours. For hamster infections, bacterial broth suspensions were centrifuged three times at 3,400 RPM for 5 minutes. Centrifuged bacterial pellets were resuspended in 5% sBHI. Infection inoculum contained 5% sBHI because *H. influenzae* suspended in plain PBS rapidly loses viability [42]. Inocula and organ homogenate bacterial titers were confirmed via serial 10-fold dilution and plating onto sCAP, followed by incubation for 13-18 hours in 5% CO2 at 37°C.

Animals

35 adult male Syrian hamsters (39—44-week-old) were obtained from Charles River Laboratory (Kingston, NY). Animals were housed individually and maintained on a 12:12 light-dark cycle at 20-25°C in an Animal Biosafety Level-3 facility at Colorado State University. Hamsters had access to food and water *ad libitum* and were acclimated for at least seven days before infection. Studies were performed in male hamsters due to their increased susceptibility and associated pathology to SARS-CoV-2 infection compared to female hamsters [13]. Additionally, it was financially infeasible to house female hamsters until the required adult age for study parameters.

Animal anesthetic procedures and pathogen challenge

For viral intranasal infection, hamsters were anesthetized by inhalation with isoflurane gas, placed in dorsal recumbency, and intranasally inoculated with 2.8×10^4 plaque-forming units (PFU) SARS-CoV-2 for a total volume of 100 uL. Post-viral infection, hamsters were manually restrained in a 60-degree position until conscious to promote the distal migration of viral inoculum into the lower respiratory tract.

For bacterial non-surgical intratracheal infection, hamsters were lightly anesthetized by inhalation with isoflurane gas followed by intraperitoneal injection of ketamine and xylazine (90 mg/kg and 9 mg/kg, respectively). Our non-surgical intratracheal approach was adapted from Sudhadevi et al. Briefly, hamsters were placed in dorsal recumbency, restrained on a 60-degree inclined board, and an otoscope light source was used to visualize the rima glottidis. Inocula were administered into the trachea via a 200 uL gel-loading pipette tip affixed to a 1 mL syringe. The base of the pipette was trimmed to ensure a secure fit onto the syringe. Before loading the syringe with bacteria, 0.5 mL of room air was aspirated into the syringe hub to facilitate distal instillation of bacterial inoculum into the lower respiratory tract. Bacterial inoculum was approximately 4.0×10^9 colony-forming units (CFU) HiB for a total volume of 160 uL.

Administering host-directed therapeutics

A delayed dosing model of VB-infected hamsters was utilized such that treatments were initiated at the start of clinical signs, which is 48 hours PVI in Syrian hamsters. This delayed dosing schedule was selected to more accurately reflect human disease progression and practical treatment timelines. Treatments were administered once daily for three consecutive days (i.e., Days 2-4 PVI). Experimental groups were as follows: PT150-only (per os [PO] 75 mg/kg), meloxicam-only (subcutaneous [SQ] 2 mg/kg), PT150 + meloxicam (PO 75 mg/kg and SQ 2 mg/kg, respectively), cenerimod-only (PO 0.3 mg/kg), and baricitinib-only (PO 10 mg/kg). Eight hamsters per group were used for PT150-only, meloxicam-only, and PT150 + meloxicam. The

four hamsters with the greatest weight loss and lowest activity level on Day 7 PVI were selected for the Day 7 study endpoint. The remaining four hamsters in each group were terminated at the Day 14 study endpoint. After the PT150 and meloxicam studies were completed, the cenerimod and baricitinib studies were performed as follow up studies to assess modulation of other inflammatory pathways. Six and five hamsters per group were used for cenerimod and baricitinib treatment groups, respectively, and all were euthanized on Day 7 PVI. These hamsters were only assessed at the Day 7 PVI endpoint because the previous studies indicated that Day 7 PVI was the critical timepoint to assess therapeutic efficacy in moderately to severely affected VBP hamsters. For the cenerimod and baricitinib groups, the four hamsters with the greatest weight loss and lowest activity level on Day 7 PVI were selected for histopathologic and microbial assessments.

Hamsters were weighed daily to deliver an appropriate drug dose, and all treatments were administered under isoflurane anesthesia. Prior to loading the oral gavage syringe with drug, 0.2 mL of room air was aspirated into the syringe hub to ensure that medications were completely evacuated from the gavage needle upon delivery. Similarly, syringes used for subcutaneous injections were aspirated with 0.02 mL room air to ensure meloxicam was evacuated from the needle shaft and hub upon subcutaneous delivery.

In humans infected with SARS-CoV-2, individuals remain infectious for approximately 10 days and the recommended length of treatment for oral SARS-CoV-2 antiviral medication is five days [1, 3]. In Syrian hamsters infected with SARS-CoV-2, viral titers are detectable for six days [6]. As such, we chose to administer PT150 for three days to simulate a similar dosing period to that recommended in humans. Meloxicam was administered for only three days to avoid NSAID-induced toxic side effects [8]. Cenerimod and baricitinib were additionally assessed as host-directed therapeutics using the same three-day dosing schedule.

PT150 was supplied by Palisades Therapeutics/Pop Test Oncology LLC. PT150 was suspended in GSP excipient solution (10% Gelucire 44/14, 10% Solutol HS 15, 30% Propylene

Glycol, 50% DPBS) to a concentration of 15 mg/mL and delivered by oral gavage at 75 mg/kg once daily for three days. PT150 was vortexed before each oral gavage dose. Animal doses were normalized to body surface area to estimate the human equivalent dose (HED); HED = animal dose in mg/kg × (animal weight in kg/human weight in kg)$^{0.33}$ [31]. Using this equation, the hamster HED was 10.7 mg/kg. Relatedly, one study assessing clinical safety dosing of PT150 in healthy human males used a PT150 dosage of approximately 11.1 mg/kg [20].

Meloxicam (OstiLox 5 mg/mL [MWI Animal Health]) was delivered subcutaneously at 2 mg/kg once daily for three days [12]. Before injection, the fur was wetted with sterile saline to visualize the skin surface better and ensure accurate drug delivery. Meloxicam was administered using a 1 mL 26G × ⅜ allergy syringe. Each of the three injections were delivered at a different subcutaneous site: left shoulder for the first treatment dose, right thorax for the second treatment dose, and left flank for the third treatment dose. For the PT150 + meloxicam treatment group, both drugs were administered at the same time.

Both cenerimod (HY-17606, MedChemExpress) and baricitinib (HY-15315A, MedChemExpress) were suspended in an excipient solution consisting of 10% DMSO, 40% PEG400, 5% Tween-80, and 45% DPBS and delivered by oral gavage once daily for three days. Both drugs were kept warm in a water bath in between administrations and vortexed before each oral gavage dose. Cenerimod (1 mg/mL) was administered at a dose of 0.3 mg/kg, based on Piali et al., which demonstrated that circulating lymphocyte counts in Wistar rats return to baseline within 24 hours at this dosage. Baricitinib (5 mg/mL) was administered at a dose 10 mg/kg, as adapted from Fridman et al., which identified this dosage as the most effective for reducing bone resorption in a Lewis rat arthritis model. When hamster-specific medication dosages are unavailable, lab animal formularies recommend extrapolating from rat-specific dosages [11].

Antibacterial therapeutics were not assessed in these studies to determine if targeting host-directed antiviral or immunomodulation pathways alone could lessen VBP disease severity in our hamster infection model. Historic controls were used for the positive (infected, untreated)

and negative (mock-infected, untreated) control groups. No mock-infected, treated controls were used in this study.

Necropsy and histopathology

On Days 7 and 14 PPI, four hamsters per group were sacrificed via lethal overdose of ketamine and xylazine (500 mg/kg and 20 mg/kg, respectively), followed by terminal intracardiac blood collection and cervical dislocation. A board-certified veterinary anatomic pathologist performed tissue harvesting and complete post-mortem examinations. Lung, kidney, and spleen tissues were collected for bacterial culture; these tissues were used instead of blood to assess for bacterial dissemination. Fresh lung tissue was also obtained for viral titers and qRT-PCR. Tissues collected for microbial and qRT-PCR analyses were homogenized using a Precellys Evolution Touch Homogenizer (Bertin Instruments). The corresponding bronchioles were ligated with a string after fresh lung tissue specimens were obtained from the right cranial and middle lobes. The remaining lung lobes were inflated by tracheal instillation of 10% neutral-buffered formalin using a 5 mL syringe attached to 30 cm IV tubing until the lung lobes were fully expanded. Standard diagnostic tissue collection for formalin fixation was performed, and select organs were reviewed for histopathology. Harvested organs were fixed in 10% neutral-buffered formalin under BSL-3 containment for three days.

Trimmed histopathological tissues were processed routinely, paraffin-embedded, and stained with hematoxylin and eosin on an automated staining system (Bond-Max; Leica). Immunohistochemistry (IHC) detection for the SARS-CoV-2 nucleocapsid was also performed in all virus-infected hamster groups using a monoclonal antibody generated by Terry et al. The initial histopathology slide review was performed as a partially masked review by a board-certified veterinary anatomic pathologist. Histopathological analysis was performed on four transverse lung sections (two left lobe [cranial and middle regions], one accessory lobe, and one right caudal lobe) using lung-specific scoring parameters. Our VBP scoring scheme was adapted from those

developed for Syrian hamster SARS-CoV-2 respiratory infections [2, 18]. Lesions were semiquantitatively scored for each of the four lung tissue sections obtained from each animal in each group, and the predominant lesion feature was used to calculate the score. Anatomic lesion categories assessed in this scoring scheme included bronchiolar, alveolar, alveolar space contents, pleural, vascular/perivascular, and overall percent of tissue affected. An additional point was awarded for the presence of hyaline membranes, intra-alveolar organizing fibrin, foci of pulmonary necrosis, or pericarditis (see Table 3 for complete scoring scheme). Lesion features, but not points, were cumulative within each category. For example, if an animal was awarded a "2" for alveolar lesions, interstitial inflammation was the predominant lesion, but alveolar type 2 (AT2) cell hyperplasia was also present. Pulmonary findings noted but not included in scoring were atypical or multinucleated epithelial cells (i.e., syncytia) and degree of pulmonary hemorrhage.

Lung tissue relative gene expression profiling using quantitative real-time PCR

For measurement of host relative gene expression, total RNA was extracted from lung homogenate with TRIzol Reagent, 5 mm stainless steel beads, and a Precellys Evolution Touch Homogenizer (Bertin Instruments) under BSL-3 conditions. Total RNA was then isolated from individual samples by TRIzol/phenol-chloroform extraction as previously described [3]. RNA purity and concentration were confirmed using a NanoDrop One C (Thermo Scientific) and Qubit 4 Fluorometer (Invitrogen). Primer pairs were developed using NCBI Primer-BLAST with PCR efficiency values of 1.95-2.1. *Actb* (Beta-actin) was used as the internal standard reference gene. Primer pairs used in qRT-PCR are listed in Table 4. cDNA was prepared from total RNA samples using RevertAid First Strand cDNA Synthesis kit (Thermo Scientific). Both the generated cDNA used in qRT-PCR assays on a Roche LightCycler 480 and the resultant Cp values used to calculate relative gene expression were performed as previously described by Rocha et al. All

biological samples (n = 3/group) were quantified independently in technical duplicate. The same genes that were assessed in Chapter 3 were also assessed in Chapter 4.

Statistical analysis

All data is presented as mean ± standard deviation (SD). Differences between two variables were identified using a two-way ANOVA statistical test followed by Tukey's *post hoc* test for multiple comparisons. Significance is denoted as $*p < 0.05$, $**p < 0.01$. All statistical analyses were conducted in Prism.

RESULTS

Host-directed therapeutics induce mixed results in adult male VB-infected hamsters.

Body weight changes were tracked daily throughout the study to indicate disease severity. Compared to infected, untreated hamsters, PT150-only treated hamsters demonstrated the least amount of weight loss at all timepoints (Fig. 14). One meloxicam-only treated hamster was humanely euthanized on Day 6 PVI; three PT150 + meloxicam treated hamsters were humanely euthanized (one on Day 5 PVI and two on Day 6 PVI). None of these four hamsters lost more than 16% of their pre-challenge weight; however, all hamsters were ataxic with subjectively cool paws suggestive of shock.

The hamsters that were part of the Day 7 PVI study endpoint were labeled as the "survival phenotype" and consisted of the following numbers of hamsters per treatment group: PT150-only (4), meloxicam-only (3), PT150 + meloxicam (1), cenerimod-only (4), and baricitinib-only (4). Similar to Chapter 3, although a subset of PT150-only, meloxicam-only, and PT150 + meloxicam treated hamsters were maintained until Day 14 PVI, these hamsters recovered unremarkably despite their relatively plateaued weight loss (Fig. 14). As such, this chapter focuses on the Day 7 PVI time point, which assesses the most susceptible hamsters in each treatment group.

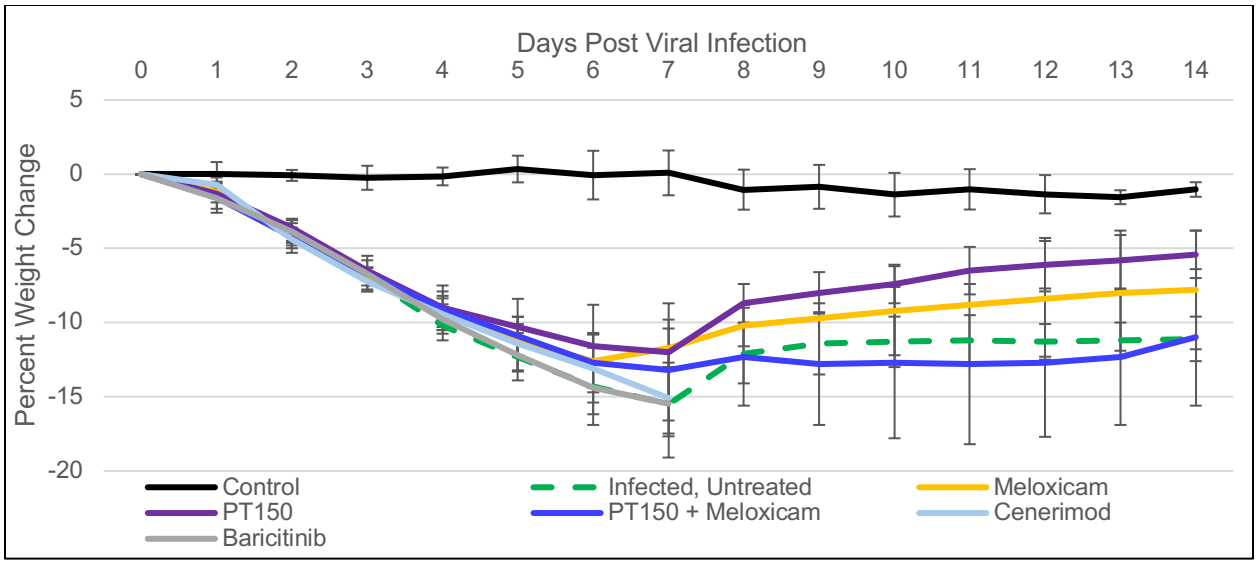

Figure 14. Body weight changes in adult male Syrian hamsters treated with HDTs during VBP infection. Body weight changes in hamsters infected with 10^4 PFU CoV2 intranasally on Day 0 and 10^9 CFU HiB intratracheally on Day 2.5, and treated with different HDTs on Days 2-4. Control, PT150, meloxicam, and PT150 + meloxicam groups had *n* = 8 hamsters/group on Days 0-7 and *n* = 4 hamsters/group on Days 8-14. Cenerimod group had *n* = 6 hamsters through Day 7, and baricitinib group had *n* = 5 hamsters through Day 7. No cenerimod or baricitinib hamster groups were maintained after Day 7. Control hamsters were administered intranasal (Day 0) and intratracheal (Day 2.5) PBS. Mean percent body weight change at Day 0 ± SD is shown at each consecutive day. HDTs: host-directed therapeutics; VBP: primary viral-secondary bacterial pneumonia; PFU: plaque-forming units; CoV2: SARS-CoV-2; CFU: colony-forming units; HiB: *Haemophilus influenzae* serotype B.

Gross pathology and histopathological analysis on Day 7 PVI.

At necropsy, PT150-only and meloxicam-only treated hamsters euthanized on Day 7 PVI demonstrated similar gross lesions of multifocal to widespread congestion with variably non-collapsing lung lobes (Figs. 15 B1-B4 and C2-C4, respectively). The one PT150 + meloxicam hamster and all cenerimod treated hamsters displayed similar but mildly increased lesion severity as the aforementioned hamster groups (Figs. 15 D4 and E1-E4, respectively); baricitinib treated hamster lungs demonstrated the most pronounced congestion and hemorrhage throughout all lung lobes (Figs. 15 F1-F4). Lung lobes of the one meloxicam-only and three PT150 + meloxicam treated hamsters euthanized prior to the Day 7 PVI endpoint displayed near diffuse pulmonary hemorrhage and markedly non-collapsing lungs (Figs. 15 C1 and D1-D3, respectively).

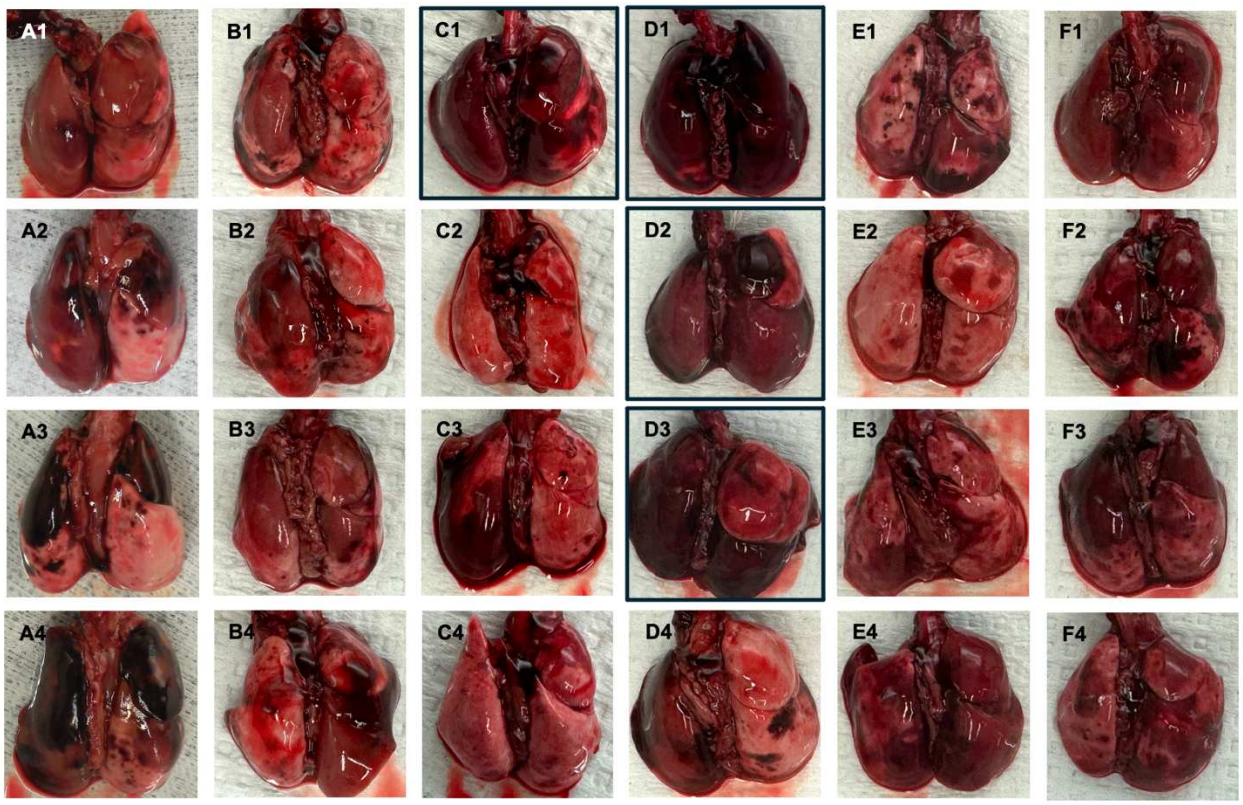

Figure 15. Gross lung pathology on Day 7 PVI of adult male Syrian hamsters treated with HDTs during VBP infection. All hamsters were treated on Days 2-4 PVI. **A1-A4**. Positive Control hamster lungs are moderately non-collapsing and include coalescing to widespread regions of congestion and hemorrhage. **B1-B4**. PT150 treated hamsters. Lungs demonstrate similar but less severe lesions as untreated hamsters. **C1-C4**. Meloxicam treated hamsters. Lungs include small, multifocal to coalescing regions of congestion. **D1-D4**. PT150 + meloxicam treated hamsters. **E1-E4**. Cenerimod treated hamsters. **F1-F4**. Baricitinib treated hamsters. Groups **D**, **E**, and **F** lungs demonstrate similar lesions as untreated hamsters. Images outlined in black indicate hamsters that were euthanized prior to the Day 7 PVI study endpoint. PVI: post-viral infection; HDTs: host-directed therapeutics; VBP: primary viral-secondary bacterial pneumonia; Positive Control: untreated hamsters infected with intranasal SARS-CoV-2 10^4 PFU on Day 0 and intratracheal *Haemophilus influenzae* serotype B 10^9 CFU on Day 2.5; PFU: plaque-forming units; CoV2: SARS-CoV-2; CFU: colony-forming units.

Pulmonary histopathology of the “survival phenotype” hamsters revealed unique, semiquantitative differences between most of the treatment groups on Day 7 PVI (Fig. 16F). PT150 treatment lungs demonstrated regionally extensive, moderate alveolar type 2 (AT2) cell hypertrophy with minimal lymphohistiocytic interstitial pneumonia and mild mononuclear cell infiltrate within alveolar spaces (Fig. 16B). This lesion pattern was reminiscent of virus-only

infected hamsters (Chapter 3). Interestingly, the meloxicam treated hamster lungs revealed multifocal, mild to moderate lymphohistiocytic interstitial pneumonia with mild AT2 cell hyperplasia and mild mononuclear cell infiltrate within alveolar spaces (Fig. 16C).

The single PT150 + meloxicam treated hamster on Day 7 PVI had near identical lesions as the infected, untreated hamsters: moderate to severe bronchointerstitial pneumonia with moderate intra-alveolar neutrophils, macrophages, cellular debris, hyaline membrane formation (HMF), and patchy organizing fibrin plugging alveolar spaces (Figs. 16A and 16D).

Although cenerimod and baricitinib affected lungs had the greatest amount of affected lung tissue (i.e., 50-100% of tissue sections comprised of moderate mixed inflammatory cell bronchointerstitial pneumonia with AT2 cell hyperplasia, HMF and/or organizing intra-alveolar fibrin; Fig. 16E), only two out of the four tissue sections assessed demonstrated these lesions. The remaining two tissue sections for hamsters in these groups had similar, but significantly less extensive, lesions occupying only 5-15% of the tissue sections.

The four hamsters euthanized prior to the Day 7 PVI study endpoint were not included in the histopathologic scoring; however, all demonstrated similar pulmonary pathology as infected, untreated VB hamsters, albeit with more hemorrhage. As in Chapter 3, all hemorrhage was attributed to decreased structural integrity of the pulmonary microenvironment secondary to inflammation, which presumably supported agonal and/or xylazine-induced perimortem hemorrhage more readily [19]. Neither gross gastric lesions nor histopathologic renal lesions were observed in these animals; however, definitive renal function in these hamsters remains unknown as serum biochemical profiles and urine analyses were not performed.

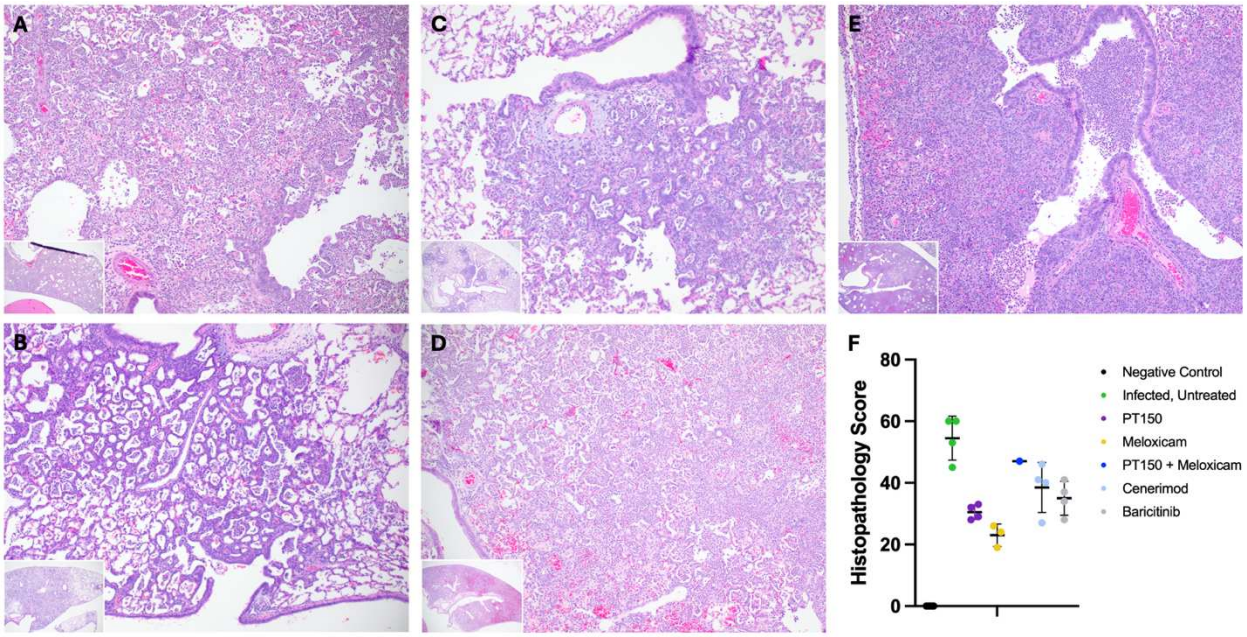

Figure 16. Combined lung histopathology photomicrographs and histopathology score summary on Day 7 PVI in adult male Syrian hamsters treated with HDTs during VBP infection. All photomicrographs are stained with hematoxylin and eosin and captured at 10× magnification; all insets are captured at 4× magnification. **A.** Positive Control hamster. Alveolar epithelium is mildly hypertrophied with low numbers of mixed inflammatory cells within interstitial spaces. Alveolar spaces are variably filled with either foamy macrophages, neutrophils, hyaline membranes or organizing fibrin. **B.** PT150 treated hamster. Alveolar septa are lined by hypertrophied AT2 cells with low numbers of mononuclear cells within alveolar spaces. **C.** Meloxicam "survival phenotype" treated hamster. Pulmonary interstitial spaces are infiltrated by lymphocytes and macrophages. Alveolar spaces contain low numbers of foamy macrophages and are lined by moderately hyperplastic AT2 cells. **D.** PT150 + meloxicam "survival phenotype" treated hamster. Similar changes are present as described in Fig. 3A. **E**. Representative image of cenerimod and baricitinib treatment groups. Bronchioles and alveolar spaces contain clusters of mixed inflammatory cells interspersed with cellular debris. Alveoli are lined by markedly hyperplastic and hypertrophied AT2 cells. Pleural surface is lined by hypertrophied mesothelial cells and a fine fibrinocellular exudate. **F**. Histopathology score summary of each hamster infection group on Day 7 PVI. Tinctorial staining differences are due to slide processing on different days. PVI: post-viral infection; HDTs: host-directed therapeutics; VBP: primary viral-secondary bacterial pneumonia; AT2 cells: alveolar type 2 cells; Positive Control: untreated hamsters infected with intranasal SARS-CoV-2 10^4 PFU on Day 0 and intratracheal *Haemophilus influenzae* serotype B 10^9 CFU on Day 2.5; PFU: plaque-forming units; CoV2: SARS-CoV-2; CFU: colony-forming units.

Bacterial dissemination can occur in HDT-treated, VB-infected hamsters on Day 7 PVI.

Bacterial cultures from lung, kidney, and spleen tissues were performed to assess for bacterial dissemination in treated, VB-infected hamsters on Day 7 PVI. None of the three "survival phenotype" meloxicam treated hamsters had detectable bacteria in any organ assessed. Among

the PT150 treated hamsters, only one had detectable bacteria (1.5×10^4 CFU/gram lung tissue; 5.0×10^2 CFU/gram kidney tissue; 6.0×10^2 CFU/gram splenic tissue) (Table 8). The single "survival phenotype" PT150 + meloxicam treated hamster also had detectable bacteria in all organs assessed (1.0×10^3 CFU/gram lung tissue; 1.0×10^4 CFU/gram kidney tissue; 3.0×10^3 CFU/gram splenic tissue) (Table 8).

In contrast, bacteria were isolated more commonly in cenerimod and baricitinib treated hamsters. Two of the four cenerimod treated hamsters had positive lung (8.0×10^7 CFU/gram lung tissue, 2.7×10^4 CFU/gram lung tissue) and kidney (2.6×10^6 CFU/gram kidney tissue, 2.0×10^4 CFU/gram kidney tissue) cultures; one of these hamsters also had detectable bacteria in the spleen (2.4×10^6 CFU/gram splenic tissue) (Table 8). Three of the four baricitinib treated hamsters had positive lung cultures (8.1×10^6 CFU/gram lung tissue, 1.9×10^5 CFU/gram lung tissue, 9.6×10^5 CFU/gram lung tissue); two of these hamsters also had positive kidney (1.5×10^7 CFU/gram kidney tissue, 1.7×10^4 CFU/gram kidney tissue) and spleen (7.2×10^6 CFU/gram splenic tissue, 1.0×10^4 CFU/gram splenic tissue) cultures (Table 8).

Tissue cultures were also performed on the hamsters euthanized before the Day 7 PVI study endpoint. The meloxicam treated hamster euthanized on Day 6 PVI had detectable bacteria in all organs assessed: 7.1×10^7 CFU/gram lung tissue; 3.2×10^5 CFU/gram kidney tissue; 3.8×10^6 CFU/gram splenic tissue. PT150 + meloxicam treated hamsters euthanized on Days 5 and 6 PVI had positive cultures in all organs assessed, with averages consisting of 2.6×10^8 CFU/gram lung tissue, 1.2×10^7 CFU/gram kidney tissue, and 4.3×10^6 CFU/gram splenic tissue.

Table 8. Bacterial tissue cultures of lung, kidney, and spleen on Day 7 PVI of adult male Syrian hamsters infected with CoV2 on Day 0 and HiB on Day 2.5 PVI and treated with HDTs on Days 2-4 PVI.

Group	Animal	Lung (CFU/g)	Kidney (CFU/g)	Spleen (CFU/g)
Meloxicam	Jn24 AM 1.3	0	0	0
	Jn24 AM 1.4	0	0	0
	Jn24 AM 1.5	0	0	0
PT150	Jn24 AM 2.12	0	0	0
	Jn24 AM 2.13	0	0	0
	Jn24 AM 2.14	0	0	0
	Jn24 AM 2.16	1.5×10^4	5.0×10^2	6.0×10^2
PT150 + Meloxicam	Jn24 AM 3.24	1.0×10^3	1.0×10^4	3.0×10^3
Cenerimod	Jn24 AM 4.26	0	0	0
	Jn24 AM 4.27	0	0	0
	Jn24 AM 4.28	8.0×10^7	2.6×10^6	2.4×10^6
	Jn24 AM 4.30	2.7×10^4	2.0×10^4	0
Baricitinib	Jn24 AM 5.31	8.1×10^6	1.5×10^7	7.2×10^6
	Jn24 AM 5.32	1.9×10^5	0	0
	Jn24 AM 5.33	9.6×10^5	1.7×10^4	1.0×10^4
	Jn24 AM 5.34	0	0	0

PVI: post-viral infection; CoV2: SARS-CoV-2; HiB: *Haemophilus influenzae* serotype B; CFU: colony-forming units; HDTs: host-directed therapeutics.

Viral persistence in HDT-treated, VB-infected hamsters.

Although SARS-CoV-2 lung viral titers in Syrian hamsters are undetectable by Day 7 post-viral infection [22], 50% of our untreated, VB-infected hamsters had detectable viral titers on Day 7 PVI (Chapter 3). To assess if host-directed therapeutics could impact viral persistence in our VBP hamster model, viral lung titers were performed on Day 7 PVI.

None of the PT150-only or “survival phenotype” meloxicam-only treated hamsters had detectable viral lung titers on Day 7 PVI. The single “survival phenotype” PT150 + meloxicam treated hamster had a detectable viral lung titer of 1.1×10^5 PFU/gram lung tissue (Table 9). Two cenerimod and two baricitinib treated hamsters had detectable viral lung titers (Table 9).

Viral lung titers were also performed on the hamsters euthanized prior to the Day 7 PVI study endpoint. Unsurprisingly, all four hamsters had positive lung viral titers. The meloxicam treated hamster euthanized on Day 6 PVI had a titer of 7.2×10^4 PFU/gram lung tissue. PT150 + meloxicam hamsters euthanized on Days 5 and 6 PVI had an average titer of 4.5×10^4 PFU/gram lung tissue.

Table 9. Plaque assay lung viral titers on Day 7 PVI of adult male Syrian hamsters infected with CoV2 on Day 0 and HiB on Day 2.5 PVI and treated with HDTs on Days 2-4 PVI.

Group	Animal	Lung (PFU/g)
Meloxicam	Jn24 AM 1.3	0
	Jn24 AM 1.4	0
	Jn24 AM 1.5	0
PT150	Jn24 AM 2.12	0
	Jn24 AM 2.13	0
	Jn24 AM 2.14	0
	Jn24 AM 2.16	0
PT150 + Meloxicam	Jn24 AM 3.24	1.1×10^{5}
Cenerimod	Jn24 AM 4.26	0
	Jn24 AM 4.27	0
	Jn24 AM 4.28	1.8×10^{3}
	Jn24 AM 4.30	9.1×10^{3}
Baricitinib	Jn24 AM 5.31	2.7×10^{3}
	Jn24 AM 5.32	5.5×10^{3}
	Jn24 AM 5.33	0
	Jn24 AM 5.34	0

PVI: post-viral infection; CoV2: SARS-CoV-2; HiB: *Haemophilus influenzae* serotype B; PFU: plaque-forming units; HDTs: host-directed therapeutics.

Baricitinib impacts relative differential expression of select genes involved in immune signaling during VBP infection.

We quantified lung tissue relative gene expression on Day 7 PVI to assess if HDT-treated animal immune responses could resemble a naïve host state. The immune response for baricitinib treated hamsters showed statistically significant relative gene expression differences for *Ifnb1* ($p = 0.049$) and *Il10* ($p = 0.0044$) when compared to negative control hamsters (Fig. 17). *Ifng* relative expression difference between negative control and baricitinib treated hamsters was nearing statistical significance ($p = 0.086$), but did not satisfy the statistical cut-off of $p \leq 0.05$.

No statistically significant relative gene expression differences were observed between the negative control, PT150-only, meloxicam-only, or cenerimod-only treated hamsters. Despite the increased relative gene expression observed in PT150, cenerimod, and baricitinib treated hamsters, as highlighted in white boxes in Fig. 17, we hypothesize that the overall paucity of statistical significance is due to a small sample size, *n* = 3/group. The PT150 + meloxicam treatment group was excluded from the statistical analysis, as it comprised of only one hamster at the Day 7 PVI study endpoint.

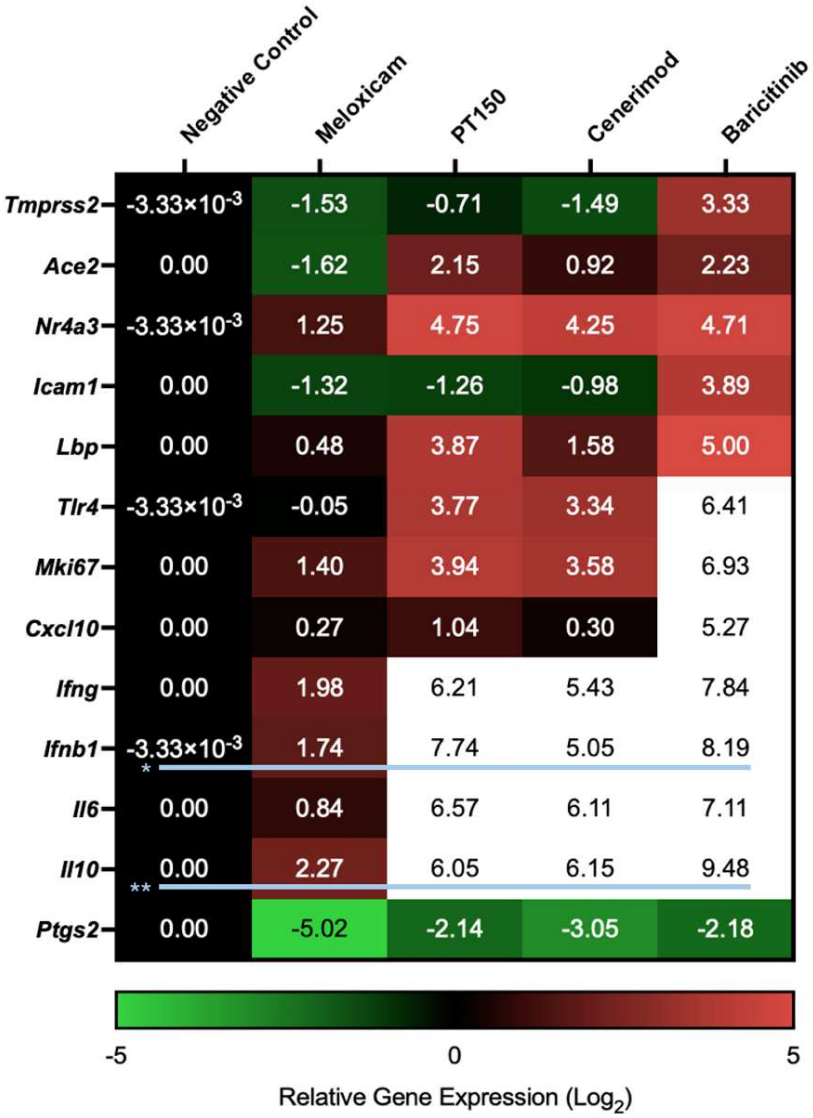

Figure 17. Relative gene expression on Day 7 PVI of Negative Control and HDT-treated hamsters during VBP infection. Gene expression was normalized to the *Actb* housekeeping gene. Fold-change of relative gene expression was calculated using delta-delta Ct against negative control hamsters (n = 3/group). White boxes represent relative gene expression (Log_2) changes greater than 5. Significance is denoted as *$p < 0.05$, **$p < 0.01$. Light blue line indicates statistically significant differences between negative control and baricitinib-treated groups. PVI: post-viral infection; Negative Control: sham infected, untreated hamsters; HDTs: host-directed therapeutics; VBP: primary viral-secondary bacterial pneumonia.

DISCUSSION

HDTs offer a promising approach to mitigating the severity of viral-bacterial pneumonia by targeting host pathways rather than the pathogens themselves. Unlike traditional antimicrobials,

which directly inhibit pathogen replication, HDTs that target host responses exploited by pathogens offers to enhance the host's ability to combat infection and prevent excessive tissue damage. In this study, our group manipulated select host pathways to assess how such perturbations would impact disease outcome in our adult male Syrian hamster VBP infection model. The HDTs assessed focused on disrupting host mechanisms necessary for viral host cell entry or modulating host pathways contributing to hyperinflammation.

The most surprising outcome was that of the PT150 + meloxicam treated hamsters. Given the success of PT150 in hamsters infected with SARS-CoV-2 [26], we hypothesized that including a NSAID to mitigate the hyperinflammatory response would result in the least amount of pulmonary damage of all treatment groups. However, the opposite proved to be true. Three of the eight hamsters receiving this treatment had to be euthanized before the first study endpoint. We suspect that the GR agonistic properties of PT150, combined with meloxicam, created an excessively broad anti-inflammatory environment, which impaired the host's ability to respond to infection and resulted in a dysregulated host state. This interpretation is supported by the bacterial dissemination detected in these hamsters and the severe pulmonary histopathology. The one "survival phenotype" hamster that was a part of the Day 7 PVI endpoint was bacteremic, had detectable lung viral titers, and displayed similar lung histopathology as VB-infected, untreated hamsters.

Although PT150 + meloxicam resulted in a detrimental outcome for a subset of hamsters, PT150 only treatment appears to be advantageous. The histopathologic lesions were similar to that of virus-only infected hamsters (Chapter 3) and no viral titers were detected on Day 7 PVI. One PT150-only treated hamster was bacteremic on Day 7 PVI; however, these titers were low, and the hamster was clinically unremarkable at the time of euthanasia. Thus, it is possible that this hamster was in the process of resolving the bacterial dissemination. Future studies will incorporate ciprofloxacin to assess if combining a broad-spectrum oral antibiotic with this antiviral HDT further mitigates pulmonary histopathologic damage.

Meloxicam-only treated “survival phenotype” hamsters demonstrated non-differentially regulated relative gene expression of most genes assessed compared to the negative control group. The single outlier was decreased *Ptgs2* relative expression, consistent with meloxicam administration. These findings, in combination with the negative microbial titers and the least amount of pulmonary histopathologic damage, suggest that incorporation of an NSAID into treatment plans may be efficacious in a subset of VBP hamsters. However, it is critical for future studies to ascertain why this treatment was fatal in one hamster.

Both cenerimod-only and baricitinib-only treatment groups included subsets of hamsters with positive bacterial and viral tissue cultures. Moreover, both groups displayed moderate to severe histopathologic pulmonary lesions. Relative expression of *Ifnb1* and *Il10* demonstrated a statistically significant increase in the baricitinib treatment group; many of the other genes assessed were similarly elevated. We suspect these hamsters were in a dysregulated immunological state; however, the small sample size likely prevented the confirmation of statistically significant relative gene expression of the pro-inflammatory markers assessed. Collectively, these findings support that baricitinib (10 mg/kg) on Days 2-4 PVI is contraindicated in our hamster VBP infection model. Similarly, given the low dosage of cenerimod used in this study (0.3 mg/kg), we infer that modulating lymphocyte and/or DC activity with cenerimod on Days 2-4 PVI is contraindicated in our VBP infection model.

Incorporating host-modulating drugs into treatment plans presents several obstacles, including determining when to initiate HDTs, optimizing dosage, and identifying the most responsive pathway for modulation based on the specific disease pathogenesis. Our study adopted a delayed dosing schedule to ensure that SARS-CoV-2 inflammatory pathways were already activated when medications were administered. Additional studies are warranted to assess if starting meloxicam on Day 3 or 4 PVI results in no fatalities while still limiting the amount of pulmonary tissue damage. This research also acknowledges study limitations such as a lack of dose range finding pilot studies, which likely impacted the outcomes observed in the PT150 +

meloxicam and baricitinib-only treatment groups. Future studies will assess whether decreasing dosages, or staggering the administration, of these HDTs results in more efficacious outcomes on Day 7 PVI. Additionally, no treated, sham infected control hamsters were included in these studies. Once the most appropriate HDTs for our hamster VBP infection model are identified, including such control animals will facilitate assessing HDT basal impact on gene expression in Syrian hamsters.

Our Syrian hamster model provides a valuable platform for investigating VBP pathogenesis and testing novel therapeutic strategies. Moreover, this study highlights the challenges of assessing HDTs in a novel small animal infection model. Our experimental findings support that PT150 holds significant clinical potential during VBP infection, and that NSAID utilization may be a viable strategy in an undetermined subset of patients. By modulating host responses, HDTs can enhance the efficacy of antimicrobial agents, reduce inflammation-induced lung damage, and improve patient outcomes. Future studies will optimize combination therapies that leverage HDTs alongside conventional treatments to provide a comprehensive approach to managing viral-bacterial pneumonia.

REFERENCES

1. Administration for Strategic Preparedness & Response/United States Department of Health and Human Services. *What Are the Possible Treatment Options for COVID-19?* https://aspr.hhs.gov/COVID-19/Treatments/Pages/Possible-Treatment-Options-for-COVID19.aspx. Accessed 7 March 2024.
2. Ali E, Owais R, Sheikh A, Shaikh A. Olumniant (Baricitinib) oral tablets: An insight into FDA-approved systemic treatment for Alopecia Areata. *Ann Med Surg (Lond).* 2022;80:104157.
3. Center for Disease Control. *Background for CDC's Updated Respiratory Virus Guidance.* https://www.cdc.gov/respiratory-viruses/guidance/background.html?CDC_AAref_Val=https://www.cdc.gov/respiratory-viruses/background/index.html. Access 1 March 2024.
4. Eken A, Yetkin MF, Vural A, et al. Fingolimod Alters Tissue Distribution and Cytokine Production of Human and Murine Innate Lymphoid Cells. *Front Immunol*. 2019;10:217.
5. Fraga-Silva TFC, Cipriano UG, Fumagalli MJ, et al. Airway epithelial cells and macrophages trigger IL-6-CD95/CD95L axis and mediate initial immunopathology of COVID-19. *iScience*. 2023;26(12):108366.
6. Frere JJ, Serafini RA, Pryce KD, et al. SARS-CoV-2 infection in hamsters and humans results in lasting and unique systemic perturbations after recovery. *Sci Transl Med*. 2022;14(664).
7. Fridman JS, Scherle PA, Collins R, et al. Selective inhibition of JAK1 and JAK2 is efficacious in rodent models of arthritis: preclinical characterization of INCB028050. *J Immunol*. 2010;184(9):5298.
8. Foley PL, Kendall LV, Turner PV. Clinical management of pain in rodents. *Comp Med*. 2019;69(6):468.
9. Gabay C. Interleukin-6 and chronic inflammation. *Arthritis Res Ther*. 2006;8 Suppl 2(Suppl 2):S3.
10. Gohibic. FDA-Authorized for Emergency Use. https://www.gohibic.com/hcp/. Accessed 17 March 2025.
11. Hawkins MG. The Use of Analgesics in Birds, Reptiles, and Small Exotic Mammals. *J Exot Pet Med*. 2006;15(3):177.
12. Heatley JJ, and Harris MC. "Hamsters and Gerbils." *Manual of Exotic Pet Practice*, Saunders Elsevier, St. Louis, Mo, 2009, pp. 406.
13. Hoang TN, Pino M, Boddapati AK, et al. Baricitinib treatment resolves lower-airway macrophage inflammation and neutrophil recruitment in SARS-CoV-2-infected rhesus macaques. *Cell*. 2021;184(2):460-475.e21.
14. Jorgensen SCJ, Tse CLY, Burry L, Dresser LD. Baricitinib: A Review of Pharmacology, Safety, and Emerging Clinical Experience in COVID-19. *Pharmacotherapy*. 2020;40(8):843.
15. Juif PE, Dingemanse J, Winkle P, Ufer M. Pharmacokinetics and Pharmacodynamics of Cenerimod, A Selective $S1P_1$ R Modulator, Are Not Affected by Ethnicity in Healthy Asian and White Subjects. *Clin Transl Sci*. 2021;14(1):143.
16. Karuppuchamy T, Behrens EH, González-Cabrera P, et al. Sphingosine-1-phosphate receptor-1 ($S1P_1$) is expressed by lymphocytes, dendritic cells, and endothelium and modulated during inflammatory bowel disease. *Mucosal Immunol*. 2017;10(1):162.
17. Kushner P, McCarberg BH, Grange L, et al. The use of non-steroidal anti-inflammatory drugs (NSAIDs) in COVID-19. *NPJ Prim Care Respir Med*. 2022;32(1):35.
18. Li G, Hilgenfeld R, Whitley R, De Clercq E. Therapeutic strategies for COVID-19: progress and lessons learned. *Nat Rev Drug Discov*. 2023;22(6):449.

19. Miller DL, Dou C, Raghavendran K. Anesthetic techniques influence the induction of pulmonary capillary hemorrhage during diagnostic ultrasound scanning in rats. *J Ultrasound Med*. 2015;34(2):289.
20. Morice C, Baker DG, Patel MM, et al. A randomized trial of safety and pharmacodynamic interactions between a selective glucocorticoid receptor antagonist, PT150, and ethanol in healthy volunteers. *Sci Rep*. 2021;11(1):9876.
21. Nidadavolu LS, Walston JD. Underlying Vulnerabilities to the Cytokine Storm and Adverse COVID-19 Outcomes in the Aging Immune System. *J Gerontol A Biol Sci Med Sci*. 2021;76:e13.
22. Oishi K, Horiuchi S, Frere J, Schwartz RE, tenOever BR. A diminished immune response underlies age-related SARS-CoV-2 pathologies. *Cell Rep*. 2022;39:111002.
23. Piali L, Birker-Robaczewska M, Lescop C, et al. Cenerimod, a novel selective $S1P_1$ receptor modulator with unique signaling properties. *Pharmacol Res Perspect*. 2017;5(6):e00370.
24. Qiao Y, Wang XM, Mannan R, et al. Targeting transcriptional regulation of SARS-CoV-2 entry factors *ACE2* and *TMPRSS2*. *Proc Natl Acad Sci U S A*. 2021;118(1):e2021450118.
25. Rhen T, Cidlowski JA. Antiinflammatory action of glucocorticoids--new mechanisms for old drugs. *N Engl J Med*. 2005;353(16):1711.
26. Rocha SM, Fagre AC, Latham AS, et al. A Novel Glucocorticoid and Androgen Receptor Modulator Reduces Viral Entry and Innate Immune Inflammatory Responses in the Syrian Hamster Model of SARS-CoV-2 Infection. *Front Immunol*. 2022;13:811430.
27. Sasaki M, Sugi T, Iida S, et al. Combination therapy with oral antiviral and anti-inflammatory drugs improves the efficacy of delayed treatment in a COVID-19 hamster model. *EBioMedicine*. 2024;99:104950.
28. Selvaraj V, Finn A, Lal A, Khan MS, Dapaah-Afriyie K, Carino GP. Baricitinib in hospitalised patients with COVID-19: A meta-analysis of randomised controlled trials. *EClinicalMedicine*. 2022;49:101489.
29. Strasser DS, Froidevaux S, Sippel V, et al. Preclinical to clinical translation of cenerimod, a novel $S1P_1$ receptor modulator, in systemic lupus erythematosus. *RMD Open*. 2020;6(2):e001261.
30. Theise ND, Arment AR, Chakravarty D, et al. Clinical stage molecule PT150 is a modulator of glucocorticoid and androgen receptors with antiviral activity against SARS-CoV-2. *Cell Cycle*. 2020;19(24):3632.
31. U.S. Center for Drug Evaluation and Research. (2005, July). Guidance for industry: estimating the maximum safe starting dose in initial clinical trials for therapeutics in adult healthy volunteers. https://www.fda.gov/media/72309/download. Access 5 March 2024.
32. Williams JA, Shacter E. Regulation of macrophage cytokine production by prostaglandin E2. Distinct roles of cyclooxygenase-1 and -2. *J Biol Chem*. 1997;272(41):25693-25699.
33. Wright JM. The double-edged sword of COX-2 selective NSAIDs. *CMAJ*. 2002;167(10):1131.
34. Wyler E, Adler JM, Eschke K, et al. Key benefits of dexamethasone and antibody treatment in COVID-19 hamster models revealed by single-cell transcriptomics. *Mol Ther*. 2022;30(5):1952.
35. Ye ZW, Yuan S, Chan JF, et al. Beneficial effect of combinational methylprednisolone and remdesivir in hamster model of SARS-CoV-2 infection. *Emerg Microbes Infect*. 2021;10(1):291.
36. Zhang J, Sheng H, Tang X, et al. Non-steroidal anti-inflammatory drugs and clinical outcomes in patients with COVID-19. *Front Cell Infect Microbiol*. 2022;12:935280.

37. Zhao Y, Usatyuk PV, Gorshkova IA, et al. Regulation of COX-2 expression and IL-6 release by particulate matter in airway epithelial cells. *Am J Respir Cell Mol Biol*. 2009;40(1):19.

Chapter 5 – General discussion and future directions

GENERAL DISCUSSION

Primary viral-secondary bacterial pneumonia (VBP) has been implicated in increased patient morbidity and mortality compared to viral pneumonia alone [21]. Such robust pathogen synergism was first observed during the 1918–1919 H1N1 influenza A virus "Spanish flu" pandemic, where most patients with severe influenza-associated pneumonia died from a secondary bacterial pneumonia [18]. Despite the medical diagnostics, therapeutics, and preventative measures that have been developed since the Spanish flu, subsets of patients in recent viral pandemics have still been negatively impacted by VBP [3, 10]. It has been generally accepted that virus-mediated structural changes and immunological dysregulation increase a host's susceptibility to secondary bacterial pneumonia [11, 31]. Multiple bacterial species have been isolated from SARS-CoV-2 patients diagnosed with a secondary bacterial pneumonia, but aged adults are consistently among those likelier to develop severe disease [15, 16]. This continued health concern has warranted experimental VBP studies using animal models to investigate respiratory viral-bacterial synergism.

Several investigators have established primary viral-secondary bacterial pneumonia models in laboratory mice [1, 13, 14, 29]; however, laboratory mice lack translational rigor for modeling human VBP disease. As such, this dissertation endeavored to create a VBP infection model using SARS-CoV-2 and the naturally susceptible, immunocompetent Syrian hamster. This dissertation's first and second research aims focused on incorporating the biological variables of (1) host age to determine the ideal VBP infection scenario and (2) determining how the pathogen infection sequence impacts disease phenotype. Surprisingly, the development of this model highlighted the critical variable of host age. The finding that adult male hamsters develop worse disease than young male hamsters is consistent with age being the most critical risk factor in humans for developing severe COVID-19 [2]. Our initial pilot studies revealed that a secondary bacterial

infection in adult males resulted in delayed pulmonary histopathologic recovery. This structural finding was validated by qRT-PCR in later studies demonstrating a dysregulated immune response in VB-infected adult hamsters, which we attributed to a consequence of immunosenescence and inflammaging. Contrastingly, a secondary bacterial infection in young males often resulted in significantly less severe pulmonary histopathology – this finding may represent the biological phenomenon of innate immune priming (IIP) [7]. IIP occurs when a primary inflammatory stimulus triggers innate immune responses, and before the immune system returns to a basal level, a secondary stimulus amplifies these responses, enhancing innate immune function that can mitigate disease severity [7, 27]. These findings highlight the necessity to incorporate an assessment of host age when modeling infectious diseases, as animal modeling phenotypes can be largely impacted by an aged immune system.

A significant challenge of this dissertation was addressing variables related to the bacterial infection: bacterial species, inoculum dose, infection route, and time interval between pathogen exposures. Pilot studies were crucial for assessing the bacterial species, dose, and infection route. These study outcomes were primarily substantiated through weight loss consistency among infection groups and histopathological assessment of the percentage of lung tissue affected. The most pressing obstacle in creating this infection model was determining the time interval between pathogen exposures. None of the published VBP animal modeling studies have provided pathophysiologic rationales for the time interval between pathogen exposures. By utilizing basic immunology principles and understanding the SARS-CoV-2 pathogenesis in Syrian hamsters, we determined an appropriate susceptibility window for the secondary bacterial infection. Providing mechanistic justifications for model design showcases the importance of a rationalized approach when attempting to recapitulate real-world disease scenarios in a laboratory setting. Comparing the ante-mortem and post-mortem analyses of virus-only, virus followed by bacteria, bacteria-only, and bacteria followed by virus infection groups, we further proved that the virus followed by bacteria infection scenario resulted in the most severe disease phenotype.

Completing the first and second research aims ultimately established a new model for assessing VBP in an underutilized laboratory animal species with greater translational utility than laboratory mice.

Treatment options for patients diagnosed with severe SARS-CoV-2 include a combination of antivirals, antibiotics, and supplemental oxygen with or without immunomodulators. The two FDA-approved anti-SARS-CoV-2 drugs target viral proteins; however, both drugs possess limitations in administration or demonstrate negative drug interactions with commonly prescribed medications [6, 22]. Although only 18% of patients with severe COVID-19 develop a secondary bacterial infection [12], this is a fatal sequela that can be prophylactically mitigated, especially when intensive care unit resources, such as beds and ventilators, are in limited supply. As such, up to 75% of COVID-19 patients received empiric antibiotics at the time of hospitalization during the pandemic [28]. Once moderate pneumonia progresses to a severe form, developing a cytokine storm becomes a clinical concern. Immunomodulators can be introduced at this stage to mitigate the host's hyperinflammatory response, a strategy that has demonstrated positive outcomes in COVID-19 patients meeting this criterion when incorporated into treatment protocols [23, 26]. Given the constraints of approved anti-SARS-CoV-2 drugs, the ongoing concern of antimicrobial resistance, and the positive clinical outcomes associated with immunomodulators, our third aim sought to assess non-antibiotic, host-directed therapeutics (HDTs) as a possible treatment strategy for VBP using our adult male hamster infection model.

HDTs modulate host cellular and immune responses to restore homeostasis and prevent excessive tissue damage. This approach is particularly relevant in COVID-19 with secondary bacterial infections, where immune dysregulation contributes significantly to morbidity and mortality [2, 20]. Based on the qRT-PCR data from our VB-infected hamsters, we selected several HDTs to assess the pathways they inhibit as potential druggable targets. Consistent with our previous report [25], PT150, an androgen and glucocorticoid receptor modulator, dampened inflammation while preserving antiviral immune defenses. Modulation of two critical proteins that

facilitate SARS-CoV-2 entry into host cells, TMPRRS2 and ACE2, in combination with PT150's ability to mitigate hyperinflammatory structural lesions, make this HDT a compelling candidate for inclusion in VBP treatment regimens. Meloxicam, a selective cyclooxygenase-2 (COX-2) inhibitor, modulates COX-2-induced inflammation to minimize pro-inflammatory prostaglandin production that contributes to tissue injury. The mild to moderate pulmonary structural changes and non-differentially regulated relative gene expression findings observed in a subset of VB-infected hamsters support that inhibition of COX-2 can be an attractive option for treating severe respiratory infections, including SARS-CoV-2 with secondary bacterial pneumonia. Moreover, these two HDTs demonstrated the potential to reduce disease severity without antibiotics – a significant advantage given the clinical concerns of pathogenic heterogeneity involved in VBP. This research reveals that select HDTs can mitigate disease severity in our Syrian hamster model and supports using this model to investigate other novel therapeutic strategies.

Our HDT studies also highlighted consequences associated with HDTs and the importance of dosage optimization. Despite the negative results associated with cenerimod, they proved that modulating lymphoid and dendritic cell functions is likely not a beneficial HDT target for VBP treatment. Baricitinib is already approved for the treatment of severe COVID-19. We hypothesize that the dose administered in this study was too high, and therefore, over-suppressed JAK1/JAK2 function. A similar rationale can be applied to the PT150 + meloxicam-treated hamsters: a combination of these drugs, at their specific dosages, may have resulted in too broad of an anti-inflammatory effect, thereby favoring pathogen survival and subsequent hyperinflammation as indicated by microbial titers and histopathology. These findings underscore the importance of assessing multiple host pathways for pilot study HDT research and the critical need for dosage calibration in HDT strategies to balance anti-inflammatory effects without compromising host defenses.

Taken together, our work reframed VBP small animal modeling selection criteria to prioritize assessing translationally relevant molecular mechanisms for successful pathogenesis

characterization and accurately identifying druggable targets. Our infection model supports pre-translational researchers in bridging gaps in basic science knowledge, while providing a platform to showcase proof-of-concept treatment rationales when addressing this complex research problem. As emerging infectious respiratory diseases continue to impact global health, research such as this is critical for developing comprehensive standard-of-care protocols based on findings from translationally relevant animal models.

FUTURE DIRECTIONS

This dissertation provided basic science information on assessing one specific virus-bacteria combination to induce disease in a naturally susceptible, immunocompetent lab animal species. These studies also assessed select pro-inflammatory pathways as targets for HDTs; however, many other pathways remain uninvestigated. Future studies should target three key areas to enhance VBP modeling and therapeutic evaluation.

Building on the success of our adult male Syrian hamster VBP model, future studies should explore other biological variables, such as sex and obesity, to understand how these often-overlooked factors influence disease phenotype. Female hamsters develop less severe SARS-CoV-2 disease than male hamsters [5, 8, 30]. Comparing VBP mechanistic differences between adult male and adult female hamsters will uncover additional insights that can be exploited to minimize disease severity in male patients. In addition to sex-based differences, obesity represents another critical biological variable that can shape immune responses and disease progression. Obesity impacts millions of Americans and is a risk factor for developing respiratory infectious disease [24]. Biologically, obesity induces a chronic, hyperinflammatory state characterized by elevated levels of TNFα, IL-6, and C-reactive protein [11]. By modeling this disease state and comparing it to findings in adult male and female VBP hamsters, we may uncover additional mechanistic insights that can be missed when exclusively using animals with adequate body condition.

No single animal model encompasses all features of human disease, which necessitates the development of multiple animal models to comprehensively study human disease in a research setting. Ferrets have been shown to be a reliable VBP model using the 2009 pandemic H1N1 influenza A virus followed by *Streptococcus pneumoniae* infection [17, 19]. This dissertation supports using SARS-CoV-2 and *Haemophilus influenzae* to assess another virus-bacteria respiratory infection combination. Cotton rats represent a third immunocompetent lab animal species that can be utilized for respiratory infectious disease modeling. Adult cotton rats, older than eight months of age, serve as the preferred model species for investigating human respiratory syncytial virus (hRSV) pathogenesis in elderly populations [9]. Future assessment of primary hRSV infection followed by a secondary bacterial infection will provide translational researchers with another rigorous VBP infection model for studying human disease. Comparative RNA-sequencing from these studies can highlight critical host immune response molecular pathways engaged across these immunocompetent animal models. These studies may also indicate whether similar HDTs can be employed as interventional strategies across different pathogen infection scenarios.

Continued investigation into the application of HDTs, in combination with pathogen-directed antimicrobials, for VBP infection scenarios remains of great clinical interest. First, conducting optimization studies on the Chapter 4 HDTs will provide a thorough evaluation of their effectiveness within our hamster VBP model. Such studies include investigating different dosages for meloxicam and baricitinib and including ciprofloxacin as an antibacterial agent. Assessment of danirixin, an investigational CXC chemokine receptor 2 (CXCR2) antagonist, is another HDT that may possess advantageous therapeutic modulation during VBP [4]. Neutrophil CXCR2 is a receptor that binds CXCL8 to facilitate neutrophil chemotaxis to sites of inflammation [31]. Antagonizing this receptor might aid in decreasing the degree of neutrophil influx observed in our VBP infection model and thus minimize the amount of host-derived pulmonary tissue damage. By refining

therapeutic strategies, we can better mitigate the impact of polymicrobial pneumonia and improve patient outcomes in future respiratory pandemics.

REFERENCES

1. Barman TK, Singh AK, Bonin JL, Nafiz TN, Salmon SL, Metzger DW. Lethal synergy between SARS-CoV-2 and Streptococcus pneumoniae in hACE2 mice and protective efficacy of vaccination. *JCI Insight*. 2022;7(11):e159422.
2. Bartleson JM, Radenkovic D, Covarrubias AJ, Furman D, Winer DA, *et al*. SARS-CoV-2, COVID-19 and the Ageing Immune System. *Nat Aging*. 2021;1:769-782.
3. Bosch AA, Biesbroek G, Trzcinski K, Sanders EA, Bogaert D. Viral and bacterial interactions in the upper respiratory tract. *PLoS Pathog*. 2013;9:e1003057.
4. Busch-Petersen J, Carpenter DC, Burman M, et al. Danirixin: A Reversible and Selective Antagonist of the CXC Chemokine Receptor 2. *J Pharmacol Exp Ther*. 2017;362(2):338-346.
5. Castellan M, Zamperin G, Franzoni G, Foiani G, Zorzan M, *et al*. Host Response of Syrian Hamster to SARS-CoV-2 Infection including Differences with Humans and between Sexes. *Viruses*. 2023;15:428.
6. Centers for Disease Control and Prevention. Types of COVID-19 Treatment. https://www.cdc.gov/covid/treatment/index.html. Accessed 3 March 2025.
7. Divangahi M, Aaby P, Khader SA, et al. Trained immunity, tolerance, priming and differentiation: distinct immunological processes [published correction appears in Nat Immunol. 2021 Jul;22(7):928. doi: 10.1038/s41590-021-00960-y.]. *Nat Immunol*. 2021;22(1):2-6.
8. Foiani G, Castellan M, Leopardi S, de Benedictis P, Monetti G, Vascellari M. Sex differences and histopathological patterns of lung damage in Syrian hamsters induced by SARS-CoV-2 experimental infection. *J Comp Pathol*. 2023;203:46.
9. Harder OE, Niewiesk S. Respiratory Syncytial Virus Infection Modeled in Aging Cotton Rats (*Sigmodon hispidus*) and Mice (*Mus musculus*). *Adv Virol*. 2022;2022:8637545.
10. Hu GN, Liu WL, Chang CH, et al. Microbial dynamics, risk factors and outcomes of secondary pneumonia in critically ill patients with COVID-19: A multicenter retrospective cohort study. *J Formos Med Assoc*. 2024;123(11):1186-1193.
11. Kumar V, Abbas A, Aster J. *Robbins and Cotran Pathologic Basis of Diseases*. 10th Edition, Elsevier, Amsterdam.
12. Langford BJ, So M, Simeonova M, Leung V, Lo J, *et al*. Antimicrobial resistance in patients with COVID-19: a systematic review and meta-analysis. *Lancet Microbe*. 2023;4:e179-e191.
13. Lee LN, Dias P, Han D, et al. A mouse model of lethal synergism between influenza virus and Haemophilus influenzae. *Am J Pathol*. 2010;176(2):800-811.
14. Lee MH, et al. A postinfluenza model of Staphylococcus aureus pneumonia. *J Infect Dis*. 2010;201(4):508-515.
15. Manohar P, Loh B, Nachimuthu R, Hua X, Welburn SC, *et al*. Secondary Bacterial Infections in Patients With Viral Pneumonia. *Front Med*. 2020;7:420.
16. Markovskaya Y, Gavioli EM, Cusumano JA, Glatt AE. Coronavirus disease 2019 (COVID-19): Secondary bacterial infections and the impact on antimicrobial resistance during the COVID-19 pandemic. *Antimicrob Steward Healthc Epidemiol*. 2022;2(1):e114.
17. Mifsud EJ, Farrukee R, Hurt AC, Reading PC, Barr IG. Infection with different human influenza A subtypes affects the period of susceptibility to secondary bacterial infections in ferrets. *FEMS Microbes*. 2022;3:xtac011.
18. Morens DM, Taubenberger JK, Fauci AS. Predominant role of bacterial pneumonia as a cause of death in pandemic influenza: implications for pandemic influenza preparedness. *J Infect Dis*. 2008;198(7):962-970.
19. Mueller Brown K, Le Sage V, French AJ, et al. Secondary infection with *Streptococcus pneumoniae* decreases influenza virus replication and is linked to severe disease. *FEMS Microbes*. 2022;3:xtac007.

20. Nidadavolu LS, Walston JD. Underlying Vulnerabilities to the Cytokine Storm and Adverse COVID-19 Outcomes in the Aging Immune System. *J Gerontol A Biol Sci Med Sci*. 2021;76:e13-e18.
21. Patton MJ, Orihuela CJ, Harrod KS, et al. COVID-19 bacteremic co-infection is a major risk factor for mortality, ICU admission, and mechanical ventilation. *Crit Care*. 2023;27(1):34.
22. Paxlovid. Drug interactions. https://www.paxlovidhcp.com/drug-interactions. Accessed 3 March 2025.
23. Piscoya A, Parra Del Riego A, Cerna-Viacava R, et al. Efficacy and harms of tocilizumab for the treatment of COVID-19 patients: A systematic review and meta-analysis. *PLoS One*. 2022;17(6):e0269368.
24. Pugliese G, Liccardi A, Graziadio C, Barrea L, Muscogiuri G, Colao A. Obesity and infectious diseases: pathophysiology and epidemiology of a double pandemic condition. *Int J Obes (Lond)*. 2022;46(3):449-465.
25. Rocha SM, Fagre AC, Latham AS, et al. A Novel Glucocorticoid and Androgen Receptor Modulator Reduces Viral Entry and Innate Immune Inflammatory Responses in the Syrian Hamster Model of SARS-CoV-2 Infection. *Front Immunol*. 2022;13:811430.
26. Selvaraj V, Finn A, Lal A, Khan MS, Dapaah-Afriyie K, Carino GP. Baricitinib in hospitalised patients with COVID-19: A meta-analysis of randomised controlled trials. *EClinicalMedicine*. 2022;49:101489.
27. Sharrock J, Sun JC. Innate immunological memory: from plants to animals. *Curr Opin Immunol*. 2020;62:69-78.
28. Sili U, Tekin A, Bilgin H, Khan SA, Domecq JP, *et al*. Early empiric antibiotic use in COVID-19 patients: results from the international VIRUS registry. *Int J Infect Dis*. 2024;140:39-48.
29. Smith AP, Williams EP, Plunkett TR, et al. Time-Dependent Increase in Susceptibility and Severity of Secondary Bacterial Infections During SARS-CoV-2. *Front Immunol*. 2022;13:894534.
30. Yuan L, Zhu H, Zhou M, et al. Gender associates with both susceptibility to infection and pathogenesis of SARS-CoV-2 in Syrian hamster. *Signal Transduct Target Ther*. 2021;6(1):136.
31. Zachary JF, ed. Pathologic Basis of Veterinary Disease. 6th ed. St Louis, MO: Elsevier; 2017.

LIST OF ABBREVIATIONS

ACE2	Angiotensin-converting Enzyme 2
AMR	Antimicrobial Resistance
ARDS	Acute Respiratory Distress Syndrome
AT1 cells	Alveolar Type 1 cells
AT2 cells	Alveolar Type 2 cells
BALT	Bronchiolar-associated Lymphoid Tissue
BAP	Blood Agar Plate
BO	Bacteria-only
BSL-3	Biosafety level-3
BV	Bacteria followed by virus
CFU	Colony-forming units
Co-infection	Simultaneous infection by two or more pathogens.
COPD	Chronic Obstructive Pulmonary Disease
COVID-19	Coronavirus Disease 2019
COX-2	Cyclooxygenase-2
CS	Cytokine Storm
DAD	Diffuse Alveolar Damage
DAMPs	Damage-associated Molecular Patterns
FDA	Food and Drug Administration
Hamster	Syrian hamster
HE	Hematoxylin and Eosin
HDT	Host-directed Therapeutics. Medications that target host-specific biology, instead of acting directly on the pathogen, to interfere with host cell functions that are either required or exploited for pathogen propagation.
H. influenzae	*Haemophilus influenzae*
HiB	*Haemophilus influenzae* serotype B
HMF	Hyaline Membrane Formation
IFN	Interferon
Ig	Immunoglobulin
IHC	Immunohistochemistry
IL	Interleukin
ILC1	Group 1 Innate Lymphoid Cells
IN/IT infection model	Intranasal/non-surgical intracheal infection model
JAK/STAT	Janus kinase-signal transducer and activator of transcription
K18-hACE2 mouse	B6.Cg-Tg(K18-ACE2)2Prlmn/J transgenic mouse
LOX	Lipoxygenase
MHCII	Major Histocompatibility Complex Class II
NF-kB	Nuclear factor-kappa B
NK cells	Type 1 Natural Killer cells
NLRP3	NOD-like receptor protein 3 inflammasome
NSAID	Non-steroidal Anti-inflammatory Drug
NSP	Non-structural protein
NTHi	Non-typeable *Haemophilus influenzae*
ORF	Open Reading Frame
PAMPs	Pathogen-associated Molecular Patterns
PFU	Plaque-forming units

PGE_2	Prostaglandin E_2
Post-viral secondary bacterial infection	Bacterial infection occurs after viral titers are no longer detectable in the host.
PPI	Post-primary infection
PRRs	Pattern-recognition Receptors
PVI	Post-viral infection
qRT-PCR	Quantitative Reverse Transcription Polymerase Chain Reaction
(h)RSV	(human) Respiratory Syncytial Virus
SARS-CoV-2	Severe Acute Respiratory Syndrome Coronavirus 2
sBHI	Supplemented Brain-Heart Infusion broth
sCAP	Supplemented Chocolate Agar Plate
Secondary infection	Single pathogen infection followed by another single pathogen infection that occurs when the first pathogen is still detectable within the host.
S. aureus	*Staphylococcus aureus*
S. pneumoniae	*Streptococcus pneumoniae*
Superinfection	Single host cell is infected by two or more pathogens (e.g., two influenza viruses undergoing reassortment to yield a new influenza virus strain).
TLR	Toll-like Receptor
TMPRSS2	Transmembrane Protease Serine 2
TNF	Tumor necrosis factor
VB	Virus followed by bacteria
VBP	Primary viral-secondary bacterial pneumonia
VO	Virus-only